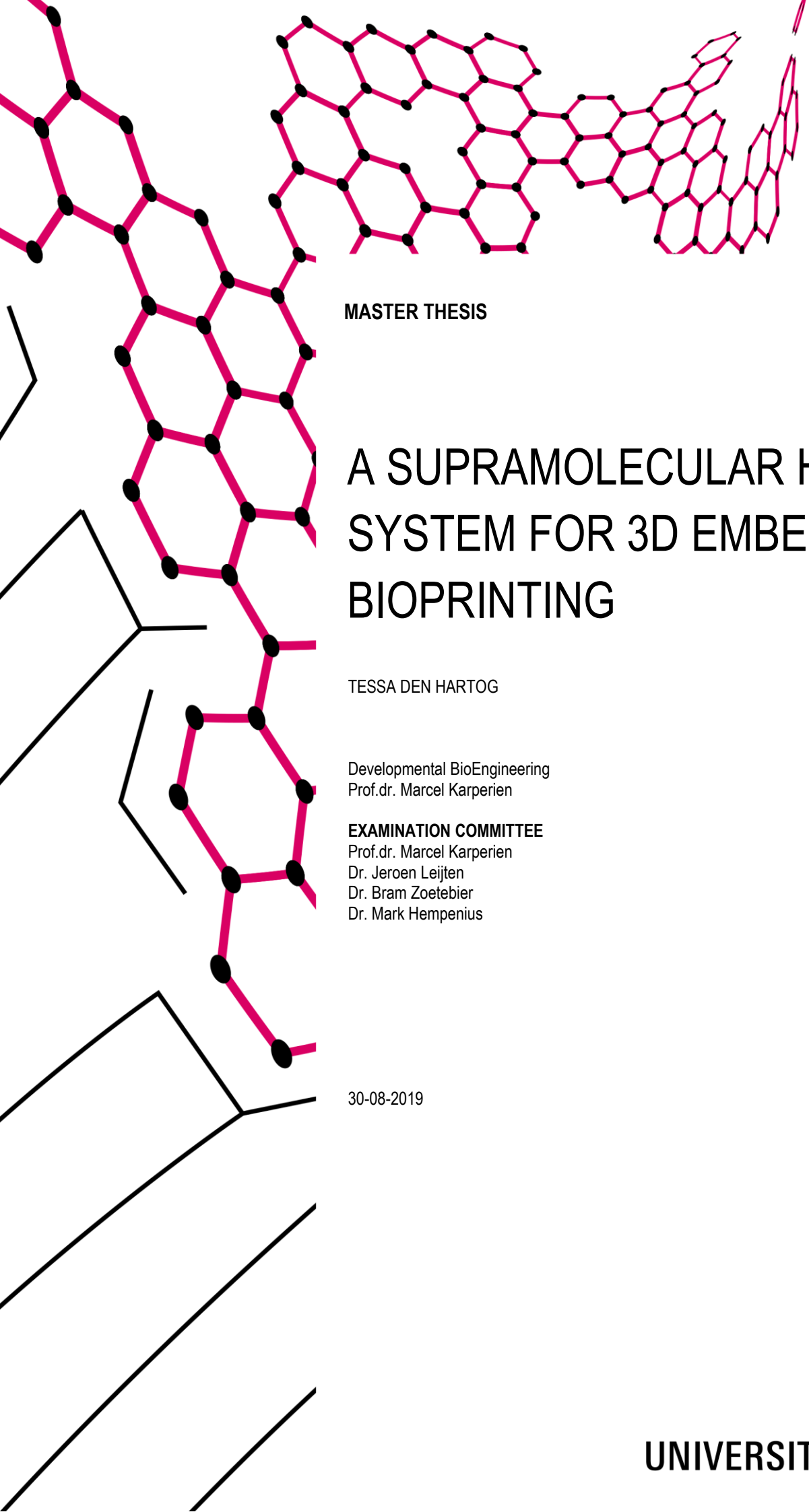

MASTER THESIS

A SUPRAMOLECULAR HYDROGEL SYSTEM FOR 3D EMBEDDED BIOPRINTING

TESSA DEN HARTOG

Developmental BioEngineering
Prof.dr. Marcel Karperien

EXAMINATION COMMITTEE
Prof.dr. Marcel Karperien
Dr. Jeroen Leijten
Dr. Bram Zoetebier
Dr. Mark Hempenius

30-08-2019

UNIVERSITY OF TWENTE.

Abstract

Biofabrication via three-dimensional bioprinting enables simultaneous and spatial positioning of cells, materials and bioactive factors. Hydrogel-based materials for embedded bioprinting have been introduced, nevertheless it is still challenging to include all the requirements of a bioink into a single biomaterial. Key factors in designing these biomaterials are the mechanical strength to ensure shape fidelity, the ability to flow under an applied shear strain (shear-thinning) and the capacity to remodel and recover from potential mechanical induced damage (self-healing). Herein, this work reports a novel biomaterial compatible with 3D embedded bioprinting based on supramolecular host-guest interactions between β-cyclodextrin (βCD, host) and tyramine (TA, guest) conjugated to either dextran or 8arm-PEG. Mechanical strength is obtained by enzymatic crosslinking of tyramine using horseradish peroxidase (HRP) as a catalyst and hydrogen peroxide (H_2O_2) as an oxidant. Adamantane (Ada) was as well conjugated to 8arm-PEG in order to compare physical crosslinking of our βCD/TA system with βCD/Ada systems.

Mixing βCD conjugated polymers with tyramine conjugated polymers did not result in hydrogels whereas mixtures with PEG-Ada as guest led to viscous hydrogel formation. Determination of the stoichiometry confirmed 1:1 H:G molar ratio binding between both βCD/TA and βCD/Ada complexations with a strong association constant for βCD/Ada complexation and a weak association constant for βCD/TA. The HRP/TA and H_2O_2/TA ratios need to be optimized in order to sufficiently crosslink the tyramines and make stable hydrogels. In conclusion, the supramolecular host-guest interactions between βCD and tyramine proved insufficient to physically crosslink the polymers and mixing them did therefore not result in a stable hydrogels. Further research is needed to design new polymers that are compatible with embedded bioprinting and could offer the desired physically crosslinked hydrogel while preserving the option of enzymatic crosslinking of the tyramines.

Abbreviations

Abs.	Absolute
Ada	Adamantane
Ada·HCl	1-Adamantane hydrochloride
βCD	β-cyclodextrin
βCD·xH_2O	β-cyclodextrin hydrate
BP	Biphosphonate
CAD	Computer-aided design
Conc. NH_3	Ammonium hydroxide solution
DEE	Diethyl ether
Dex	Dextran
DMF	*N,N*-dimethylformamide
DS	Degree of substitution
DSC	*N,N'*-disuccinimidyl carbonate
EtOH	Ethanol
FBS	Fetal bovine serum
FRESH	Freeform reversible embedding of suspended hydrogels
FTIR	Fourier-transform infrared spectroscopy
GelMA	Gelatin methacrylate
H_2O_2	Hydrogen peroxide
HA	Hyaluronic acid
HG	Host guest
^{1}H NMR	Proton nuclear magnetic resonance
HRP	Horseradish peroxidase
HUVEC	Human umbilical vein endothelial cell
LiCl	Lithium chloride
MA	Micheal-type addition
Me	Methacrylate
MeOH	Methanol
MSC	Mesenchymal stem cell
MW	Molecular weight
NaN_3	Sodium azide
NaOH	Sodium hydroxide
NH_4Cl	Ammonium chloride
PBS	Phosphate-buffered saline
Pd/C	Palladium on active charcoal
PEG	Poly(ethylene glycol)
PEO-b-PHM	Poly(ethylene oxide)-b-PHM
pHEMA	Poly(hydroxyethyl methacrylate)
PLA	Polylactide
PNC	4-Nitrophenyl chloroformate
PPh_3	Triphenylphosphine
PS	Penicillin-streptomycin
ROESY	Rotating frame Overhause effect spectroscopy
SH	Thiol
SI	Supplementary info
TA	Tyramine
TA·HCl	Tyramine hydrochloride
TE	Tissue engineering
TEA	Triethylamine
TEM	Transmission electron microscopy
V	Volume
Wt%	Weight percentage

Table of Contents

1. Introduction

1.1. Bioprinting as up-and-coming biofabrication technique

The biofabrication of functional tissue replacements and organ models is in increasing demand for applications in tissue engineering (TE), regenerative medicine strategies and pharmaceutical screening.[1-4] Within the TE field there are various biofabrication technologies that aim to engineer 3D tissue constructs. Some of the more traditional biofabrication techniques are solvent casting or solvent leaching,[5-8] freeze drying[9-12] and gas foaming.[13-16] All these techniques offer great pore size control, which is important for the diffusion of molecules, waste products and gases within the 3D scaffold. Pore size control aids cell migration, proliferation and spreading as well.[5] However, none of them can encapsulate cells or bioactive molecules during their fabrication process or offer precise control of spatial cell placement.[8,12,16] A relatively new biofabrication technique that does enable simultaneous spatial positioning of cells, materials and bioactive factors is bioprinting.[2,17-19] Biomaterials that incorporate cells are referred as bioinks and are carefully engineered in order to offer cell-cell and cell-matrix interaction. These interactions facilitate matrix remodelling and cell migration, differentiation and maturation.[20,21] Bioprinting is a computer-assisted technology that through imaging techniques and computer-aided design (CAD) enables the design of personalized tissue or organ constructs.[22,23]

Considering the mentioned advantaged that bioprinting offers, it is a fast growing field and various bioprinting techniques have been developed. The bioprinting techniques can be classified in two main approaches, *i.e.* direct and indirect bioprinting. Direct bioprinting includes extrusion, droplet and laser assisted printing techniques and all deposit the selected cell type(s) and materials in a layer-by-layer fashion in order to create a 3D construct (Figure 1).[18,24-26] Although each of these direct bioprinting techniques have their own advantages and disadvantages, as of yet it is not possible to print materials into 3D space at any specific point with high resolution and multiple length scales.[27,28] The maximum amount of stacked layers does mostly not exceed 10 layers due to weak mechanical properties. Post-printing cell viability is inadequate due to poor vascularization and insufficient nutrient supply. When mechanical properties are adjusted to ensure shape fidelity, the encapsulated cells within the rigid bioink show poor cell activity.[17,18,29-31] Additionally, biological tissues consist of multiple cellular layers, extra cellular matrix (ECM) and biomolecules, all positioned in a tissue specific hierarchical order. This complex structure plays an important role in the tissue function and is therefore vital to replicate when constructing a 3D tissues. Since the direct printing techniques deposit the materials in a layer-by-layer fashion this complex hierarchical structure can only be constructed to a certain extent.[1,30,32]

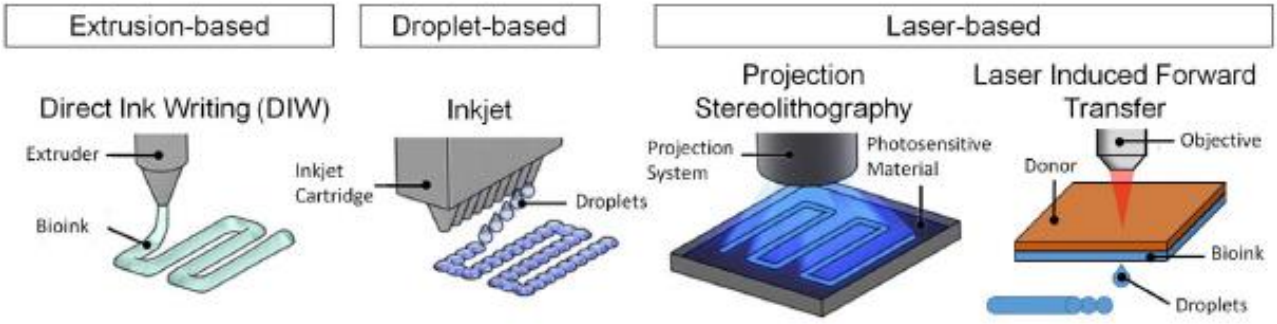

Figure 1. Direct bioprinting techniques for printing of tissues and organs in a layer-by-layer fashion, copied from Ji et. al. [33]

The other main approach is indirect bioprinting and can be subdivided into free-form and embedded bioprinting. Where free-form bioprinting uses a sacrificial negative mold that provides support, does embedded bioprinting utilize a print bath to overcome gravitational forces.[17,23,34,35] These methods are designed to enable direct patterning of structures, creation of fine channels, positioning of structures with large internal voids and offer physical support during construct maturation (Figure 2). Low viscosity materials can be processed and the complex 3D tissue structure can be replicated to a better extend. Through this additional support the used materials can be freely positioned, overcoming the conventional layer-by-layer filament extrusion.[1,17,19,36]

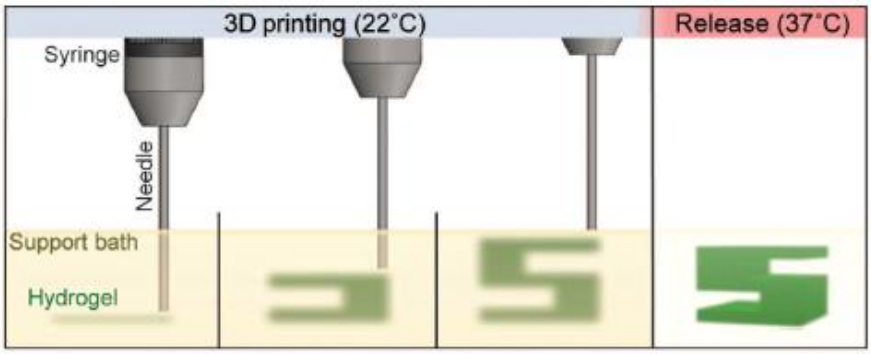

Figure 2. A schematic representation of the embedded bioprinting process presented by Hinton et al.[34] A hydrogel (green) is extruded and cross-linked in a gelatin support bath (yellow). The printed 3D construct is harvested by removing the gelatin by heating it to 37 °C.

1.2. Biomaterial requirements for bioprinting

Bioprinting materials are designed to mimic the native tissue architecture and composition, though balancing the physical and chemical properties remains challenging.[27] Generally considered ideal properties of bioinks include the ability to print constructs with adequate mechanical strength while maintaining shape fidelity at high resolution and tunable gelation time to aid extrusion.[37-39] Also, bioinks should be biocompatible, mimic native cellular environment, facilitate reproducibility and provide chemical modifications.[40-45]

Widely used biomaterials for bioinks are hydrogels, as they are easily designed to be similar to soft tissues and are compatible with most bioprinting techniques. Hydrogels are constructed by polymer networks that swell to retain large quantities of water without dissolving. They can be categorized into chemical and physical networks.[46-48] Chemically crosslinked hydrogels are comprised of polymeric chains that are interconnected by irreversible bonds and are commonly obtained via photo-initiated, redox-initiated or Michael-type addition (MA) polymerization.[49,50] Chemical crosslinking can be easily tuned to adjust mechanical properties, however as the polymers are covalently crosslinked these hydrogels are often brittle and cannot recover after induced damage.[51,52] Post-injection crosslinking of polymer solutions is undesirable, due to limited access of the injection site, slow crosslinking kinetics and potential cytotoxicity of crosslinking agents.[53] Physical hydrogel formation is driven by molecular self-assembly, such as temperature, pH, hydrogen bonds, supramolecular host-guest (HG), ionic, hydrophobic interactions and dynamic covalent bonds. Their mechanical properties are directly related to the number and strength of the interactions used.[53-56]

Polymers used in hydrogels commonly include natural polymers, such as alginate, gelatin, fibrin, dextran, collagen, gelatin methacrylate (GelMA) and hyaluronic acid (HA). Also synthetic polymers are widely used, including poly(ethylene glycol) (PEG), polylactide (PLA) and poly(hydroxyethyl methacrylate) (pHEMA).[17,18,57-59] These polymers have their own advantages and disadvantages, and when combed their specific advantages can be promoted while their disadvantages can be reduced. But even combined they rarely satisfy the mechanical requirements for bioprinting while simultaneously maintaining desired cell activities. Even fewer systems allow for molecular design of mechanical and biological properties.[60-62]

Therefore it remains vital to develop new bioprinting systems that can meet these aforementioned requirements. Key factors in accomplishing these demands are the ability to flow under an applied shear strain (shear-thinning) and the capacity to remodel and recover from potential mechanical induced damage (self-healing).[50,53,62] Shear-thinning properties eases extrusion through a nozzle or syringe, as the viscosity of the bioink decreases when shear strain is applied. Once the shear strain is removed the viscosity will increase, aiding mechanical strength of the filaments and limiting diffusion of the encapsulated components. Self-healing abilities are favourable since it allows the medium to withstand repeated damage caused by potential mechanical stress and assists nozzle movement through the viscous media. Self-healing properties facilitates as well medium deformation as response to migration and maturation of encapsulated cells.[49,53,63,64] Providing shape stability to a material with shear-thinning and self-healing abilities remains a challenge, as the previous mentioned traits are both associated with weak mechanical properties.[49,50,53,65]

1.3. State-of-the-art 3D bioprinting systems

1.3.1. Direct extrusion systems

An emerging strategy for designing novel direct bioprinting materials that feature general bioink requirements, while providing mechanical stability is based on combining reversible physical crosslinking with covalent chemical crosslinking. These systems are known as dual-crosslinking systems, in which physical crosslinking provides shear-thinning and self-healing abilities and secondary chemical crosslinking enhances the mechanical properties.

Rodell et al.[64] introduced a self-assembling hydrogel that is based on the hydrophobic HG interactions between β-cyclodextrin (βCD, host) and adamantane (Ada, guest). HA was used as polymer backbone, which was modified with either the host molecule (HA-βCD) or guest molecule (HA-Ada). The mechanical instability was addressed by a secondary crosslink based on MA which occurs through the reaction of a nucleophile, such as a thiol (SH) and an activated olefin. HA was modified by esterification with 3,3'-dithiodipropionic acid followed by reduction with dithiothreitol, resulting in HA-SH. They modified multiple Michael-receptors of HA, including methacrylate (Me), acrylate, vinyl sulfone and maleimide derivatives. From these HA-Me proved to be viable for clinical use. When the HG hydrogels were modified for MA, they retained their native mechanical properties and were observed to have similar injectable properties. MA gels alone did not have sufficient mechanics for retention, whereas HG and the dual-crosslinked hydrogels were both well retained. Rheological time sweeps showed that upon initial formation, dual-crosslinked hydrogels had moduli similar to HG hydrogels, yet the secondary crosslinking via MA resulted in a more rigid viscoelastic solid with increased shear modulus. This dual-crosslinking system is designed for percutaneous delivery and the crosslinking kinetics should be adjusted in order to meet the desired bioprinting material properties.

A bioprinting system based on HG interactions and a secondary crosslinking using photopolymerization was shown by Ouyang et al.[66]. Adamantane (guest) and βCD (host) moieties were separately coupled to HA, to create two hydrogel-precursors that formed a supramolecular assembly upon mixing. The designed bioink was not laden with cells and the filaments were positioned in a layer-by-layer fashion with an extrusion-based system. To enhance the structural integrity of the supramolecular cross-linked hydrogel, they introduced photocrosslinkable methacrylate groups onto the polymers and afterwards cells were seeded onto the 3D structures. Structures of more than 16 layers were printed and showed to be stable for over a month. The filament size ranged from 100 to 500 µm and the material proved to have shear-thinning and self-healing properties.

Liu et al.[62] reported a strategy that allows direct bioprinting of 3D cell-laden pure GelMA constructs by utilizing GelMA physical gels as bioink. At 37°C the GelMA solution was liquid and upon cooling to 21 °C or lower it became a physical hydrogel with shear-thinning and self-healing characteristics due to the coil-helix transition aided by intermolecular bonds. Further stabilization of the hydrogel was achieved through UV photocrosslinking of the present methacryloyl groups. Cell-laden constructs up to 10 layers were printed and could maintain the predesign structures without deformation allowing subsequent photocrosslinking. This printing process did not rely on fast chemical crosslinking upon extrusion. This enabled positioning of relatively low concentrations, 3% as compared to the otherwise applied 7% solutions. The lower concentration constructs featured higher porosity and lower stiffness, resulting in better cell activities. The resolution of the bioprinted constructs was limited to ~500 µm due to the used nozzle size, but was improved by using a smaller sized nozzle.

Another dual crosslinking system was developed by Zhang et al.[67], where they blended GelMA loaded with human umbilical vein endothelial cells (HUVECs) with alginate. When divalent calcium ions were added the alginate underwent rapid ionic crosslinking. Afterwards a secondary photocrosslinking of the GelMA components followed in order to further stabilize the structure. They obtained a 30-layer bioprinted scaffold within 10 minutes with microfibers of approximately 100-150 µm in diameter. The fiber diameter was limited due to the diffusion barrier of the crosslinking agent $CaCl_2$. Also $CaCl_2$ may be toxic to certain endothelial cell types that are more fragile than HUVECs. The encapsulated HUVECs were able to migrate and at day 16 they formed lumen-like structures. These lumen-like structures were not sufficiently hollow and were unable to perfuse the bioprinted scaffolds.

1.3.2. Embedded bioprinting systems

The increased mechanical stability provided by secondary crosslinking in the direct bioprinting methods proved to be as of yet insufficient in printing large scale cell laden constructs while maintaining the desired cell activity. Indirect bioprinting methods could potentially meet the set requirements, particularly embedded bioprinting has shown great promise and has gained much interest over the last decade.[27,34,68]

Hinton et al.[34] demonstrated a 3D bioprinting technique termed freeform reversible embedding of suspended hydrogels (FRESH), where alginate hydrogels were printed within a second gelatin hydrogel support bath that maintains the designed structure during printing while increasing shape fidelity (Figure 2). The support bath is composed of gelatin that behaves solid like at low shear stresses, but under higher shear stresses it flows as a viscous liquid. This behaviour permits nozzle movement through the bath with little mechanical resistance while the bath is held in place after depositioning. After printing the construct was released by heating to 37 °C in order to remove the gelatin in a non-destructive manner. They successfully mimicked the external structures of human femur with a length of ~35 mm, embryonic chick heart of about ~25 mm and complex external surface structures based on an MRI image of the human brain. It was demonstrated that FRESH can 3D print mechanically robust

parts with biomimetic structure, high repeatability and embedded cells, with a resolution of ~200 µm. FRESH is not limited to standard layer-by-layer printing and can deposit materials with high shape fidelity as long as the extruder does not pass through previously deposited material.

Highley et al.[69] developed a hydrogel-based approach that permits the printing of shear-thinning hydrogel inks directly into a self-healing hydrogel support bath. Both the ink and bath are based on supramolecular assembly through HG interactions. The hydrogels used were modified HA with either adamantane (HA-Ada) or βCD (HA-βCD). The mechanical properties could be altered through modification of the degree of substitution of the HA backbone with the host or guest molecules, through adjusting of the polymer concentration and through the ratio of host-to-guest moieties. These HA polymers could be further modified by introducing methacrylates, enabling secondary crosslinking by UV photopolymerization without affecting the HG hydrogel properties. Linear filaments were printed with a diameter up to 35 µm and the printing process was non-toxic to cells (>90%) with minimal loss in viability over several days in culture.

Shi et al.[70] expanded the range of reversible crosslinking strategies by introducing a shear-thinning and self-healing system based on reversible metal-ion-chelating ligand dynamic coordination bonds between bisphosphonate (BP) groups on a HA backbone and free Ca^{2+} ions. Secondary chemical crosslinking using UV light was applied in the final stage ensuring mechanical stability of the construct. The HA-BP·Ca^{2+} hydrogel was found to be pH responsive, at neutral pH the hydrogel was stable for one day though it dissolved within 2 hours in acidic environment (pH 5.0). When the printed structure was efficiently photo-crosslinked the support gel could be removed by incubation in slightly acidic medium. They demonstrated high cell survival of >88% in a photo-crosslinked HA-BP·Ca^{2+} hydrogel immediately after 3D printing and a cell survival of >80% during a 6 days culture.

2. Proposed supramolecular hydrogel for embedded bioprinting

Assessing these state-of-the-art systems it has become clear that 3D embedded bioprinting hydrogels based on supramolecular HG assembly and secondary chemical crosslinks allows printing of multiple materials, complex free-standing and hollow structures at high resolution and desired cell viability. The state-of-the art systems mostly use photopolymerization or crosslinking agents such as calcium ions for secondary crosslinking. However, UV radiation is correlated with suboptimal cell survival and potential genetic damage, and many crosslinking agents are correlated with cytotoxic properties.[67,71] Further development of supramolecular materials and exploring other secondary crosslinking mechanisms could increase the complexity and functionality of the designed 3D embedded bioprinting materials.

Therefore we investigated a supramolecular HG hydrogel system based on hydrophobic interactions between βCD (host) and tyramine (TA, guest) molecules and an enzymatic chemical crosslinking of TA (Figure 3). The host and guest molecules were separately coupled to either dextran or PEG to create precursor polymers that could self-assemble into a self-healing and shear-thinning hydrogel. To enhance the mechanical strength of the supramolecular hydrogel TA was oxidative crosslinked under mild conditions by horseradish peroxidase (HRP) catalyzed crosslinking. PEG was also modified with adamantane (guest) in order to compare our supramolecular βCD/TA system with the more extensively reported βCD/Ada system. Adamantane is included and held strongly in the cavity of βCD, though it is not capable of a secondary crosslinking by HRP and hydrogen peroxide (H_2O_2) due to the lack of a phenol or aniline group.[48,72-74]

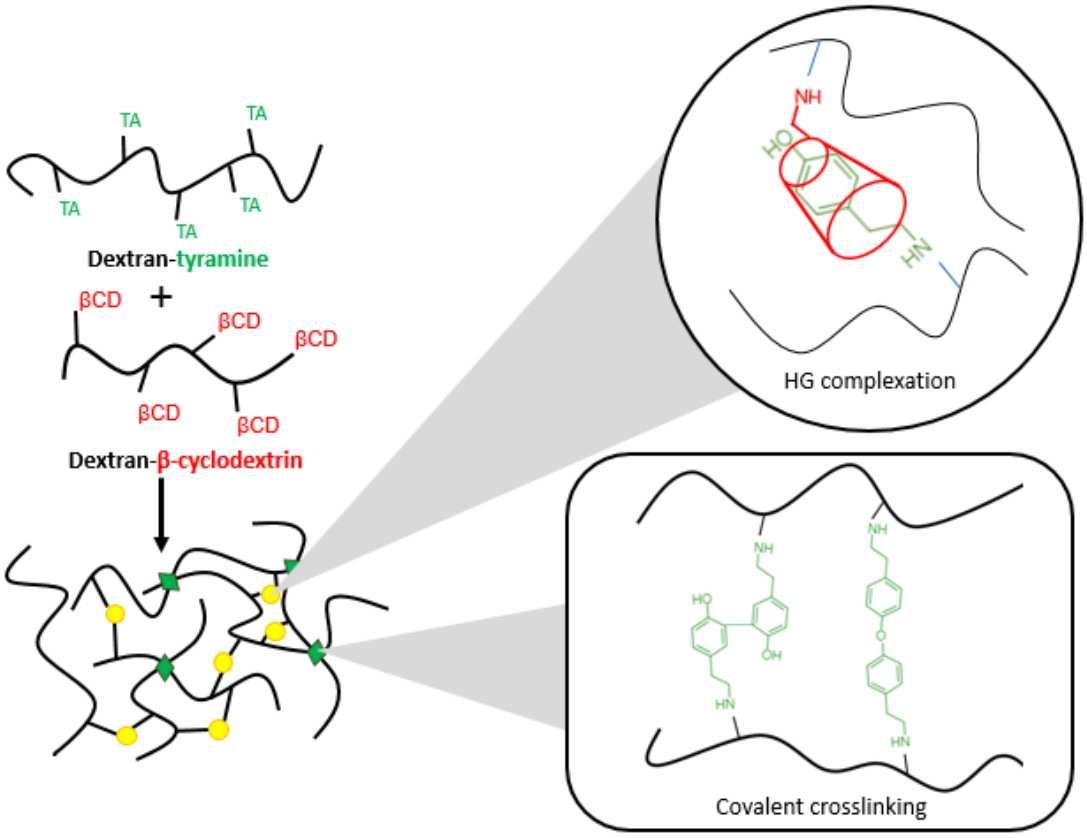

Figure 3. Supramolecular hydrogel system based on the polymers βCD/TA complexation and secondary covalent crosslinking of TA. HG complexation of βCD and TA are providing shear-thinning and self-healing abilities and the secondary chemical crosslinking of the phenol groups on TA yields in a mechanical stable gel by the covalent C-C and C-O bonds.

2.1. Physical crosslinking by HG complexation

2.1.1. β-Cyclodextrin as host

Supramolecular interactions are based on the direct association of molecular components which results in noncovalent dynamic networks. HG complexation based on hydrophobic forces has been widely used for the preparation of supramolecular hydrogels with self-healing and shear-thinning properties. Commonly used host molecules are cyclodextrins, which are cyclic oligosaccharides consisting of six to eight α-(1,4)-glycosidic linked D-glucose units, α-, β-, and γ-cyclodextrins, respectively (Figure 4a).[53,75,76] The glucose unit has a chair conformation (Figure 4b).[77] Their 3D structure can be represented as a truncated cone with the primary hydroxyl groups positioned at the narrower rim, the secondary hydroxyl groups at the wider rim and with an inner cavity size of 4.7-5.3 Å, 6.0-6.5 Å and 7.5-8.3 Å for respectively α-, β-, and γ-CD.[78] The hydrophilic outer surface is composed of the protons H-1', H-2', H-4' and H-6', while the hydrophobic cavity is lined with H-3' and H-5' protons (Figure 4c).[79] Hydrophobic and van der Waals forces in the cavity between the host and guest facilitates the driving forces for HG interactions. The hydroxyl groups on the outer surface promotes solubility in aqueous environments induced by hydrogen bonding.[50,72]

βCDs are the most regular used cyclodextrins for pharmaceutical, drug delivery and nanotechnology applications. Their cavity size can interact with many branched alkyl chains and aromatic groups and is therefore compatible with a wide variety of organic, inorganic, biological and pharmaceutical guest molecules. Also the βCDs are lowest in price.[76,80]

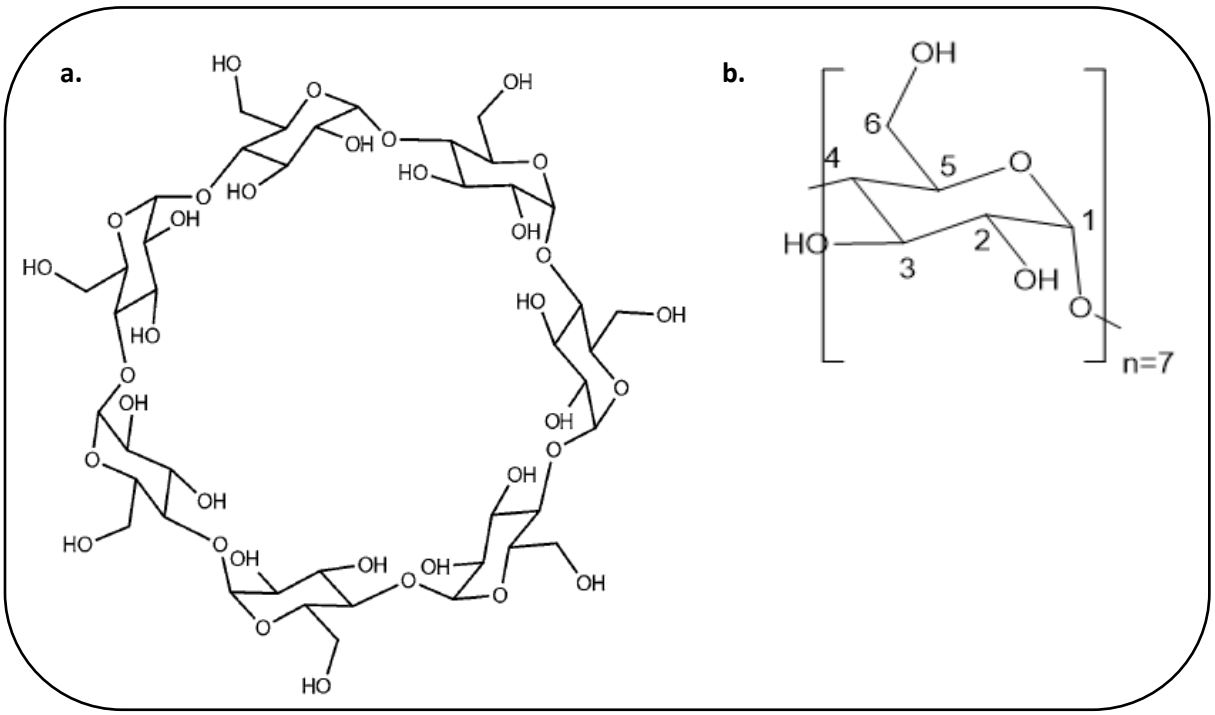

Figure 4. General structure of (a) the host βCD, (b) the position of its protons on the D-glucose unit.

2.1.2. Tyramine as guest

One known guest molecule of βCD is tyramine, a naturally occurring neurotransmitter derived from the amino acid tyrosine.[80,81] As shown in Figure 5 tyramine is a hydrophobic molecule that consists of a phenolic aromatic ring with a flexible aminoethyl side group. In its gauche conformation tyramine has a molecular size of 6.3×4.3×4.2 Å which makes it accessible for entering the βCD cavity resulting in HG complexation (Figure 5).[82]

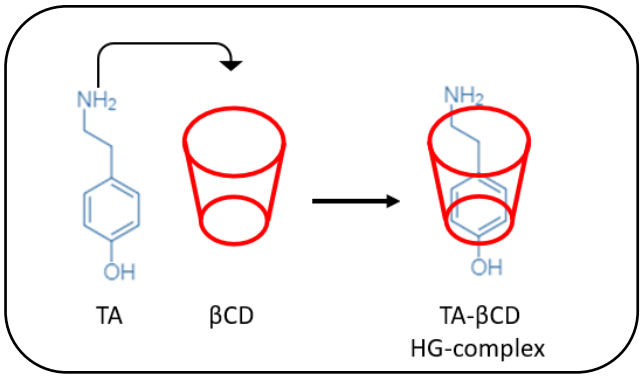

Figure 5. The schematic assemble of tyramine (TA, guest) and βCD (host) into a HG complexation.

In general the strength in which the HG complexes are formed is expressed by the association (binding) constant K_a. Size matching between the host and guest and environmental conditions, such as temperature, pH and light, can influence the K_a. The association constant increases with the degree of space filled of the βCD cavity and is related to the increase of hydrophobic interactions and non-polar van der Waals interactions.[83]

According to Roy et al.[80] tyramine is a suitable guest molecule for βCD. With its hydrophobic phenolic aromatic ring and molecule diameter of 4.3 Å tyramine should adequately fit into the βCD cavity (6.0-6.5 Å) (Figure 6a and c). Adamantane is a strain free highly symmetrical structure with a diameter of 6.4 Å and is almost a perfect fit for the βCD cavity (6.0-6.5 Å). Inclusion complexes of βCD/Ada·HCl are formed in a 1:1 ratio (Figure 5 and Figure 6b and c).[74,84] Adamantane (or water soluble Ada·HCl) have a reported K_a value of 10^4-10^5 M^{-1} where bound adamantane guest units have a reported K_a value of 1500 M^{-1}.[72-74,85]

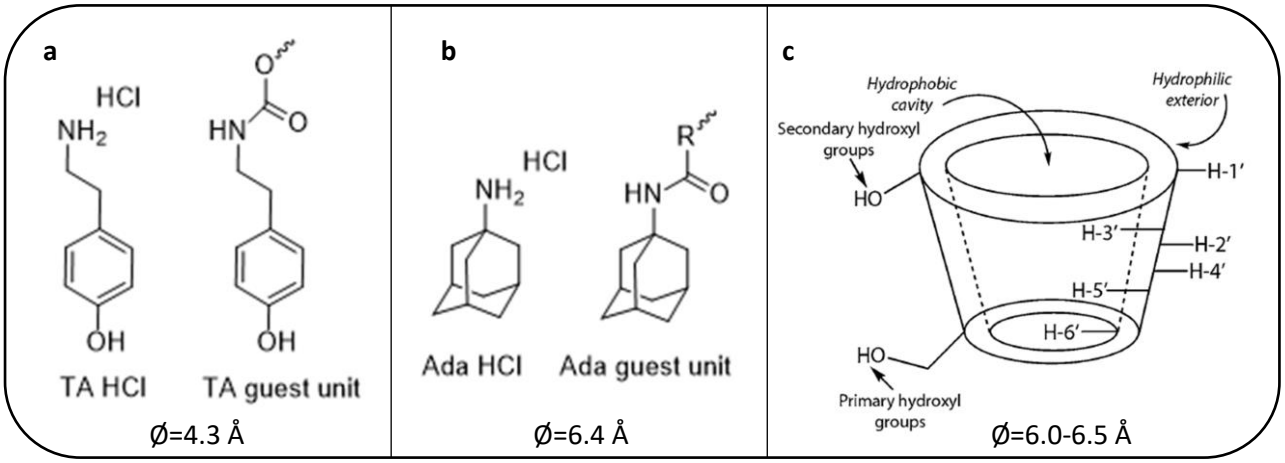

Figure 6. Chemical structure and diameter of (a) tyramine hydrochloride and tyramine bonded to a polymer and (b) adamantane hydrochloride and adamantane bonded to a polymer. (c) Truncated cone shape model of βCD indicating the hydrophilic outer surface, hydrophobic inner cavity, cavity diameter and the position of the H1'-H6' protons.[79]

2.2. Secondary enzymatic crosslinking of tyramine

To provide the hydrogel with sufficient mechanical strength a secondary chemical crosslinking will be performed. Chemically crosslinked hydrogels can be obtained by the use of additives, such as photo-initiators, crosslinking agents, or organic solvents. A major drawback of these additives is the possible chance to be cytotoxic, leading to non-biocompatible hydrogels. One method to avoid harsh chemicals or photoinitiated-crosslinking is based on the horseradish peroxidase (HRP)-catalysed crosslinking reaction under mild H_2O_2 conditions.[86-88] Here the phenol group of tyramine is polymerized by the single-chain β-type hemoprotein of HRP via the oxidative decomposition of H_2O_2. The resulting covalently crosslinked polyphenol structures are bound at the aromatic ring by C-C and C-O coupling of phenols (Figure 3).[48,89] This HRP/H_2O_2 crosslinking takes place under physiological conditions and does not require harsh chemicals. Induced cell damage by the oxidative nature of H_2O_2 is neglectable due to its rapidly conversion by HRP.[58,71]

Within the DBE research group many papers has been published that prove the fast formation of biocompatible dextran hydrogels based on dextran-tyramine (Dex-TA) enzymatic crosslinking, with high cell survival and good mechanical properties.[48,58,71,90] Dex-TA gels, 10 weight percentage (wt%), had an storage modulus of 30 kPa making them compatible for musculoskeletal tissues, such as cartilage (20-30 kPa) and bone (25-40 kPa). [91,92] To make the gel compatible with softer tissue, such as nerve or brain (0.1-1 kPa) and fat (3 kPa), the mechanical properties could be easily altered by modifying the wt% of the gel and the substitution degree of dextran.[48,58]

2.3. Research aims and workflow

Our research aims can be summarized in five main objectives (Figure 7):

1. ***Synthesis and characterization of* dextran or PEG based polymer precursors**

First the polymeric precursors were functionalized, and afterwards their composition and degree of substitution (DS) were characterized with proton nuclear magnetic resonance (^{1}H NMR) spectroscopy and Fourier-transform infrared spectroscopy (FTIR). Dextran was functionalized with either βCD or tyramine (Dex-βCD; Dex-TA) with various DS. Prior experiments with 40 kDa dextrans (10 wt%) functionalized with either βCD or tyramine have been performed to test the supramolecular hydrogel formation. Upon mixing these 40 kDa functionalized polymers a large phase separation was observed and no hydrogel was formed. Therefore in this study we utilized larger dextran polymers of 150 kDa, 250 kDa and 500 kDa. These high MW dextrans can absorb more water in their hydrophilic groups and can make more crosslinks between the polymer chains as compared to the lower 40 kDa dextran.[93,94] 8arm-PEG of 40kDa was functionalized with either βCD, tyramine or adamantane (PEG-βCD; PEG-TA; PEG-Ada). PEG was functionalized with adamantane in order to compare our supramolecular βCD/TA system with the more extensively explored βCD/Ada system.

2. ***Testing supramolecular hydrogel formation***

By mixing the prepared polymers in vials their gelation ability was visually observed via the vial tilting method. Polymers of various molecular weights (MW) and DS were mixed in different weight percentages and ratios. The enzymatic crosslinking of tyramine was investigated as well.

3. ***Determination stoichiometry of the HG complexations***

The stoichiometry of βCD/TA complexation was determined by UV-vis absorption Job plot experiments and via the linear Benesi-Hildebrand regression method the association constant K_a was determined. As βCD and adamantane are both spectroscopically inert their stoichiometry could not be investigated by UV-vis experiments.

Therefore the assembly ratio and K_a of βCD/TA and βCD/Ada complexes were also determined via a ^{1}H NMR titration experiments and calculated with computer-based non-linear regression method provided by Pall Thordarson.[95]

4. Testing printability supramolecular hydrogels

Printability of the supramolecular hydrogels were investigated in two different test setups. For the first test an ink consisting of PEG-βCD/PEG-Ada was prepared and printed in a pre-crosslinked Dex-TA support bath. In the second test gelatin soaked with 0.03% H_2O_2 acted as bioink and was dispositioned in a support bath consisting of Dex-βCD/Dex-TA hydrogel.

5. Testing cytotoxicity of the supramolecular hydrogels

Finally the cytotoxicity of PEG-βCD/PEG-TA and Dex-βCD/Dex-TA hydrogels were tested by a routine live/dead assay using Jurkat cells.

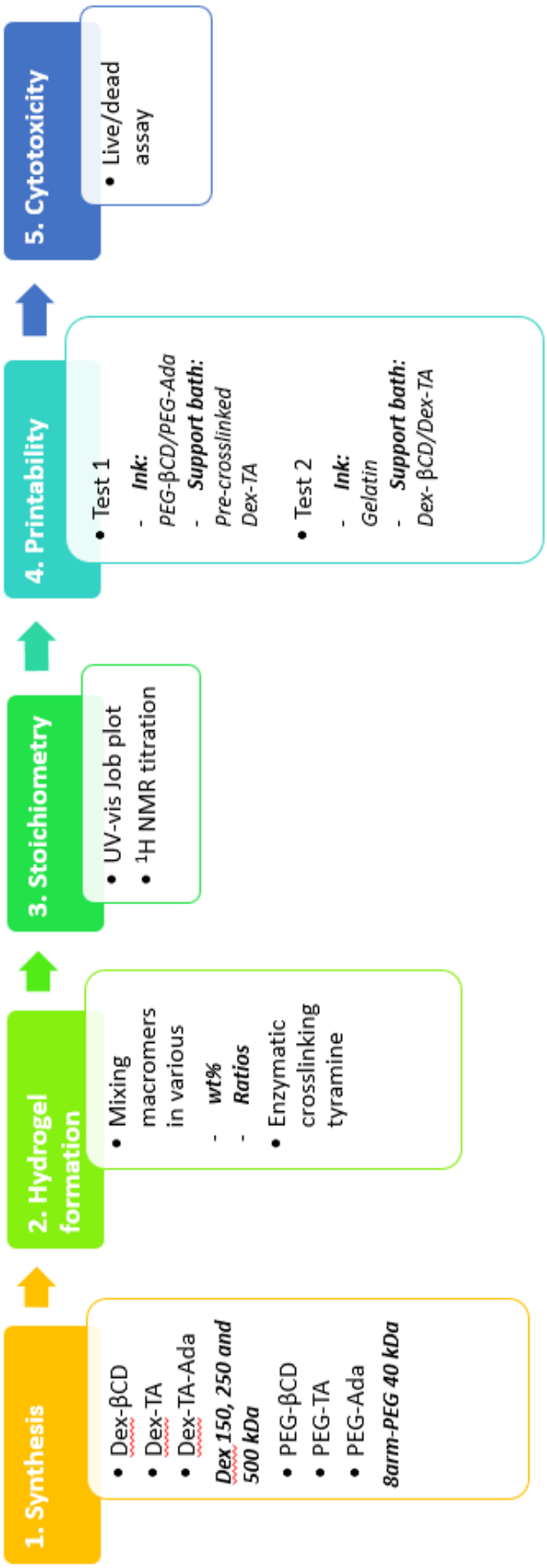

Figure 7. Schematic workflow of the five main objectives towards our proposed supramolecular hydrogel.

3. Materials and methods

3.1. Materials

Dextran MW ca. 150 kDa (Dex_{150}, powder), dextran MW ca. 250 kDa (Dex_{250}, powder), dextran MW ca. 500 kDa (Dex_{500}, powder), imidazole (99%), dichloromethane (anhydrous DCM, 99.7+%), p-toluenesulfonyl chloride (98%), β-cyclodextrin hydrate (βCD·xH_2O) , β-cyclodextrin (βCD), sodium hydroxide (NaOH, 98% flakes), ammonium chloride (NH_4Cl, 98%), absolute methanol (abs. MeOH, 99.8+%) and ethylene glycol (99%) were purchased from Alfa Aesar and used as received. Lithium chloride (LiCl, 99.0%), *N,N*-dimethylformamide (anhydrous DMF, ≥99.8%), pyridine (anhydrous, 99.8%), sodium azide (NaN_3, ≥99.5%), palladium on activated charcoal (Pd/C, 10% Pd basis), activated charcoal (100 particle size mesh), triphenylphosphine (PPh_3, 99%), ammonium hydroxide solution (conc. NH_3, 28.0-30.0% NH_3 basis), tyramine (TA, 99%), 1-adamantanamine hydrochloride (Ada·HCl), *N,N*'-disuccinimidyl carbonate (DSC, ≥95%), triethylamine (TEA, ≥99.5%), D_2O (99.9 atom % D), DMSO-d_6 (99.9% atom % D), $CDCl_3$ 99.8 atom % D), peroxidase from horseradish (HRP, 263 u/mg solid), Xanthan gum from Xanthomonas campestris, gelatin from porcine skin (powder, gel strength ~300 g Bloom, Type A) and trypan Blue (0.04%) were obtained from Sigma Aldrich and used as received. 4-Nitrophenyl chloroformate (PNC, 96%) was obtained from Sigma Aldrich and sublimated before use. Ethanol (EtOH) and dry acetonitrile (≥99.5%) were purchased from Merck, Germany. Diethyl ether (DEE, AnalaR NORMAPUR® analytical reagent), ethyl acetate (AnalaR NORMAPUR® analytical reagent), n-heptane (AnalaR NORMAPUR® analytical reagent), acetone (AnalaR NORMAPUR® analytical reagent), toluene (AnalaR NORMAPUR® analytical reagent), hydrogen peroxide (H_2O_2, 30%) and silica gel 60 (for column chromatography, 0.040-0.063 mm, 230-400 mesh particle size) were purchased from VWR. Spectra/Por 6 Standard RC pre-wetted dialysis tubing (MWCO 1.0 kDa and MWCO 3.5 kDa) were obtained from Spectrum™ Labs (now called Repligen). 8-Arm poly(ethylene glycol) (PEG-OH, tripentaerythritol core) MW 40 kDa was obtained from JenKem Technology USA. Tyramine hydrochloride (TA·HCl, 99%) was purchased from Acros Organics, Belgium. 1 M HCl solution was prepared by dilution of 83.3 mL 12.0 M HCl solution to 1.0 L water and 1.0 M NaOH solution by dissolving 40.0 g NaOH in 1.0 L water. MilliQ water was used in all experiments. Green food colour (NaCl, tartrazine, E102 and Brilliant Blue FCF E133) was purchased from TRS Foods, UK. Jurkat Clone E6-1 (ATCC® TIB-152™) was obtained from ATCC and stored at -80 °C (Box 9, 8, spot 7, p8-p9, 3-5-2017 LK 2M). RPMI-1640 medium (1x, [+] L-Glutamine), penicillin-streptomycin (PS, 10.000 U/mL) and fetal bovine serum (FBS) were obtained from Gibco. Phosphate-buffered saline (PBS) was purchased from Lonza. The culture medium for Jurkat cells contained RPMI-1640 with 10% FBS and 1% PS. Live/dead viability/cytotoxicity Kit was obtained from Invitrogen, containing ethidium homodimer (200 µl, 2.0 mM) and calcein AM (80 µl, 4.0 mM).

3.2. Techniques

The synthesized products were analyzed by ^{1}H NMR and FTIR. ^{1}H NMR spectra were recorded on a Brucker Avance III 400 MHz instrument in DMSO-d_6, D_2O or $CDCl_3$. ^{1}H proton shifts were based on solvent residual signals.[96] FTIR spectra were measured with a Brucker ALPHA FTIR spectrometer on lyophilized samples. Rheological measurements were carried out with a MCR 301 rheometer (Anton Paar). The viscosity η [Pa·s], storage moduli G' and loss moduli G'' were observed as function of shear rate γ from 0.1-10 000 s^{-1} under constant temperature (2, 5, 10, 15, 20, 25, 30, 35 and 37^{o}C) using a standard double gap measuring system DG26.7 (Anton Paar) filled with 3 mL sample. UV-vis absorption spectra were recorded on a Cary 300 spectrophotometer from Agilent Technologies. 3D printing was performed using a Cellink+ 3D printer, where the extrusion of the ink was performed at RT, with a velocity of 10 mm/s, a nozzle diameter of 22G (0.64 mm) and a pressure of 163 kPa and 181 kPa for respectively test 1 and 2. The G-code was written using Repetier-Host V2.1.3 software. Cells for the cytotoxicity assay were counted on a Bürker-Türk counting chamber and their viability was recorded on an EVOS fluorescence microscope with a RFP/GFP filter. Cell suspensions were centrifuged at 300 rcf for 5 minutes and incubation was performed at 37 ^{o}C with 5% CO_2.

3.3. Polymer synthesis

Dextran-p-nitrophenyl chloroformate **1.** Dextran (5.0 g, 30.83 mmol r.u.) and LiCl (4 g, 94.35 mmol) were dried under vacuum for 2 hours at 95 °C. Afterwards the flask was filled with nitrogen and 200 mL of anhydrous DMF was added through a double tipped needle, heated to 95°C and stirred until al was dissolved. The clear dextran solution was cooled down on an ice bath and kept on 0-0.5 °C while pyridine was added under nitrogen atmosphere. Subsequently small portions of PNC (2.0 g, 9.92 mmol) were added while the temperature was prevented from exceeding 2 °C. The solution was stirred for 60 minutes. Separately under nitrogen condition, 2 g of sublimated PNC was dissolved in 10 mL anhydrous DMF and 2 mL pyridine resulting in a yellow/orange suspension. The solvent containing PNC was added to the reaction mixture and stirred for 1 hour. Afterwards the reaction was precipitated in 2L ice cooled EtOH and kept in the fridge for 60 minutes. Afterwards the solution was filtered over POR4 glass filter and washed 5 times with EtOH and 5 times with DEE. The product residue was collected, grinded with a glass spatula and dried overnight under vacuum. The product was collected and the degree of substitution (DS) was defined as the number of conjugated groups per 100 anhydroglucose units in dextran. Dex-PNC conjugates were expected to have a DS of 20%. DS ^{1}H NMR (400 MHz, DSMO-d_6) δ: 2.5-4.0 (m, –CH_2–CH_2–), 4.2-5.8 (m, 4H, glucosidic protons dextran), 7.4-7.7 (m, 2H, aromatic protons PNC), 8.2-8.5 (m, 2H, aromatic protons PNC). ATR-FTIR: 3341 (O-H, stretch), 2923 (C-H, stretch), 1765 (C=O carbonate, stretch), 1650 (C=C, stretch), 1346 (C-H, bend), 1524 (N-O, stretch) 1217 (C-O, stretch) and 1010 (O-H, bend) cm^{-1}.

Dex_{150}-PNC DS 3% **1a.** Dextran 150 kDa (5.0 g, 30.83 mmol r.u.). Yielded in 4.98 g (32.5 µmol, 98%), DS 3%. ^{1}H NMR (400 MHz, DMSO-d_6) δ: 2.5-4.0 (m, –CH_2–CH_2–), 4.2-5.8 (m, 4H, glucosidic protons dextran), 7.5-7.7 (m, aromatic protons PNC), 8.2-8.6 (m, 2H, aromatic protons).

Dex_{250}-PNC DS 18% **1b.** Dextran 250 kDa (5.0 g, 30.83 mmol r.u.). Yielded in 5.54 g (18.7 µmol, 94%), DS 18%. ^{1}H NMR (400 MHz, DSMO-d_6) δ: 2.5-4.0 (m, –CH_2–CH_2–), 4.2-5.8 (m, 4H, glucosidic protons dextran), 7.5-7.6 (m, 2H, aromatic protons PNC), 8.2-8.4 (m, 2H, aromatic protons PNC).

Dex_{250}-PNC DS 9% **1c.** Dextran 250 kDa (1.0 g, 6.17 mmol r.u.) was dissolved in water and precipitated in 100 mL EtOH. The solution was centrifuged at 5000 rpm for 5 minutes and the EtOH was removed. Next, the residue was washed twice with 10 mL EtOH, centrifuged at 5000 rpm for 5 minutes and EtOH was drained. The residue was dissolved in 5 mL water and dialysed

for 3 days against water in a 1000 kDa MWCO dialysis membrane. The product was collected by lyophilization and the purity of Dextran 250 kDa was established by comparing its ^{1}H NMR spectra to unpurified dextran. Subsequently, the protocol was followed as described above. Purified dextran 250 kDa (0.84 g, 3.36 µmol), lithium chloride (0.67 g, 15.8 mmol), pyridine (0.34 mL, 4.30 mmol) and PNC (0.34 g, 1.69 mmol). Dissolved in 50 mL anhydrous DMF, stirred for 2 hours and precipitated in 250 mL cold ethanol. Yielded in 0.79 gram (2.89 µmol, 86.1%), DS 9%. ^{1}H NMR (400 MHz, DSMO-d_6) δ: 2.5-4.0 (m, –CH_2–CH_2–), 4.2-5.8 (m, 4H, glucosidic protons dextran), 7.5-7.7 (m, 2H, aromatic protons PNC), 8.3-8.4 (m, 2H, aromatic protons PNC).

Dex_{500}-PNC DS 12% 1d. Dextran 500 kDa (5.0 g, 30.83 mmol r.u.). Yielded in 5.33 g (9.49 µmol, 94.9%), DS 12%. ^{1}H NMR (400 MHz, DSMO-d_6) δ: 2.5-4.0 (m, –CH_2–CH_2–), 4.1-6.0 (m, 4H, glucosidic protons dextran), 7.4-7.6 (m, 2H, aromatic protons PNC), 8.2-8.4 (m, 2H, aromatic protons PNC).

1-(p-Toluenesulfonyl)-imidazole[97] 2. To a solution of imidazole (65 g, 0.95 mol) in 250 mL dry DCM cooled at 0 °C, a solution of p-toluenesulfonyl chloride (80 g, 0.42 mol) in 250 mL dry DCM was added dropwise over 1.5 hours. Subsequently the mixture was warmed up to room temperature (RT) and stirred vigorously for 3 hours. The reaction mixture was filtered through a silica pad (~100 g) and washed with 500 mL of 1:1 ethyl acetate-n-heptane. The filtrate was concentrated under vacuum for 1.5 hours and afterwards the residue was added to 50 mL ethyl acetate and finally to 500 mL n-heptane. The resulting suspension was filtered over a POR3 glass filter and dried overnight under vacuum resulting in white crystals with an yield of 84.3 gram (0.38 mol, 90.3%). ^{1}H NMR (400 MHz, $CDCl_3$) δ: 2.44 (s, 3H), 7.08 (s, 1H), 7.29 (s, 1H), 7.36 (d, 2H), 7.83 (d, 2H), 8.02 (s, 1H). ATR-FTIR: 3160-3125 (N-H, stretch), 3101-2974 (C-H, stretch), 1593 (N-H, bend), 1463 (C=C, stretch), 1377 (S=O, sulfonyl, stretch) and 1047 (S=O, sulfoxide, stretch) cm^{-1}.

6^A-O-Toluenesulfonyl-β-cyclodextrin [97] 3. βCD hydrate (βCD·xH_2O, 66.7 g, 58.7 mmol) was dissolved in 1500 mL water by vigorously stirring at 60 °C. Stirring was continued while the solution was cooled down to RT and to the resulting milky white suspension finely powdered **2** (52.2 g, 234.7 mmol) was added in one portion. After stirring for 2 hours, NaOH (30 g, 0.75 mol) dissolved in 84 mL water was added dropwise over 20 minutes. Unreacted **2** was removed after 10 minutes by filtration through a POR4 glass filter and the remaining solution was quenched by the addition and subsequently swirling of NH_4Cl (80.3 g, 1.50 mol). Shortly after NH_4Cl was completely dissolved precipitation started of **3** and the resulting suspension was reduced in volume by blowing an airstream over its surface overnight. Afterwards the volume was reduced by approximately 1/3 and the remaining suspension was filtered through a POR4 glass filter and the residue was washed with two 165 mL portions of ice water and one 300 mL portion of acetone resulting in a white sticky paste. This paste was transferred into a petri dish and dried overnight under vacuum. The dried product was crushed with a pestle and mortar resulting in a fine white powder with a 36% #1 yield (27.6 g, 21.4 mmol). ^{1}H NMR (400 MHz, DMSO-d_6) δ: 2.49 (overlap with DMSO-d_6, s, 3H) 3.11- 3.83 (m. overlap with HDO), 4.11-4.23 (m, 1H), 4.27-4.41 (m, 2H), 4.41-4.48 (m, 2H), 4.52 (br s, 3H), 4.76 (br s, 2H), 4.83 (br s, 5H), 5.58-5.92 (m, 14H), 7.43 (d, 2H), 7.75 (d, 2H). ATR-FTIR: 3310 (O-H, stretch), 2923 (C-H_2, stretch), 1362 (S=O, sulfonyl, stretch), 1153 (C-C, stretch) and 1047 (S=O, sulfoxide, stretch), 1024 (O-H, bend) cm^{-1}.

6-monodeoxy-6-monoazide-β-cyclodextrin[98,99] 4. Product **3** (28.0 g, 21.7 mmol) was dissolved in 137 mL abs. DMF and NaN_3 (1.69 g, 26.0 mmol) was added. The reaction mixture was heated up to 105-110 ^oC, and stirred for 1 h at this temperature. Afterwards the almost clear solution was cooled to RT and treated with 380 mL acetone to precipitate the product. The precipitate was filtered over a POR5

glass filter and redissolved in 40 mL water at 80 °C. Subsequently, the solution was cooled to RT and the product was recrystallized by addition of 400 mL acetone. The suspension was stored in the fridge for 1 hour to promote precipitation, filtered over POR4 glass filter and dried overnight under vacuum yielding the product in 24.9 g white crystals (21.5 mmol, 99.1%). ^{1}H NMR (400 MHz, DMSO-d_6) δ: 3.21-3.45 (m, overlap with HDO), 3.48-3.81 (m, 28H), 4.41-4.58 (m, 6H), 4.82 (br s, 6H), 4.87 (shoulder, 1H), 5.61-5.85 (m, 14H). ATR-FTIR: 3304 (O-H), 2923 (C-H_2), 2101 (N≡N, stretch), 1228 (C-N), 1146 (C-C) and 1024 (O-H, bend) cm^{-1}.

6-monodeoxy-6-monoamino-β-cyclodextrin, reduction by palladium charcoal[98] **5a.** Product **4** (2.5 g, 2.16 mmol) was suspended in 23 mL abs. MeOH under nitrogen atmosphere and cooled to -20 °C. Pd/C (0.25 g) was suspended in 2 mL water and added, and the bottle was washed-in with another 2 mL water. The reaction mixture was heated to RT and hydrazine hydrate (0.55 g, 17.2 mmol) was added. After stirring for 20 minutes at reflux temperature (65 °C), the mixture was cooled to 50 °C, poured on a paper filter and washed twice with 10 mL warm water (50 °C). Afterwards the solvents were evaporated and the crude product was redissolved in 6.5 mL water. pH was adjusted to ∼2.5 by the addition of 1M HCl and the solution was clarified by active charcoal for 30 minutes. The suspension was filtered through a paper filter and washed twice with 1.5 mL water. Next, 40 mL acetone was added and the precipitated product was filtered over a POR5 glass filter and dried overnight under vacuum. The product was collected as a fine white crystal with a yield of 12.8% (0.29 g, 0.25 mmol). ^{1}H NMR (D_2O, 400 MHz) δ: 2.84 (s, 0H), 2.99 (s, 0H), 3.24 (dd, 1H), 3.40-3.72 (m), 3.72-4.02 (m), 5.00-5.19 (m, 7H).

6-monodeoxy-6-monoamino-β-cyclodextrin, reduction by triphenylphosphine[98,100,101] **5b.** To a solution of product **4** (20 g, 17.2 mmol) in 350 mL DMF was triphenylphosphine (PPh_3, 10 g, 38.1 mmol) added. When dissolved, 100 mL of conc. NH_3 was added and stirred at RT for 4 hours. Afterwards 2 L acetone was added to precipitate product **5b** and the suspension was stored for 1 hour in the fridge to promote precipitation. Subsequently, the product was filtered over a POR4 glass filter and dried overnight under vacuum. The product was collected as a white brittle solid, was crushed with a glass rod in a petri dish and redissolved in 100 mL water which was heated up to 60 °C. The solution was cooled to RT, 1 L acetone was added to recrystallize the product and the resulting suspension was filtered over a POR4 glass filter and dried overnight under vacuum resulting in fine white crystals with a yield of 82.9% (16.2 g, 14.3 mmol). ^{1}H NMR (400 MHz, D_2O) δ: 2.85 (dd, 1H, H-6'), 3.09 (dd, 1H, H-6'), 3.45 (t, 1H, H-4'), 3.49-3.74 (m), 3.75-4.11 (m), 4.99-5.16 (m, 7H, H-1'). ATR-FTIR: 3350 (N-H, stretch), 3333 (O-H, stretch), 2925 (C-H_2, stretch), 1654 (N-H, bend), 1226 (C-N), 1152 (C-C, stretch) and 1026 (O-H, bend) cm^{-1}.

Dextran- β cyclodextrin[48] **6.** Product **1b** was dissolved in anhydrous DMF under nitrogen atmosphere. Solution time variated from 1 to 2 hours, depending on the used dextran (250 kDa or 500 kDa). βCD was added to the solution and stirred for 1 hour. Afterwards the reaction was precipitated in cooled EtOH and kept in the fridge for 1 hour to promote product sedimentation. Subsequently, the mixture was filtered over a POR4 glass filter and washed 5 times with EtOH and 5 times with DEE. Remaining solvent was removed in vacuum overnight and the resulting yellow solid was redissolved in minimal amounts of water of which the pH was adjusted to 11-12 by the addition of 1M NaOH solution to promote dissolution. When dissolved, the pH was neutralized with 1M HCl solution, transferred into a 3500 Da MWCO dialysis membrane and dialysed against water for 7-9 days, until product **6** has become clear of colour and the product was collected by lyophilisation. The degree of substitution (DS) was based on the anomeric protons of dextran, peak at 4.96 ppm, and set to an integral of 1. The peak integrals assigned to the anomeric βCD H-1' protons (Figure 4b) were 5.04 ppm. βCD consists of seven repeating D-glucose units, hence the DS can be expressed as:

$$DS = \frac{Int_{\beta CD}}{7} \times 100\% \quad (1)$$

ATR-FTIR: 3335 (O-H, stretch), 2923 (C-H, stretch), 1685 (C=O urethane, stretch), 1215 (C-N, stretch), 1150 (C-C, stretch) and 1013 (O-H, bend) cm^{-1}.

Dex_{250}-βCD DS 6% #1 **6a.** Product **1b** (150 mg, 0.92 mmol r.u.; 0.14 mmol PNC) and βCD-NH_2 (206 mg, 0.18 mmol). Dissolved in 3 mL anhydrous DMF, precipitated in 30 mL EtOH, redissolved in 7 mL water. Yielded in 85.4 mg (0.23 µmol, 45.0%), DS 6% #1. ^{1}H NMR (400 MHz, D_2O) δ: 4.96 (s, 1H, anomeric proton dextran), 5.04 (s, 7H, anomeric proton βCD).

Dex_{250}-βCD DS 6% #2 **6b.** Product **1b** (2.00 g, 12.33 mmol r.u.; 1.88 mmol PNC) and βCD-NH_2 (2.75 g, 2.42 mmol). Dissolved in 40 mL anhydrous DMF, precipitated in 400 mL EtOH, redissolved in 15 mL water. Yielded in 1.73 g (4.81 µmol, 71.3%), DS 6% #2. ^{1}H NMR (400 MHz, D_2O) δ: 4.96 (s, 1H, anomeric proton dextran), 5.05 (s, 7H, anomeric proton βCD).

Dex_{250}-βCD DS 5% **6c.** Product **1c** (395 mg, 2.44 mmol r.u.; 0.20 mmol PNC) and βCD-NH_2 (542.47 mg, 0.48 mmol). Dissolved in 8 mL anhydrous DMF, precipitated in 80 mL EtOH, redissolved in 5 mL water. Yielded in 315 mg (0.95 µmol, 66.0%), DS 5%. ^{1}H NMR (400 MHz, D_2O) δ: 4.97 (s, 1H, anomeric proton dextran), 5.06 (s, 7H, anomeric proton βCD).

Dex_{500}-βCD DS 2% **6d.** Product **1d** (1.41 g, 8.69 mmol r.u.; 0.93 mmol PNC) and βCD-NH_2 (1.41 g, 2.53 mmol). Dissolved in 28 mL anhydrous DMF, precipitated in 280 mL EtOH, redissolved in 40 mL water. Yielded in 1.14 g (1.96 mmol, 77.5%), DS 2%. ^{1}H NMR (400 MHz, D_2O) δ: 4.96 (s, 1H, anomeric proton dextran), 5.05 (s, 7H, anomeric proton βCD).

Dextran-tyramine[48] **7.** Product **1** was brought under nitrogen atmosphere and anhydrous DMF was added through a syringe and stirred until all was dissolved. Solution time variated from 1 to 2 hours, depending on the used dextran (250 kDa or 500 kDa). TA was added to the solution and dissolved quickly, turning the solution yellow, and the solution was stirred for 1 hour. The reaction was precipitated in cooled EtOH and kept in the fridge for 1 hour to promote sedimentation of the product. Subsequently, the mixture was filtered over POR4 glass filter and washed 5 times with EtOH and afterwards washed 5 times with DEE. Remaining solvent was removed in vacuo overnight and the resulting solid was redissolved in minimal amounts of water, transferred into a 1000 Da MWCO dialysis membrane and dialysed against water for 3 days. The product was collected by lyophilization and the DS was defined as the number of conjugated groups per 100 anhydroglucose units in dextran. DS (^{1}H NMR, 400 MHz, DSMO-d_6) δ: 2.5-4.0 (m, –CH2–CH2–), 4.2-5.4 (m, 4H, glucosidic protons dextran), 6.6-6.8 (m, 2H, aromatic protons TA), 6.9-7.1 (m, 2H, aromatic protons TA). ATR-FTIR: 3361 (O-H), 2923 (C-H), 1689 (C=O urethane, stretch), 1650 (C=C, stretch), 1205 (C-N, stretch), 1151 (C-C, stretch) and 1012 (O-H, bend) cm^{-1}

Dex_{250}-TA DS 8% **7a.** Product **1b** (1.00 g, 6.17 mmol r.u.; 0.94 mmol PNC) and TA (0.26 g, 1.88 mmol). Dissolved in 20 mL anhydrous DMF, precipitated in 200 mL EtOH, redissolved in 10 mL water. Yielded in 0.65 g (2.44 µmol, 72.2%), DS 8% ^{1}H NMR (400 MHz, DSMO-d_6) δ: 2.5-4.0 (m, –CH_2–CH_2–), 4.2-5.5 (m, 4H, glucosidic protons dextran), 6.6-6.7 (m, 2H, aromatic protons TA), 6.9-7.1 (m, 2H, aromatic protons TA).

Dex_{250}-TA DS 4% **7b.** Product **1c** (395 mg, 2.44 mmol r.u.; 0.20 mmol PNC) and TA (54.8 mg, 0.40 mmol). Dissolved in 7 mL anhydrous DMF, precipitated in 70 mL EtOH, redissolved in 5 mL water. Yielded in 321 g (2.24 µmol, 86.1%), DS 8% ^{1}H NMR (400 MHz, DSMO-d_6) δ: 2.5-4.0

(m, –CH_2–CH_2–), 4.1-5.4 (m, 4H, glucosidic protons dextran), 6.6-6.7 (m, 2H, aromatic protons TA), 6.9-7.1 (m, 2H, aromatic protons TA).

Dex_{500}-TA DS 4% **7c.** Product **1d** (1.41 g, 8.69 mmol r.u.; 0.93 mmol PNC) and TA (169.7 mg, 1.24 mmol). Dissolved in 28 mL anhydrous DMF, precipitated in 280 mL EtOH. Redissolved in 37 mL water of which the pH was adjusted to 11-12 by addition of 1M NaOH solution. When the solution was dissolved, the pH was neutralized with 1M HCl solution and transferred into the dialysis membrane. Yielded in 1.07 g (2.07 µmol, 82.5%), DS 4% ^{1}H NMR (400 MHz, DSMO-d_6) δ: 2.5-4.0 (m, –CH_2–CH_2–), 4.2-5.3 (m, 4H, glucosidic protons dextran), 6.6-6.7 (m, 2H, aromatic protons TA), 6.9-7.1 (m, 2H, aromatic protons TA).

Dextran-tyramine-adamantadine **8.** Product **1b** (2.29 g, 14.12 mmol r.u.; 2.15 mmol PNC) and 1-Ada (0.40 mg, 2.15 mmol) were dissolved in 46 mL anhydrous DMF under nitrogen atmosphere and stirred for 1 hour. TA (0.59 g, 4.30 mmol) was added to the solution and the procedure was subsequently followed as described for **7**. The solution was precipitated in 460 mL EtOH, redissolved in 15 mL water and 150 mL DMSO and dialysed for 7 days. The composition of 8 was established by comparing its ^{1}H NMR spectra to the spectra's of the pure substances. DS TA 7%, DS Ada 0%. 1H NMR (400 MHz, DSMO-d6) δ: 2.5-4.0 (m, –CH2–CH2–), 4.2-5.4 (m, 4H, glucosidic protons dextran), 6.6-6.7 (m, 2H, aromatic protons TA), 6.9-7.0 (m, 2H, aromatic protons TA).

Poly(ethylene glycol) succinimidyl carboxyl methyl ester **9.** PEG-OH-8arm 40 kDa (10.6 g, 0.27 mmol) was dissolved in 20 mL toluene in a warm water bath at 40 ^oC, precipitated in 200 mL DEE, filtered over a POR4 glass filter and dried under vacuum for 1 hour. The product was then dissolved in 200 mL toluene and subsequently connected to a rotary evaporator in order to evaporate the solvent. This was repeated twice. The resulting white solid was dried over the weekend under vacuum yielding in a final weight of 10.3 g (0.26 mmol, 97.7%). Purified PEG-OH (10.3 g, 2.06 mmol OH) was dissolved in 28 ml dry acetonitrile and treated with DSC (1.04 g, 4.11 mmol) under argon conditions. Subsequently pyridine (0.82 ml, 10.44 mmol) was added and the mixed solution was stirred for a minimum of 16 hours under argon. Afterwards the now clear solution was precipitated in 280 mL DEE and dried under vacuum overnight. Product **9** was obtained as white powder with a yield of 95.1% (10.5 g, 0.26 mmol), DS 100%. ^{1}H NMR (400 MHz, $CDCl_3$) δ: 3.20-3.95 (m, 3636H, protons PEG), 4.43-4.50 (t, 2H, urethane bond). The DS (percentage of functionalized arms) was based on the peak integrals assigned to urethane bond between PEG and SC at 4.43-4.50 ppm to the total 3636 protons of PEG at 3.60-3.40 ppm. As the bond represents 2 protons the DS could be expressed as:

$$DS_{PEG-SC} = \frac{\frac{Int_{SC}}{2}}{8\ (arms)} \times 100\% \qquad (2)$$

ATR-FTIR: 2880 (C-H, stretch), 1811 (C=O, stretch), 1742 (C=O, stretch), 1466 (C-H, bend), 1340 (C-H, bend), 1279 (O-H, stretch), 1240 (O-H, stretch), 1197 (C-O, ester stretch), 1146 (C-N, stretch), 1099 (C-O-H, bend), 960 (C-H, bend) and 840 (C-H, bend) cm^{-1}.

Poly(ethylene glycol)-β cyclodextrin[102] **10.** To a solution of **5** (1.25 g, 1.10 mmol) and trimethylamine (TEA, 219 µL, 1.59 mmol) in 9 mL dry DMF, a solution of **9** (2.50 g, 61.1 µmol, 0.48 mmol NHS) in 9 mL dry DMF and 1.5 mL dry DCM was added, all under argon conditions. The solution was stirred under argon for 4 hours and afterwards the product was precipitated in 200 mL DEE and filtered over a POR4 glass filter. The precipitate was dried under vacuum overnight, redissolved in 10 mL water and transferred into a 3500 Da MWCO dialysis membrane and dialysed against water for 3 days. The product was collected by lyophilization yielding the product as a though white foam of 2.73 g (55.8

mmol, 91.4%), DS 99%. ^{1}H NMR (400 MHz, $CDCl_3$) δ: 3.23-4.00 (m, 3636H, protons PEG), 5.00-5.11 (s, 7H, anomeric βCD H-1'). The DS (percentage of functionalized arms) was based on the peak integrals assigned to the anomeric βCD H-1' protons at 5.05 ppm and the combined signals of the remaining six protons of βCD and the protons of PEG at 3.23-4.0 ppm. The integration of the PEG + βCD region was expressed as:

$$Int_{PEG+\beta CD} = 7 \times 6(protons\ \beta CD) + 3636(protons\ 40\ kDa\ PEG) = 3678$$

From this the integral of the anomeric βCD H-1' protons were determined and the DS was expressed as:

$$DS_{PEG-\beta CD} = \frac{\frac{Int_{\beta CD}}{7}}{8\ (arms)} \times 100\% \quad (3)$$

ATR-FTIR: 3380 (O-H, stretch), 2878 (C-H, stretch), 1467 (C-H, bend), 1342 (C-H, bend), 1279 (O-H, stretch), 1240 (O-H, stretch), 1146 (C-N, stretch), 1100 (C-O-H, bend), 960 (C-H, bend) and 840 (C-H, bend) cm^{-1}.

Poly(ethylene glycol)-tyramine 11. The same protocol was followed as for **10**, though **5** was replaced by TA (150.70 mg, 1.10 mmol) and the redissolved **11** was dialysed in 1000 Da MWCO dialysis membrane. The product was collected by lyophilization yielding the product as a white foam of 2.23 g (54.4 mmol, 89.0%), DS 103%. ^{1}H NMR (400 MHz, $CDCl_3$) δ: 3.08-4.06 (m, 3636H, protons PEG), 4.16-4.26 (t, 2H, urethane bond PEG-TA), 6.75-6.82 (m, 2H, aromatic protons TA), 6.97-7.04 (m, 2H, aromatic protons TA). The peak integrals of PEG at 3.08-4.06 ppm were set to the total 3636 protons of PEG, and from this the integrals of the urethane bond between PEG and TA at 4.15-4.26 ppm and the aromatic TA protons at 6.75-6.82 ppm and 7.00-7.04 ppm were determined. As the bond represents 2 protons the DS (percentage of functionalized arms) could be expressed as:

$$DS_{PEG-TA} = \frac{\frac{Int_{TA\ bond}}{2}}{8\ (arms)} \times 100\% \quad (4)$$

ATR-FTIR: 3343 (O-H, stretch), 2880 (C-H, stretch), 1717 (C=O, urethane, stretch), 1467 (C-H, bend), 1342 (C-H, bend), 1279 (O-H, stretch), 1242 (O-H, stretch), 1146 (C-N, stretch), 1098 (C-O-H, bend), 960 (C-H, bend) and 840 (C-H, bend) cm^{-1}.

Poly(ethylene glycol)-adamantine[57] 12. Ada·HCl (1.0 g, 5.33 mmol) was suspended in 20 mL dry DCM and TEA (750 µL, 5.44 mmol) was added. Separately **9** (2.50 g, 61.1 µmol, 0.48 mmol NHS) was dissolved in 30 mL dry DCM, added to the Ada·HCl suspension and stirred overnight. Next, the solvent was removed under vacuum and rinsed with dry DCM which was repeated three times. To the resulting solid 50 mL water was added, as **12** will dissolve in water though unreacted 1-adamantadine will not. The suspension was centrifuged for 10 minutes at 5000 rpm and the supernatant was dialyzed for 3 days in a 1000 Da MWCO dialysis membrane against water. The product was subsequently lyophilized and yielded in a firm white foam. ^{1}H NMR spectra indicated that unbound adamantane was still present, therefore the product was redissolved in water and dialysed for another 3 days and collected by lyophilisation. The product yielded in 2.12 g (51.8 µmol, 84.8%), DS 92%. ^{1}H NMR (400 MHz, $CDCl_3$) δ: 3.14-3.89 (m, 3636H, protons PEG), 4.12-4.18 (t, 2H, urethane bond PEG-TA). Remaining proton signals indicated that unbound adamantane was still presents (SI 2, Figure S22). The peak integrals of PEG at 3.14-3.89 ppm were set to the total 3636 protons of PEG, and from this the integrals

of the urethane bond between PEG and adamantane at 4.12-4.18 ppm were determined. As the bond represents 2 protons the DS could be expressed as:

$$DS_{PEG-Ada} = \frac{\frac{Int_{Ada\ bond}}{2}}{8\ (arms)} \times 100\% \quad (5)$$

ATR-FTIR: 3325 (O-H, stretch), 2880 (C-H, stretch), 1719 (C=O, urethane, stretch), 1467 (C-H, bend), 1342 (C-H, bend), 1279 (O-H, stretch), 1240 (O-H, stretch), 1146 (C-N, stretch), 1098 (C-O-H, bend), 960 (C-H, bend) and 840 (C-H, bend) cm^{-1}.

3.4. Hydrogel formation

Supramolecular hydrogels were prepared by mixing the synthesized host polymers with the guest polymers according to the Table 1, with either 1:1 (5 wt%, 10 wt%, 15 wt%), 1:2 (10 wt%) or 2:1 (10 wt%) H:G molar ratio. The hydrogels were prepared from dissolved individual polymers in PBS at the desired concentration which were then combined in vials with a final volume of 200 µL and mixed by vortexing. Upon vial tilting the mixtures were visually assessed to be in the gel or liquid state.

Table 1. Polymer mixing table for HG hydrogel formation

Host \ Guest	Dex_{250}-TA DS 8%	Dex_{250}-TA DS 4%	Dex_{500}-TA DS 4%	PEG-TA	PEG-Ada
Dex_{250}-βCD DS 6% #1					
Dex_{250}-βCD DS 6% #2					
Dex_{250}-βCD DS 5%					
Dex_{500}-βCD DS 2%					
PEG-βCD					

Secondary HRP/H_2O_2 crosslinking of our HG hydrogel system was investigated by two tests:

1. Dex_{250}-βCD DS 6% #2 + HRP
   Dex_{250}-TA DS 4% + H_2O_2
   } mixed and pipetted in cooled molds.
2. Dex_{250}-βCD DS 6% #2 + HRP
   Dex_{250}-TA DS 4%
   } mixed and waited until equilibrium was reached. Then H_2O_2 was added, mixed in and solution was pipetted in cooled molds.

Both tests had a final 10 wt% polymer concentration with 1:1 H:G molar ratio in a volume of 700 µL with 4 U/mL HRP and 0.03% H_2O_2 concentration. In test 1 the individual polymers were dissolved in 280 µL PBS and 70 µL HRP (40 U/mL HRP stock solution) was added to the Dex_{250}-βCD DS 6% #2 solution and 70 µL H_2O_2 (0.3% H_2O_2 stock solution) was added to Dex_{250}-TA DS 4% solution. The polymer solutions were mixed shortly by vortexing and pipetted into cooled molds. The stable gels were removed from the molds, kept in PBS and saved until later evaluation. For test 2 the individual polymers were dissolved in 280 µL PBS and 70 µL HRP (40 U/mL stock solution) was added to the Dex_{250}-βCD DS 6% #2 solution and the polymer solutions were mixed shortly by vortexing. After equilibrium was reached 70 µL H_2O_2 (0.3% stock solution) was added to the hydrogel, vortexed shortly and pipetted into cooled molds. The stable gels were removed from the molds, kept in PBS and saved until later evaluation.

3.5. Viscosity measurements of dextran

40 kDa, 150 kDa, 250 kDa and 500 kDa dextran solutions series were prepared of 2.5 wt%, 5 wt%, 7.5 wt% and 10 wt% and the viscosity η [Pa·s] was measured with shear rates from 0-10 000 s^{-1}. A shear-thinning fluid is characterized by as decreasing viscosity with an increasing share rate.

3.6. Stoichiometry determination using Job's plot method

Job's method of continuous variation was applied to investigate the stoichiometry of the HG complexation of the synthesized βCD and tyramine polymers by UV-vis spectroscopy. Absorbance measurements were carried out at RT using a 2 mL quartz cell with 1.0 cm path length. Since both βCD and tyramine have poor solubility in water βCD·H_2O and TA·HCl were used as host and guest. The concentrations of the host and guest were varied in each sample, from respectively 1-0 equivalent and 0-1 equivalent, whereas the sum of the concentrations was kept constant at 100 µM (See Table S1 and Table S2 in SI 4). Water was used as blanco to correct for background noise. βCD·H_2O is spectroscopically inert, though TA·HCl has absorption maxima at 221 nm and 274 nm. Therefore the absorbance was measured from 200 to 350 nm and the absorbance of TA·HCl at 221 nm and 274 nm for each mole fraction of guest ($X_{TA\cdot HCl}$) was used for the Job's plot analysis. Job plots were constructed by plotting the change in absorbance (ΔA) x R versus R, with

$$\Delta A = A_{[H]=0} - A_{HG} \tag{6}$$

and R

$$R = \frac{[G]}{[G] + [H]} \tag{7}$$

The value of R at the maximum deviation gives the HG assembly ratio, e.g., R=0.5 for 1:1 HG complexes; R=0.33 for 1:2 HG complexes; R=0.66 for 2:1 complexes, etc.[80]

The association constant was graphically evaluated by Benesi-Hildebrand plots by plotting the inverse relative absorbance $\frac{1}{A-A_0}$ at 221 nm, where A is the corresponding absorbance intensity at the measured wavelength and A_0 is the absorbance intensity in the absence of the host molecule, against the inverse of the corresponding βCD concentration $\frac{1}{[\beta CD]}$. From this linear relationship the association constant K_a was determined by

$$\frac{1}{\Delta A} = \frac{1}{K_a \times (A_{max} - A_o) \times [\beta CD]} + \frac{1}{A_{max} - A_o} \tag{8}$$

where A is the measured absorption, A_0 is the absorption of free TA and A_{max} is the saturated absorption of the HG complex.[80,103-105]

3.7. Stoichiometry determination by ^{1}H NMR titration

Two separate ^{1}H NMR titration experiments were executed, both with βCD·H_2O as host with a fixed concentration [H_0]=4.4 mM and D_2O as solvent. In the first titration TA·HCl was used as guest and in the second titration Ada·HCl. The guests solutions of TA·HCl ([$G_{TA\cdot HCl,\ 0}$]=441 mM) and Ada·HCl ([$G_{Ada\cdot HCl,\ 0}$]=441 mM) were prepared at a 100 fold higher concentration ([G_0]= 100[H_0]). ^{1}H NMR spectra were recorded from the range of 0-10 equivalent with 10 data points from 0-1.50 equivalent and 4 data points from 2.50-10 equivalent. The raw titration data was fitted into 1:1 binding isotherm and the associating constant was obtained by non-linear regression of the isotherm using Thordarson Group – Software.[106]

3.8. Printability

HG polymer combinations were selected that formed a gel or a solution with high viscosity to serve as ink or support bath. Diverse stock solutions in water were prepared: 3.0% Xantan, 40 U/mL HRP and 0.03% H_2O_2. Also green food colouring was dissolved in water and used to prepare green 0.3% and 0.03% H_2O_2 solutions. Two 3D printing tests were conducted with the Cellink+ 3D printer (Figure 8) in order to study the printability:

1. The ink consisted of PEG-βCD mixed with PEG-Ada (10 wt%, 1:1 HG molar ratio, V=1 mL) and H_2O_2 (0.03% final concentration). Pre-crosslinked Dex_{250}-TA DS 8% (5 wt%, 0.003% H_2O_2, 4 HRP U/mL) stacked on 3.0% Xanthan was used as support bath. The ink was transferred into a cartridge and subsequently printed in a straight line in the support bath and visually investigated (Figure 9a).

2. Green gelatin ink (5 wt%) was prepared and to promote smooth extrusion the gelatin ink was broken down by extrusion through needles which were successively decreasing in size. The ink was transferred into a cartridge and saved until later use. Dex_{250}-βCD DS 6% #2/Dex_{250}-TA DS 4% (4 units HRP/mL HRP, 1:1 HG molar ratio, 15 wt%) stacked on 3.0% Xanthan was used as support bath. The ink was subsequently printed in a straight line in the support bath and visually investigated (Figure 9b).

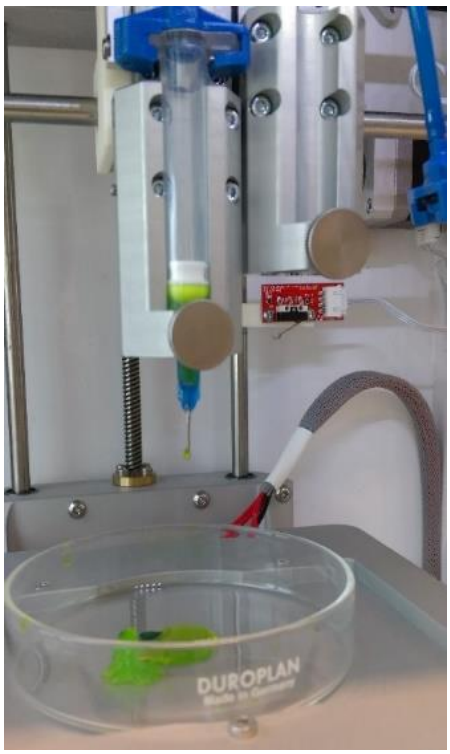

Figure 8. Printer set-up of the Cellink+ 3D printer. Ink was extruded through a 22G nozzle with a velocity of 10 mm/s and a pressure of 163 kPa and 181 kPa for respectively test 1 and 2.

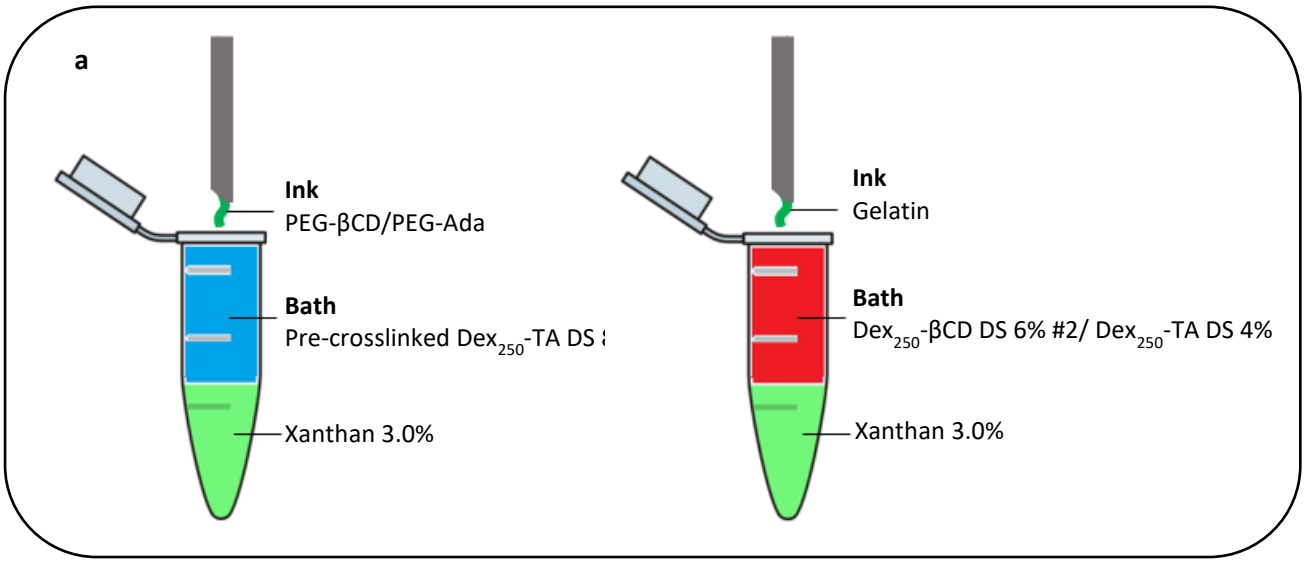

Figure 9. Schematic representation of printing tests (a) 1 and (b) 2.

3.9. Cytotoxicity assay

A viability study of Jurkat cells was performed on two gels: (1) Dex_{250}-βCD DS 6% #2/Dex_{250}-TA DS 4% (10 wt%) and (2) PEG-Ada/PEG-βCD (10 wt%). As control culture medium was used. In a 48-wells untreated culture plate 150 µL of each gel and the control were pipetted in triplicates and 200 µL of cell suspension was added to each well (~15 000 cells per well) and incubated for 4 hours. The Jurkat cells were cultured and subcultured according the procedure as describe in Supplementary info (SI) SI 1SI 1. Live/dead staining solution was prepared by the addition of 15 µL of ethidium homodimer stock solution and 1.25 µL of calcein AM stock solution to 5 mL PBS, resulting in a final concentration of 6 µM ethidium homodimer and 1 µM calcein AM. After incubation the cells were transferred into a Greiner tube, centrifuged and medium was aspirated. Cells were washed twice with 3 mL pre-warmed PBS and afterwards resuspended in 500 µL PBS and transferred into a 6-wells plate (untreated). Next, 500 µL staining solution was added and the cells were incubated for 30 minutes. Viability was visualized by fluorescence microscopy where dead cells fluoresce red and the viable cells green.

4. Results

4.1. Polymer synthesis

The DS of PNC coupled to high MW (≥150 kDa) dextrans varied from 3-18% and with low repeatability. After dissolution of 150 kDa, 250 kDa and 500 kDa dextran in anhydrous DMF sublimated PNC was added, though PNC did not dissolve completely. Prolonged dissolution time of both dextran and PNC did not result in absolute dissolved PNC. To compensate extra PNC was added to the mixture which resulted in DS of 3.3%, 18% and 12% for respectively 150 kDa, 250 kDa and 500 kDa dextran. Figure 10shows the integrals of the aromatic PNC protons of 250 kDa. 250 kDa dextran was purified and functionalized with PNC. A new bottle of pyridine was used in this reaction, however the same problems were encountered and 250 kDa dextran was functionalized with a DS of 9%. Due to the low DS dextran 150 kDa was excluded from successive experiments.

The reduction of βCD-N_3 by Pd/C resulted in low yields (~12%) where in literature[98] yields of 90% were reached. After reduction of βCD-N_3 by Pd/C the mixture was filtered over paper and subsequently connected to the rotary evaporator to remove the solvents. After evaporation the crude product was weighted and proved to be nearly gone. Also its ^{1}H NMR spectra did not agree with the literature (Figure 11).[101] Therefore another mild azide reduction method was tried, the Staudinger reaction, which resulted in a yield of 82.9% (Figure 12).[22]

Dex_{250}-TA-Ada synthesis proved to be difficult, as the polymer could not be dissolved in water. DMSO was added to promote dissolution however the product was still not completely dissolved and was present as gel-like lumps during dialysis. Ada could not be detected by ^{1}H NMR spectra, though TA was present with a DS of 6.8%.

The calculated DS of PEG-TA was 103%. Remaining reactions were performed without significant complications and their DS, yield, MW and MW per host or guest unit (g/mol_{moiety}) are summarized in Table 3 and Table 2. Their ^{1}H NMR and FTIR spectra are provided in SI 2 and SI 3.

Table 3. DS, yield (%) and MW (Da) of the synthesized precursors.

Precursor	*DS (%)*	*Yield (%)*	*MW (Da)*
Dex_{150}-PNC	3	97.6	257 689
Dex_{250}-PNC	18	93.5	296 148
Dex_{250}-PNC	9	86.1	273 074
Dex_{500}-PNC	12	94.9	561 481
Tosyl-imidazole	-	90.3	222
Tosyl-βCD	-	36.4	1289
βCD-N_3	-	99.1	1160
βCD-NH_2 (Pd/C)	-	12.8	1134
βCD-NH_2 (PPh_3)	-	82.9	1134
PEG-SC	100	95.1	40 913

Table 2. DS, yield (%), MW (Da) and MW per host or guest unit (g unit/mol) of the synthesized polymers.

Polymer	*DS*	*Yield (%)*	*MW (Da)*	*g/mol_{moiety}*
Dex_{250}-βCD	6 #1	45.0	362 156	3666
Dex_{250}-βCD	6 #2	71.3	360 404	3705
Dex_{250}-βCD	5	66.0	330 585	4656
Dex_{500}-βCD	2	77.5	580 585	8177
PEG-βCD	99	91.4	48 928	6116
Dex_{250}-TA	8	72.2	266 988	2153
Dex_{250}-TA	4	86.1	259 223	3812
Dex_{500}-TA	3	82.5	516 988	4170
Dex_{250}-TA-Ada	7 (TA)	-	-	-
PEG-TA	103	89.0	40 953	5119
PEG-Ada	92	84.8	40 934	5848

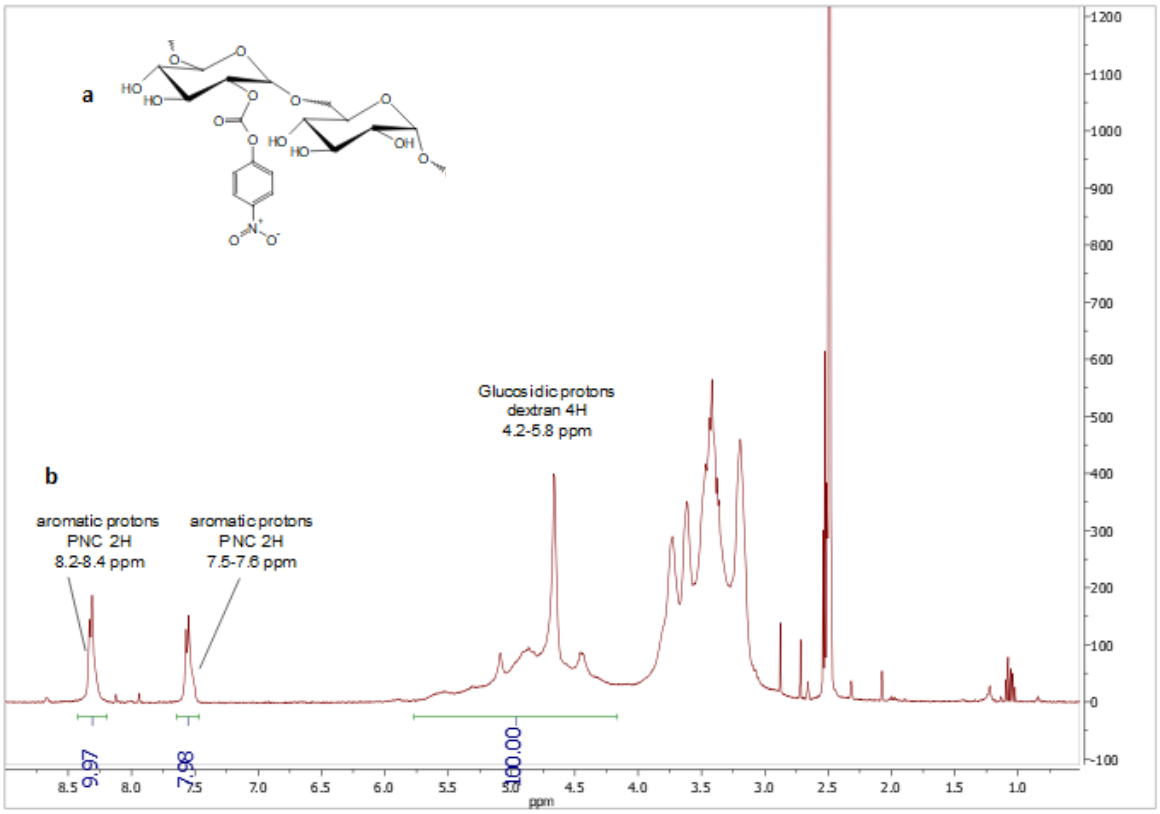

Figure 10. Dex$_{250}$-PNC DS 18% (a) structure and (b) ^{1}H NMR (400 MHz, DSMO-d$_6$) δ: 2.5-4.0 (m, –CH$_2$–CH$_2$–), 4.2-5.8 (m, 4H, glucosidic protons dextran), 7.5-7.6 (m, 2H, aromatic protons PNC), 8.2-8.4 (m, 2H, aromatic protons PNC).

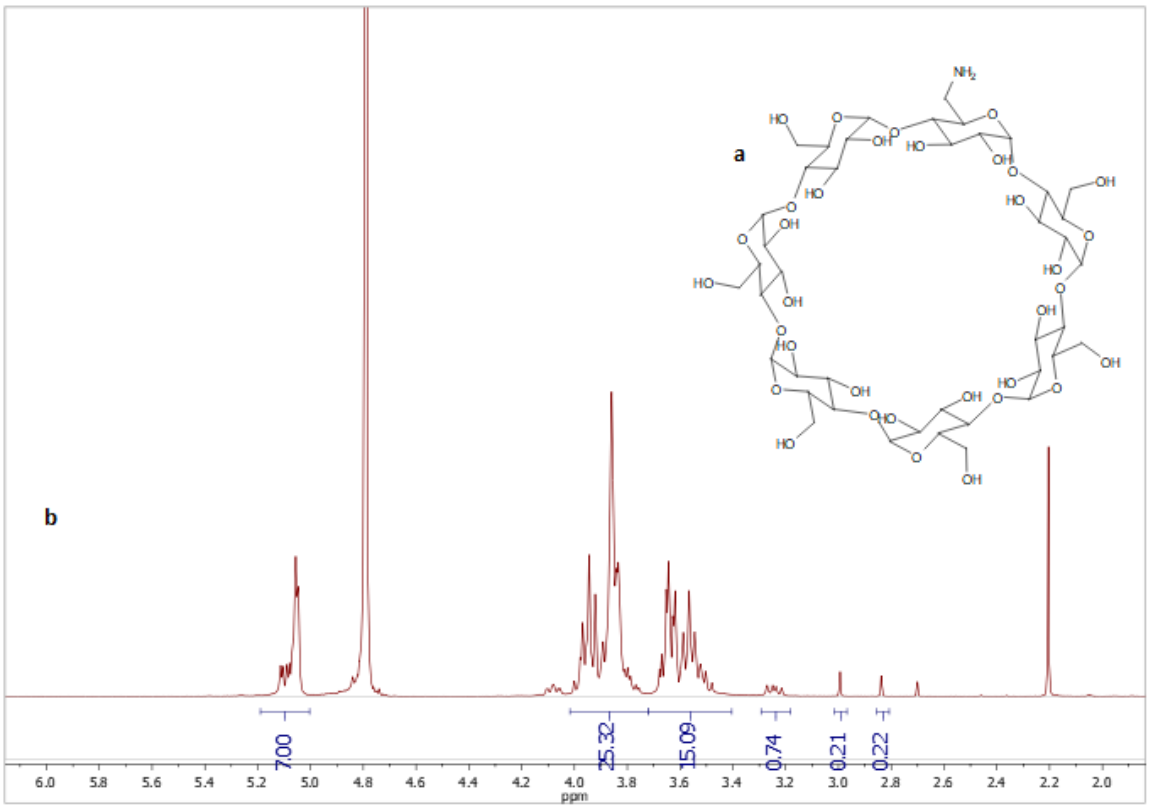

Figure 11. βCD-NH$_2$ reduced by Pd/C (a) structure and (b) ^{1}H NMR (D$_2$O, 400 MHz) δ: 2.84 (s, 0H), 2.99 (s, 0H), 3.24 (dd, 1H), 3.40-3.72 (m), 3.72-4.02 (m), 5.00-25.19 (m, 7H).

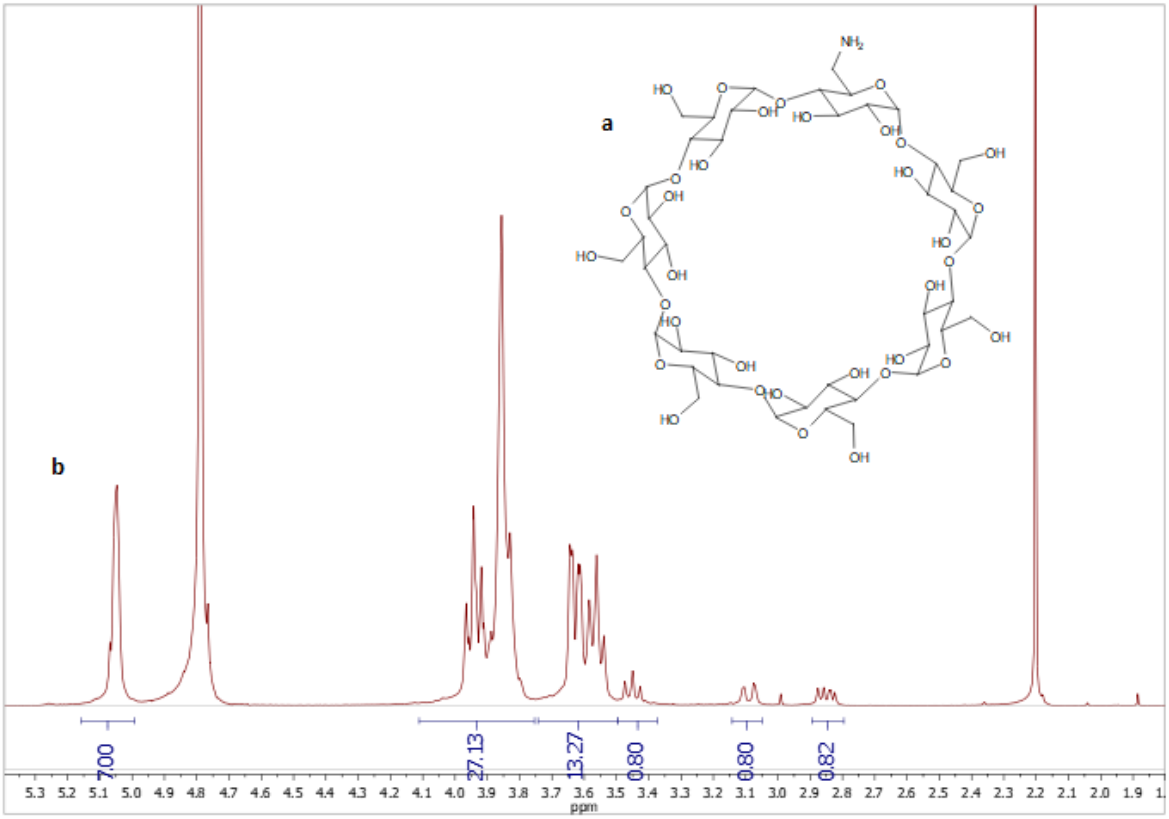

Figure 12.βCD-NH_2 reduced by PPh_3 (a) structure and (b) ^{1}H NMR (400 MHz, D2O) δ: 2.85 (dd, 1H, H-6'), 3.09 (dd, 1H, H-6'), 3.45 (t, 1H, H-4'), 3.49-3.74 (m), 3.75-4.11 (m), 4.99-5.16 (m, 7H, H-1').

4.2. Hydrogel formation

4.2.1. Polymer mixing

The formation of supramolecular hydrogels by mixing the prepared host polymers with the guest polymers was visually investigated. Table 4 shows the results of 1:1 H:G molar ratio (10 wt%) mixing. Temporary gels were rapidly formed by mixing Dex_{250}-βCD DS 6% #1 with Dex_{250}-TA DS 8% and Dex_{250}-TA DS 4% for respectively 15 minutes and 45 minutes. Hereafter the hydrogels remained in a stable viscous state and contained fibers as listed in Table 4. Both gels were opaque coloured. Figure 13 shows that mixed Dex_{250}-βCD DS 6% #1/Dex_{250}-TA DS 4% at t=0 minutes formed a hydrogel. Afterwards the hydrogel started flowing and reached a stable viscous state after 45 minutes. Mixtures containing PEG-Ada as guest polymers resulted in weak gels which became more stable over time. By tilting the vials PEG-βCD mixed with PEG-Ada proved the most stable. PEG-Ada/Dex_{250}-βCD DS 5% was opaque coloured and the remaining PEG-Ada mixtures were colourless. The other mixtures resulted in opaque coloured viscous liquids which were not able to remain in the vial tip upon tilting. Fibers were present in the dextran polymer mixtures and absent in PEG mixtures.

Figure 13. Mixed Dex_{250}-βCD DS 6% #1 and Dex_{250}-TA DS4%, from gel state towards fluid state at (a) t=0 min, (b) t=45 min and (c) t=60 min.

Table 4. Results of mixing host and guest polymers, 1:1 H:G molar ratio, 10 wt%

Host \ Guest	Dex_{250}-TA DS 8%	Dex_{250}-TA DS 4%	Dex_{500}-TA DS 4%	PEG-TA	PEG-Ada
Dex_{250}-βCD DS 6% #1	Gel for 15 min After: fibers, viscous	Gel for 45 min After: fibers, viscous	No gel, fibers, lightly viscous	No gel, no fibers, liquid/viscous	Weak gel, no fibers
Dex_{250}-βCD DS 6% #2	No gel, fibers, viscous	No gel, fibers, viscous	No gel, fibers, viscous	No gel, no fibers, liquid/viscous	Weak gel, no fibers
Dex_{250}-βCD DS 5%	No gel, no fibers, viscous	No gel, fibers, viscous	No gel, fibers, viscous	No gel, no fibers, liquid/viscous	Weak gel, no fibers
Dex_{500}-βCD DS 2%	No gel, fibers, lightly viscous	No gel, fibers, lightly viscous	No gel, fibers, lightly viscous	No gel, no fibers, liquid/viscous	Weak gel, no fibers
PEG-βCD	No gel, no fibers, liquid/viscous	No gel, fibers, liquid/viscous	No gel, no fibers, liquid/viscous	No gel, no fibers, liquid/viscous	Weak gel, No fibers

Based on the results in Table 4 Dex_{250}-βCD DS 6% #2/Dex_{250}-TA DS 8% and Dex_{250}-βCD DS 6% #2/Dex_{250}-TA DS 4% were selected to test if wt% can influence hydrogel formation. Mixing the selected polymers in 5 wt% or 15 wt% (1:1 H:G molar ratio) did not result in stable hydrogels (Table 5). As a control the selected polymers were mixed in 10 wt% (1:1 H:G molar ratio), however both did not result in stable hydrogels as shown in Table 4. All gels were opaque coloured.

Table 5. Results of mixing host and guest polymers, 1:1 H:G molar ratio, (a) 5 wt% and (b) 15 wt%

a. 5 wt%

Host \ Guest	Dex_{250}-TA DS 4%
Dex_{250}-βCD DS 6% #2	No gel, fibers, lightly viscous
Dex_{250}-βCD DS 5%	No gel, fibers slightly viscous

b. 15 wt%

Host \ Guest	Dex_{250}-TA DS 4%
Dex_{250}-βCD DS 6% #2	No gel, fibers, viscous/gel
Dex_{250}-βC DS 5%	No gel, fibers, viscous

Table 6 shows the results of 1:2 H:G molar ratio (10 wt%) mixing. Mixtures containing PEG-Ada as guest polymers resulted in weak gels of which PEG-βCD/PEG-Ada proved the most stable. The other mixtures listed in Table 6 resulted in viscous liquids. Fibers were present in the dextran polymer mixtures and absent in PEG mixtures. Eight of the twenty mixtures where colourless while the other 12 were opaque. No relation was found between specific polymers and the colour obtained upon mixing.

Table 6. Results of mixing host and guest polymers, 1:2 H:G molar ratio, 10 wt%

Guest / Host	*Dex$_{250}$-TA DS 8%*	*Dex$_{250}$-TA DS 4%*	*Dex$_{500}$-TA DS 4%*	*PEG-TA*	*PEG-Ada*
Dex$_{250}$-βCD DS 6% #2	No gel, fibers, viscous	No gel, no fibers, viscous	No gel, fibers, lightly viscous	No gel, no fibers, liquid	Weak gel, no fibers
Dex$_{250}$-βCD DS 5%	No gel, fibers, lightly viscous	No gel, fibers, viscous	No gel, fibers, lightly viscous	No gel, fibers, lightly viscous	Weak gel, no fibers
Dex$_{500}$-βCD DS 2%	No gel, no fibers, viscous	No gel, fibers, lightly viscous	No gel, fibers, lightly viscous	No gel, no fibers, liquid/viscous	Weak gel, no fibers
PEG-βCD	No gel, no fibers, liquid/viscous	No gel, fibers, liquid/viscous	No gel, no fibers, liquid/viscous	No gel, no fibers, liquid/viscous	Weak gel, no fibers

Mixing the host and guest polymers in 2:1 H:G molar ratio (10 wt%) resulted in viscous liquids which were as well not able to remain in the vial tip upon tilting. PEG-Ada mixed with the dextran polymers resulted in weak gels (Table 7). Eleven of the twenty mixtures were colourless and the remaining mixtures were opaque. Again, no relation was found between specific polymers and the colour obtained upon mixing.

Table 7. Results of mixing host and guest polymers, 2:1 H:G molar ratio, 10 wt%

Guest / Host	*Dex$_{250}$-TA DS 8%*	*Dex$_{250}$-TA DS 4%*	*Dex$_{500}$-TA DS 4%*	*PEG-TA*	*PEG-Ada*
Dex$_{250}$-βCD DS 6% #2	No gel, no fibers, lightly viscous	No gel, fibers, lightly viscous	No gel, no fibers, lightly viscous	No gel, no fibers, lightly viscous	Weak gel, no fibers
Dex$_{250}$-βCD DS 5%	No gel, fibers, lightly viscous	No gel, fibers, lightly viscous	No gel, fibers, lightly viscous	No gel, fibers, lightly viscous	Weak gel, no fibers
Dex$_{500}$-βCD DS 2%	No gel, fibers, lightly viscous	No gel, fibers, lightly viscous	No gel, no fibers, lightly viscous	No gel, no fibers, liquid/viscous	Weak gel, no fibers
PEG-βCD	No gel, fibers, lightly viscous	No gel, fibers, liquid/viscous	No gel, no fibers, lightly viscous	No gel, no fibers, liquid/viscous	No gel, fibers, lightly viscous

Preparing hydrogels by enzymatic HRP/H_2O_2 crosslinking did not yield in stable gels. The mixture of test 1 gelated fast in the Eppendorf tube and could not be pipetted into the molds. The mixture of test 2 was successfully pipetted into the molds, though did not gelate afterwards.

4.2.2. Fiber investigation

Fibers were in addition investigated. Figure 13 shows a microscopic picture of a fiber formed after polymer mixing, with a length of ~450 µm and a width of ~25 µm. In order to determine the fiber composition some extra experiments were conducted. Fibers proved to be insensitive for pH and temperature change. When DMSO was added the fibers did disintegrate. Fibers of the mixtures Dex250$_{250}$-βCD DS 6% #1/Dex$_{250}$-TA DS 4% (1:1, 1:2) and Dex250$_{250}$-βCD DS 5%/Dex$_{250}$-TA DS 4% (1:1, 1:2) were centrifuged, the supernatant was discarded and the precipitate was freeze dried. Figure 15 shows the stacked ^{1}H NMR spectra of Dex$_{250}$-TA DS 8%, βCD and fibers in DMSO-d_6. The fibers contained both βCD and tyramine (1.0:1.7 H:G ratio).

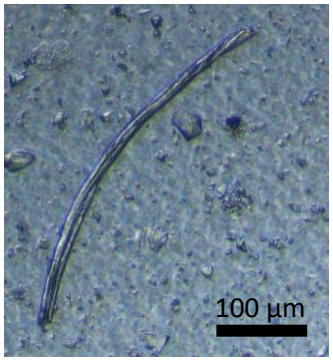

Figure 14. Microscopic picture of a fiber in mixed Dex$_{250}$-βCD DS 4% with Dex$_{250}$-TA DS 4% (1:1 molar ratio, 10 wt%) after viscous equilibrium was reached.

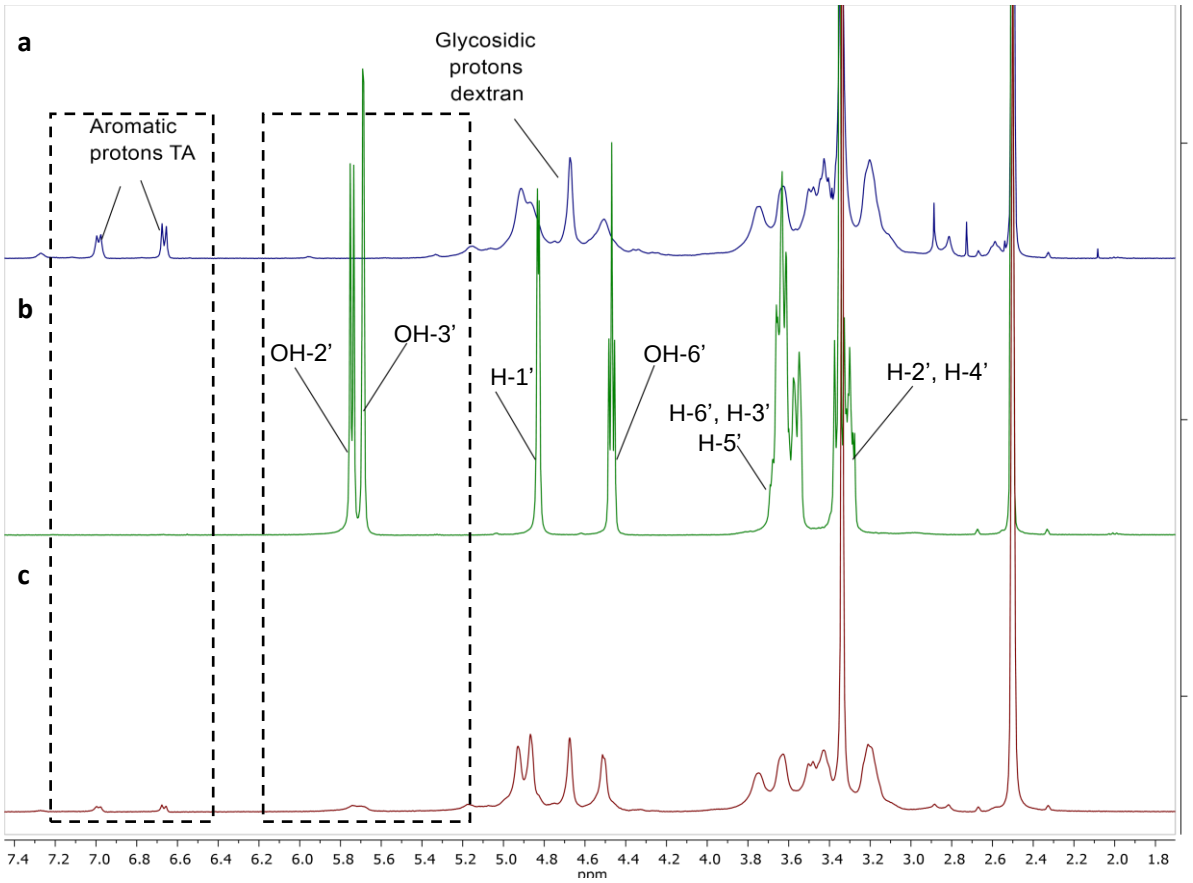

Figure 15. Stacked ^{1}H NMR (DMSO-d_6) spectra of (a) Dex_{250}-TA DS 8%, (b) βCD and (c) fibers (1.0:1.7 H:G ratio).

4.3. Viscosity measurements of dextran

The effect of MW, temperature and wt% on the viscosity (η) of 40, 150, 250 and 500 kDa dextran solutions are shown in Figure 17. When the viscosity decreases with an increasing shear rate the polymer can be characterized as shear-thinning (Figure 16).

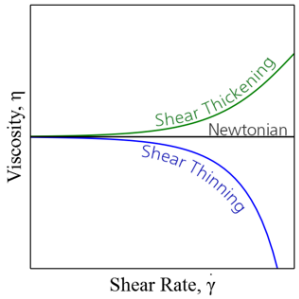

Figure 16. Viscosity of Newtonian, shear-thinning and shear-thickening fluids as a function of shear rate. Copied from [107].

Figure 17a shows the relation between polymer MW and the shear rate (2 °C, 10 wt%). It is observed that the overall viscosity is lower for lower MW dextrans as compared to higher MW dextrans. The viscosity of 40, 150 and 250 kDa dextrans remained constant, except at high shear rate (>7500 s^{-1}). The viscosity of 500 kDa did gradual decrease with increasing shear rate, showing shear-thinning behaviour. How the viscosity is influenced by temperature is shown in Figure 17b (250 kDa dextran, 10 wt%). Higher temperature have a lower viscosity as compared with lower temperatures. Up to 20 °C the viscosity remained constant, though the viscosity at temperatures from 2-15 °C show shear-thinning behaviour. The influence of wt% is shown in Figure 17c (250 kDa dextran, 2 °C). With increasing wt% the viscosity of dextran increased as well. The viscosity of 2.5 and 5 wt% dextran

solutions remained constant up to a shear rate of 5000 s^{-1}, after which the viscosity increased. The viscosities of dextran solutions of 7.5 and 10 wt% remained constant with increasing shear rate.

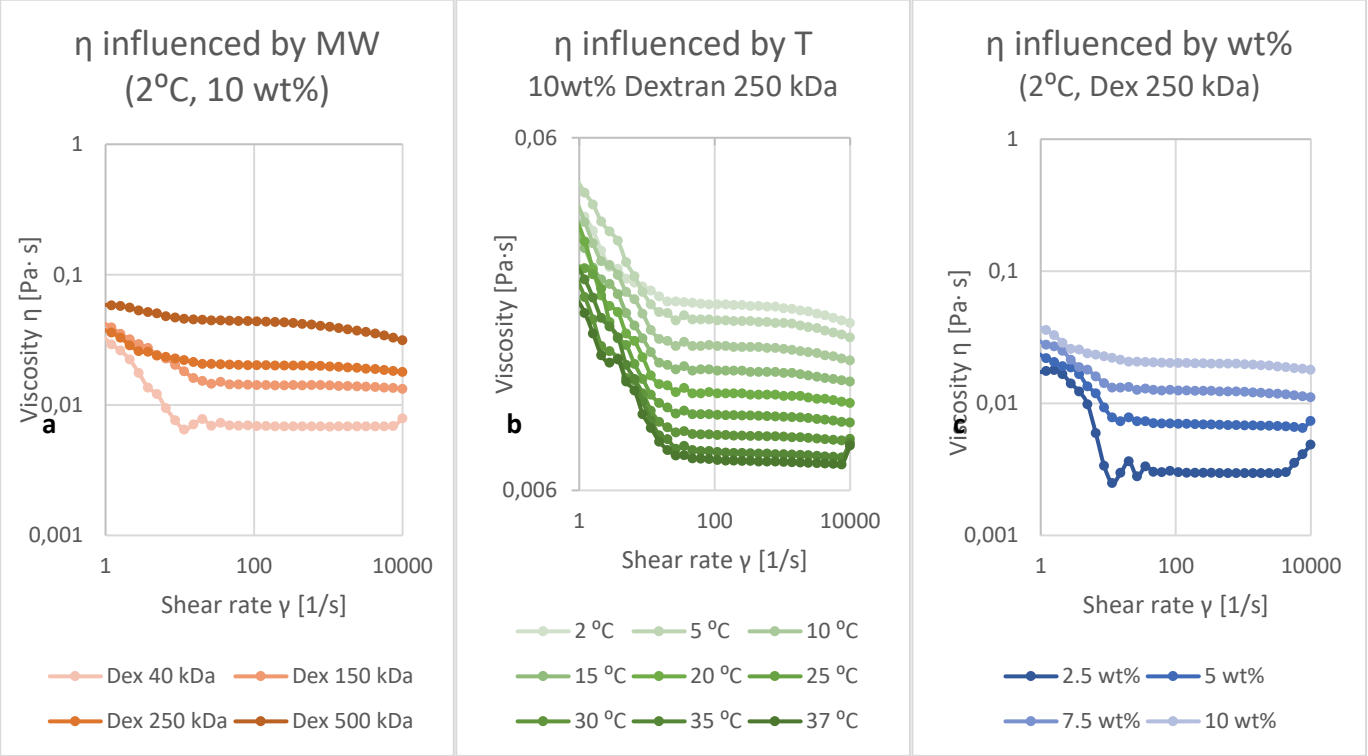

Figure 17. The effect of (a) MW (2 °C, 10 wt%),(b) temperature (250 kDa dextran, 10 wt%) and (c) wt% (2 °C, 250 kDa dextran) on the viscosity (η) of dextran solutions. η [Pa·s] was measured with shear rate=0-10 000 s^{-1}.

4.4. Stoichiometry determination using Job's plot method

Stoichiometry of βCD·H_2O, TA·HCl and the synthesized polymers were studied using the Job's plot method, as shown in Figure 18 and SI 4. The absorbance of TA·HCl at 221 nm (blue plot) and 274 nm (orange plot) for each mole fraction of guest ($X_{TA\,HCl}$) was used for the Job's plot analysis. Two trend lines were constructed in order to determine the ratio, through the first and last four data points. At the maximum deviation R=0.5 was found (Figure 18a) and a linear Benesi-Hildebrand plot could be constructed (Figure 18b). The absorption spectra of TA·HCl in Figure 18c depict the spectral changes upon TA·HCl addition (0-100 µM). The absorption maxima bands at 221 nm and 274 nm increased graduallyand and no blue nor red shift was observed. Using equation 8 a K_a was calculated of 1299 M^{-1} (Table 8). Simular results were found for all measured HG complexes (SI 4), and using equation 8 the association constants were calculated (Table 8). The K_a values of the polymers increased as follows: PEG-TA (1164 M^{-1}) < Dex_{250}-βCD DS 5% (1174 M^{-1}) < Dex_{500}-βCD DS 2% (1176 M^{-1}) < Dex_{250}-βCD DS 6% #2 (1193 M^{-1}) < PEG-βCD (1217 M^{-1}) < βCD·H_2O + TA·HCl (1299 M^{-1}) < Dex_{500}-TA DS 4% (1417 M^{-1}) < Dex_{250}-TA DS 8% (1449 M^{-1}) < Dex_{250}-TA DS 4% (1457 M^{-1}).

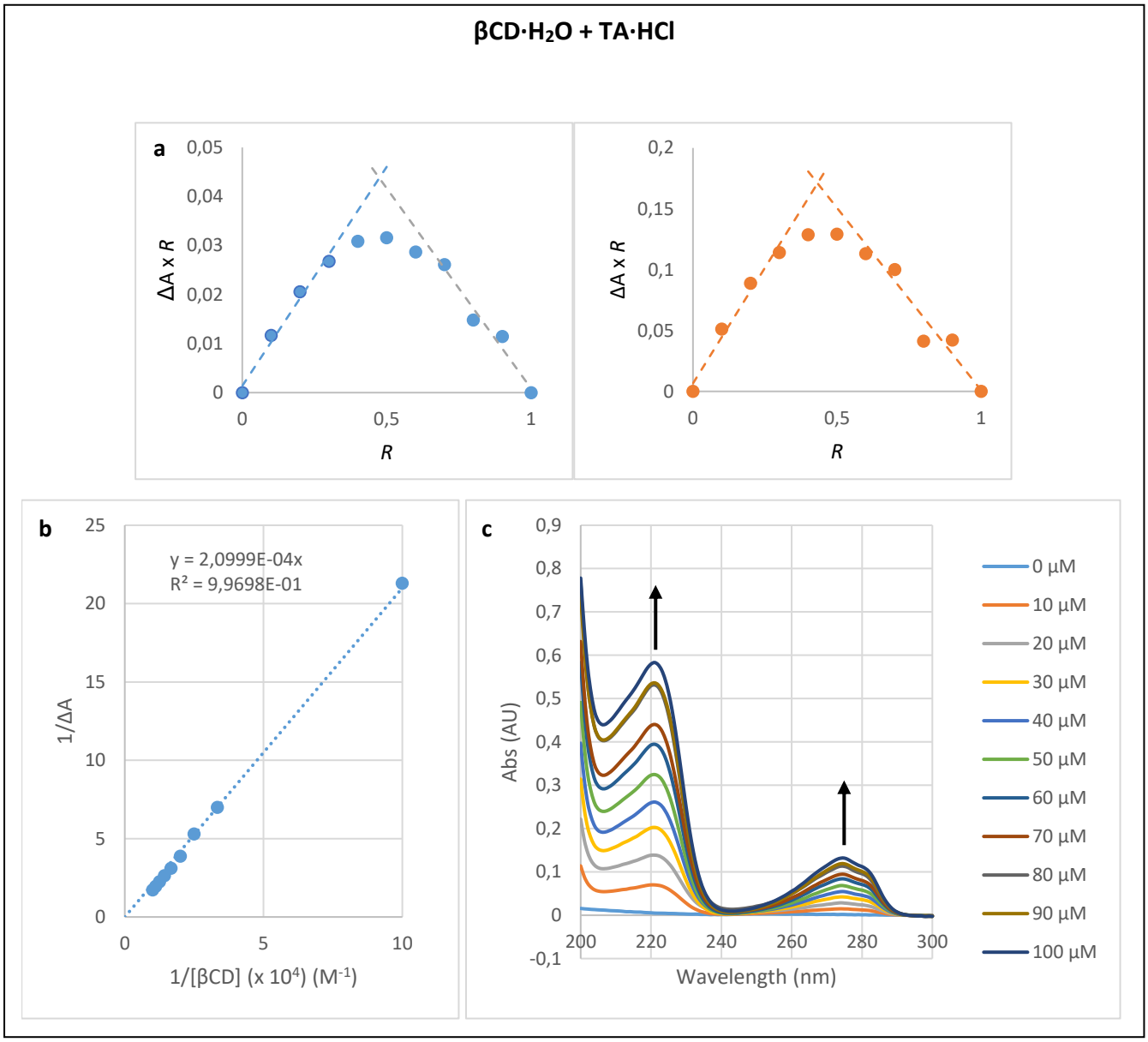

Figure 18. (a) Job plots of βCD·H_2O/TA·HCl complex at 274 nm (blue) and 221 nm (orange). (b) Benesi-Hildebrand plot (221nm) for 1:1 inclusion βCD·H_2O/TA·HCl complex. (c) UV-vis spectral changes of βCD·H_2O upon addition of TA·HCl (0-100 µM).

Table 8. Association constants K_a (M^{-1}) for each HG complex, calculated using equation 8, with dark green indicating the higher K_a values.

HG complex	K_a (M^{-1})
βCD·H_2O + TA·HCl	1299
Dex_{250}-βCD DS 6% #2 + TA·HCl	1193
Dex_{250}-βCD DS 5% + TA·HCl	1174
Dex_{500}-βCD DS 2% + TA·HCl	1176
PEG-βCD + TA·HCl	1217
βCD·H_2O + Dex_{250}-TA DS 8%	1449
βCD·H_2O + Dex_{250}-TA DS 4%	1457
βCD·H_2O + Dex_{500}-TA DS 4%	1417
βCD·H_2O + PEG-TA	1164

4.5. Stoichiometry determination by ^{1}H NMR titration

The supramolecular complexation stoichiometry between Ada/βCD and TA/βCD was investigated by ^{1}H NMR titration experiments. Using the Thordarson Group – Software the $\Delta\delta$ of the H-3' and H-5' βCD signals were plotted against the [G]/[H] molar ratio resulting in 1:1 binding isotherms (Figure 19). Corresponding association constants of 1.19×10^{4} M^{-1} and 46.6 M^{-1} were determined for respectively Ada/βCD and TA/βCD complexes.

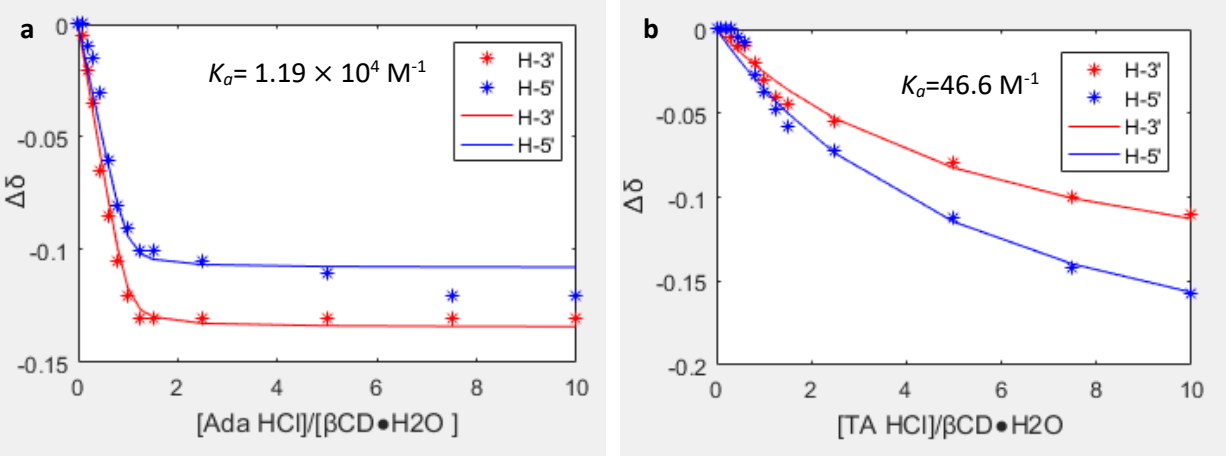

Figure 19. Experimental data (asterisk) and corresponding fitted curve (solid line) of the ^{1}H NMR titration binding isotherms of (a) βCD with Ada·HCl and (b) βCD with TA HCl.

The resulting ^{1}H NMR spectra are given in Figure 20 and Figure 20 respectively. In both spectra an upfield shift of the H-3' and H-5' signals of βCD was observed upon guest addition. The remaining βCD protons (H-1', 2', 4', 6') also showed shift changes but these were negligible compared to H-3' and H-5'. In the βCD/Ada·HCl complex was the $\Delta\delta$ of the H-3' signal higher as compared to the H-5' signal, where in the βCD/TA·HCl complex the $\Delta\delta$ of the H-5' signal was more pronounced than the H-3' signal. The $\Delta\delta$ of the βCD protons upon adamantane or tyramine addition are listed in SI 5 Table S3 and Table S4.

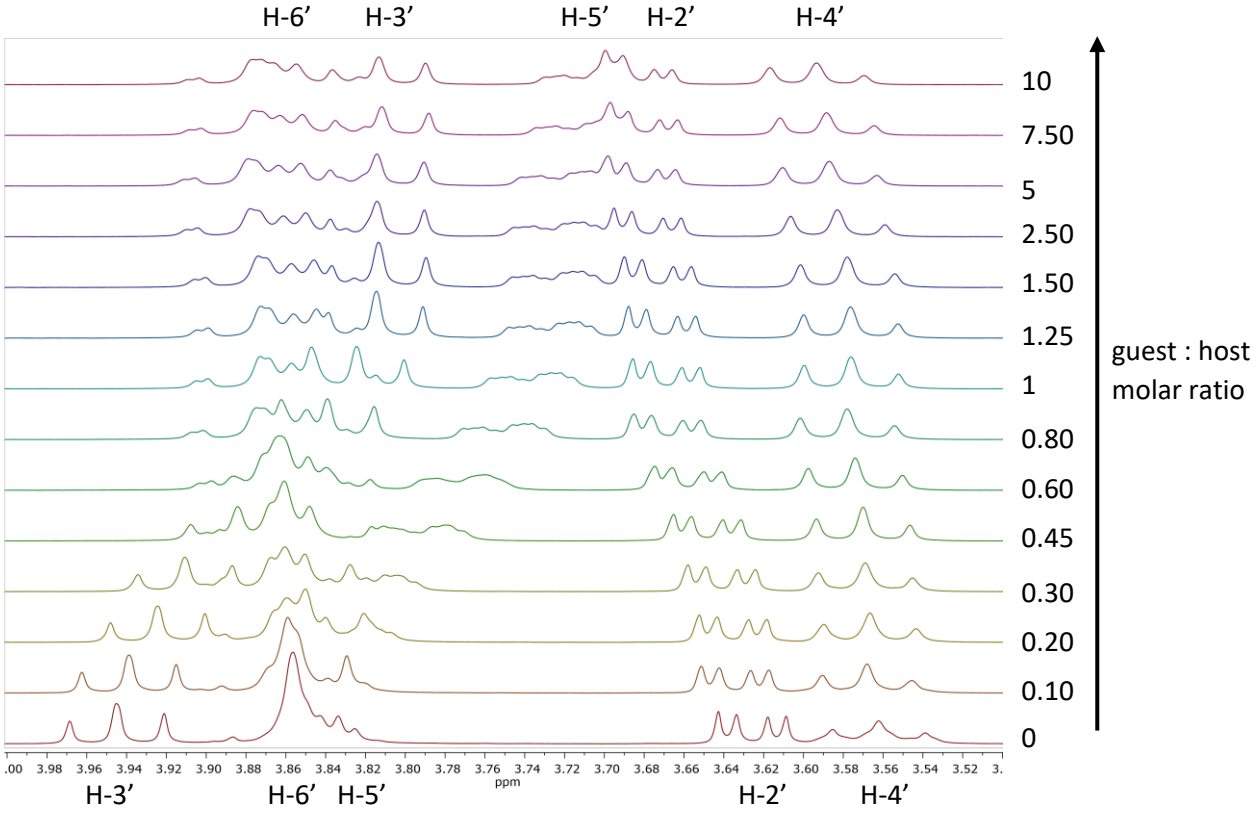

Figure 21. ^{1}H NMR spectra of βCD H-2’ – H-6’ region upon adamantane addition of 0-10 equivalent in D_2O.

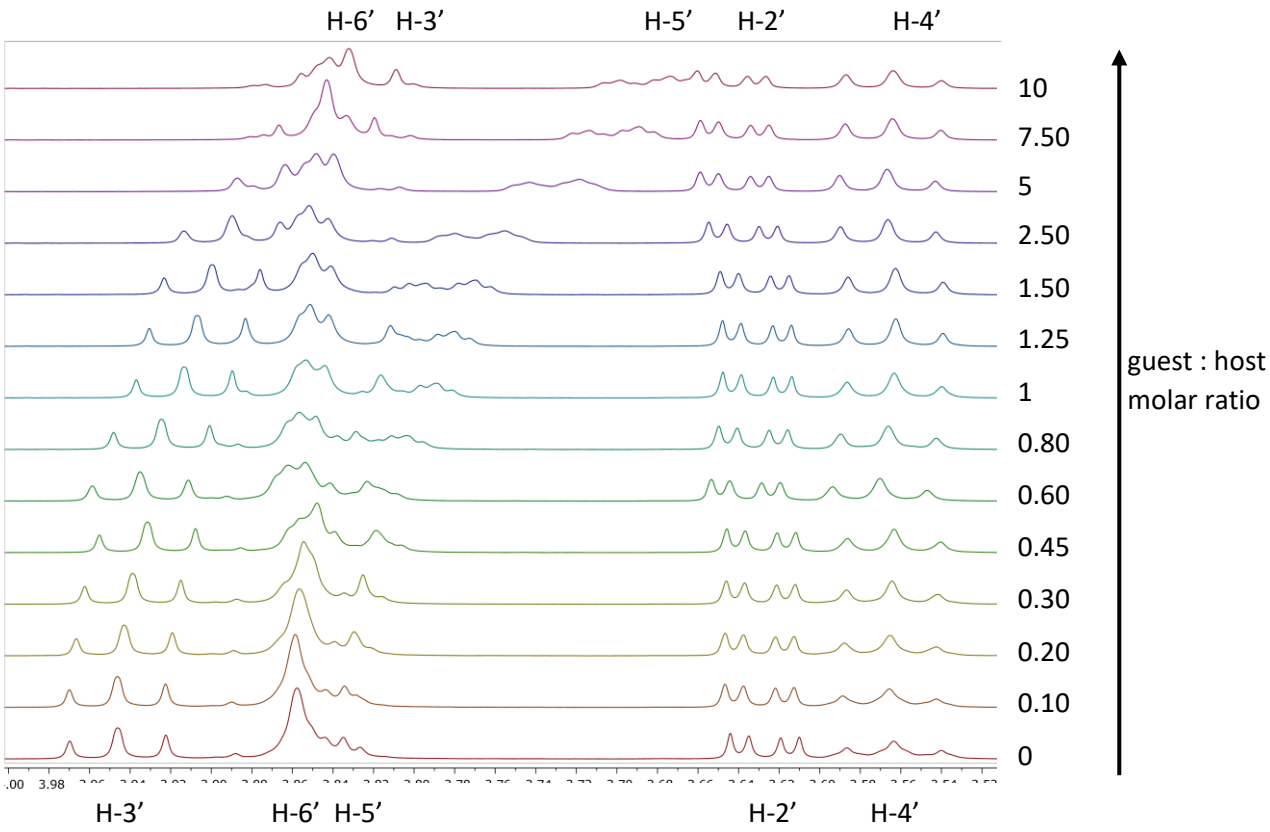

Figure 20. ^{1}H NMR spectra of βCD H-2’ – H-6’ region upon tyramine addition of 0-10 equivalent in D_2O.

4.6. Printability

Figure 8 shows the general 3D printing set-up of the Cellink+ 3D printer. The ink extrusion performed at RT, with a velocity of 10 mm/s, a nozzle diameter of 22G (0.64 mm) and a pressure of 163 kPa and 181 kPa for respectively test 1 and 2.

In test 1 PEG-βCD/PEG-Ada (1:1 H:G molar ratio, 10 wt%) containing 0.03% H_2O_2 ink was printed in 3.0% Xanthan stacked on pre-crosslinked Dex_{250}-TA DS 8% (5 wt%). Figure 22 shows the resulting printed filaments in green. In Xanthan the green ink was printed in a continuous straight line and was visible for 2 hours. The pre-crosslinked Dex_{250}-TA printing bath did not result in a homogeneous hydrogel, though was stable enough to support the ink. The green ink was printed in this bath in a straight line, but was discontinued at some places. Directly after printing the green printed filament could be observed in both support baths (Figure 22a). The green ink did not form a periphery crosslinked "shell" and after two hours the ink printed in the pre-crosslinked Dex_{250}-TA bath was no longer visible (Figure 22b and c).

Figure 23 shows the results of test 2, where green gelatin (0.03% H_2O_2) ink was printed in either Dex_{250}-βCD DS 6% #2/Dex_{250}-TA DS 4% (1:1 H:G molar ratio, 15 wt%, 4 HRP U/mL) or Xanthan (3.0%) support baths. In both baths the ink was printed in continuous straight lines, though the green dye of the ink printed in Dex_{250}-βCD/Dex_{250}-TA could diffuse through the medium (Figure 23a). Photos of the top view (Figure 23b and c) showed that after 2 hours the ink printed in Xanthan remained in place, while the ink printed in Dex_{250}-βCD/Dex_{250}-TA was distributed through the medium. No periphery crosslinked "shell" were formed.

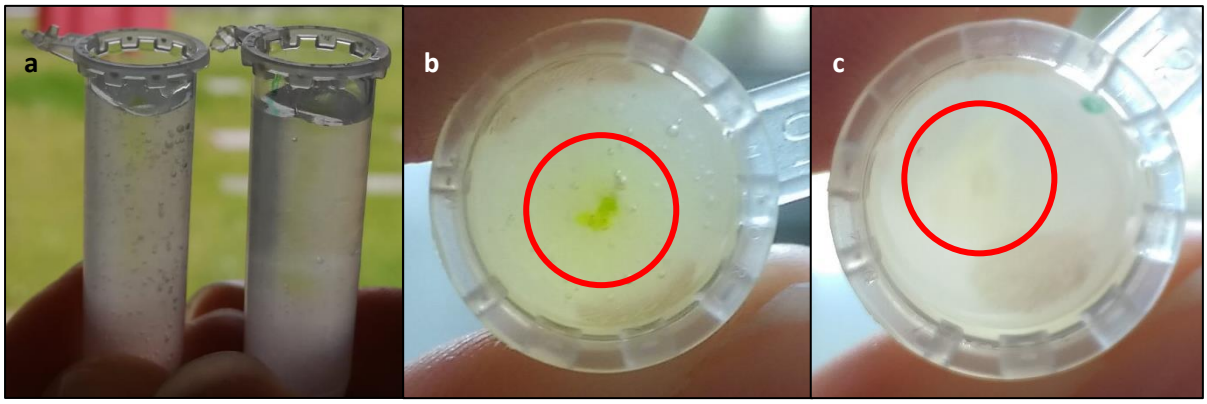

Figure 22. 3D printing test 1 in 2 mL Eppendorf tubes. PEG-BCD/PEG-Ada (1:1 H:G molar ratio, 10 wt%) with 0.03% H_2O_2 ink printed in (a) Xanthan (3.0%, left) vs pre-crosslinked Dex_{250}-TA DS 8% (5 wt%, right). Top views of PEG-βCD/PEG-Ada ink 2 hours after printing in (b) Xanthan and (c) pre-crosslinked Dex_{250}-TA DS 8% (5 wt%).

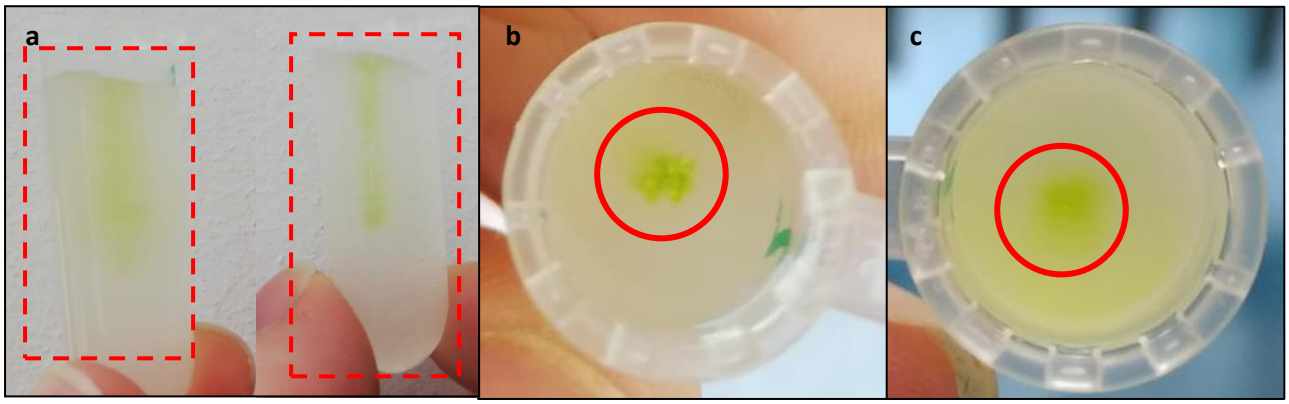

Figure 23. 3D printing test 2 in 2 mL Eppendorf tubes. Green gelatin 0.03% H_2O_2 ink printed in (a) Dex_{250}-βCD DS 6% #2/Dex_{250}-TA DS 4% (1:1 H:G molar ratio, 15 wt%, left) and Xanthan (3.0%, right). Top views of gelatin ink after 2 hours in (b) Xanthan and (c) Dex_{250}-βCD DS 6% #2/Dex_{250}-TA DS 4%.

4.7. Cytotoxicity assay

Jurkat cells were cultured in the gels Dex_{250}-βCD DS 6% #2/Dex_{250}-TA DS 4% (1:1 H:G molar ratio, 10 wt%) and PEG-Ada/PEG-βCD (1:1 H:G molar ratio, 10 wt%). As control culture medium was used. Cytotoxicity of these gels was evaluated by cell survival using a live/dead calcein-AM/ethidium homodimer assay. As shown in Figure 24, relatively no cell content was left in the wells. No life cells were visible that incubated in the gels nor in the control. Some debris or deformed cells remained and were stained red. In the control a deformed cell was visible and was stained both red and green.

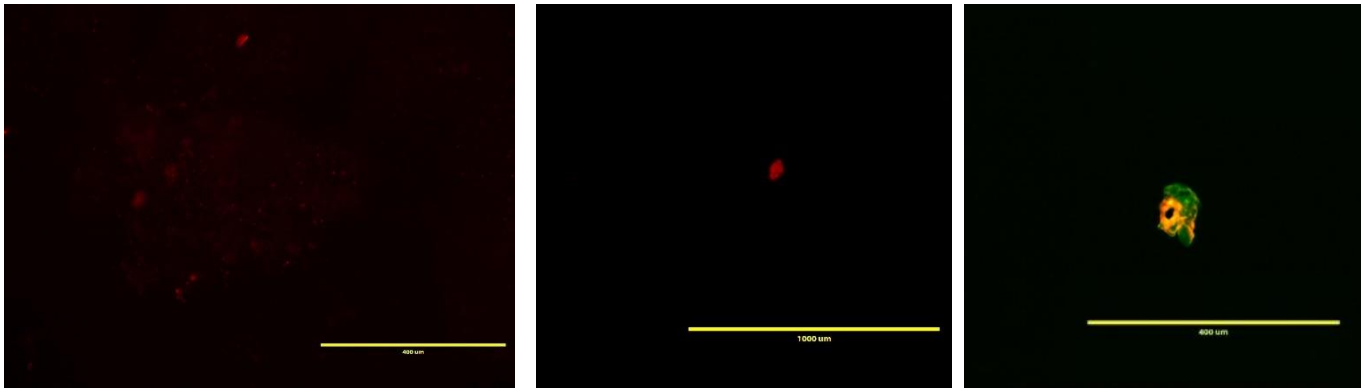

Figure 24. Live/dead assay of Jurkat cells in: (a) Dex_{250}-βCD DS 6% #2/Dex_{250}-TA DS 4% (1:1 H:G molar ratio, 10 wt%). 4x, scale bar=400 µm and (b) PEG-βCD + PEG-TA (1:1 H:G molar ratio, 10 wt%), scale bar=1000 µm. Culture medium was used as control, scale bar= 400 µm (c). Cells were stained with calcein-AM/ethidium homodimer (living cells stained green, and dead cells pale red).

5. Discussion

5.1. Polymer synthesis

When following a literature protocol as described in the Materials and methods section the DS of conjugated PNC is around 20%.[48,58] When the same protocol was applied for high MW (≥150 kDa) dextrans the DS varied from 3-18% and with low repeatability. PNC did not dissolve completely upon addition to the polymer solution. Larger polymers are in general less soluble as it is harder for solvent molecules to surround the long entangled polymer branches.[93] Incomplete dissolution of the dextran hinders dissolution of other additives. To promote complete dissolution of the polymers their solution time was extended, though this did not result in absolute dissolution of PNC. Purification of the obtained high MW dextrans and the usage of uncontaminated pyridine did not affect the dissolution of PNC. The synthesis procedure proved difficult to reproduce, as various DS (9% and 18%) were obtained. The low DS could result from the fact that high MW polymers have higher viscosity and poorer processability. Also, in case of natural polymers, their purest form are mixtures of molecules of different molecular weights.[93] Instead of linear polymer chains it is more likely that they are branched, though their branching degrees are not specified by their manufacturers. Dextran 250 kDa and 500 kDa had both sufficient DS of PNC (9-18%) and were selected for follow-up experiments. Dextran 150 kDa was excluded from successive experiments due to the low DS (2%) of PNC.

The initial reduction reaction of βCD-N_3 into βCD-NH_2 by Pd/C was adopted from Jicsinszky et al, where a yield of 90% was collected.[98] The active Pd/C reducing catalyst is deactivated by being soaked in water for longer than 10 minutes (poisoning effect). This water poisoning effect leads to decreased conversion acceleration of azide into amines and causes lower conversion and less reproducibility.[98] Unaware of this water poisoning effect, the in water suspended Pd/C was not directly added to the reaction solution and could therefore have caused the low βCD-NH_2 yield of 12.8%. Other possible causes of the low yield are alongside evaporation of the product with the solvents while on the evaporator rotary and adsorption of the product to the filtration filter. A yield of 82.9% was obtained by the mild azide reduction (Staudinger reaction). Here PPh_3 was used to react with the azide to generate a phosphazide, which loses N_2 to form an iminophosphorane. Our yield was lower by 7.1% as compared to the obtained yield by Jicsinszky et al. The reduced βCD-NH_2 via the Stauding reaction was characterized by ^{1}H NMR and FTIR spectroscopy which confirmed the product's purity. The Staudinger reaction was easier, faster and cheaper to perform as compared to the Pd/C catalysed reduction reaction.

The calculated DS of the polymers based on the corresponding ^{1}H NMR spectra are estimations, and could deviate from the actual DS. Notable are the DS estimations of Dex-βCD polymers. Here the DS were based on the anomeric dextran peak at 4.96 ppm and the anomeric βCD H-1' protons at 5.04 ppm. These two indicative signals partly overlap, resulting in overestimated DS. The calculated H:G molar ratios could therefore deviate from reality and influence the outcomes of successive experiments.

Dex_{250}-TA-Ada synthesis resulted in contradicting outcomes. Following the protocol, adamantane was added to a solution of Dex_{250}-PNC DS 18%. After the solution was stirred for 1 hour tyramine was added and the solution was stirred for another hour. The collected product was poorly soluble in water. Addition of DMSO did promote dissolution of the product, however not completely. Addition of hydrophobic adamantane groups onto the polymer could have caused this behaviour. However ^{1}H NMR spectra (Figure S18) revealed that adamantane was not present nor bound to dextran while tyramine proved to be successfully conjugated to the polymer with a DS of 6.8%. These contradicting results cannot be explained from our data and should be further investigated. Furthermore, the synthesis protocol should be adjusted in order to synthesize Dex-TA-Ada.

5.2. Hydrogel formation

Dextran consists of hydrophilic sugar molecules and has good solvability in aqueous solutions. This feature can be modified by the addition hydrophobic moieties, such as adamantane and tyramine. Earlier investigations within this research group have shown that a DS of tyramine above 15% resulted in poor solubility of the Dex-TA, while Dex-TA polymers with a DS lower than 15% were soluble in aqueous solutions. This study has shown that the guest polymers synthesized with high MW dextran, all with a DS <15%, were soluble in water with Dex_{250}-TA-Ada as the exception. These dissolved guest polymer solutions coloured opaque as a result of attracting hydrophobic interactions between the guest moieties. Hydrophobic associations between guest moieties, as depicted in Figure 25, colours the solution opaque by scattering light.[108] Inclusion of the hydrophobic guest into the βCD cavity disrupts these hydrophobic associations and result in a clear solution instead of opaque.[108] The more stable hydrogels formed with PEG-Ada (1:1 H:G molar ratio, 10wt%) were clear of colour, suggesting sufficient HG complexation. The viscous mixtures were opaque coloured, suggesting hydrophobic associations between the guest moieties instead of saturated HG complexation. However, the mixture PEG-Ada/Dex_{250}-βCD DS 5% (1:1 H:G molar ratio, 10 wt%) was a stable weak gel but opaque coloured, undermining the aforementioned reasoning.

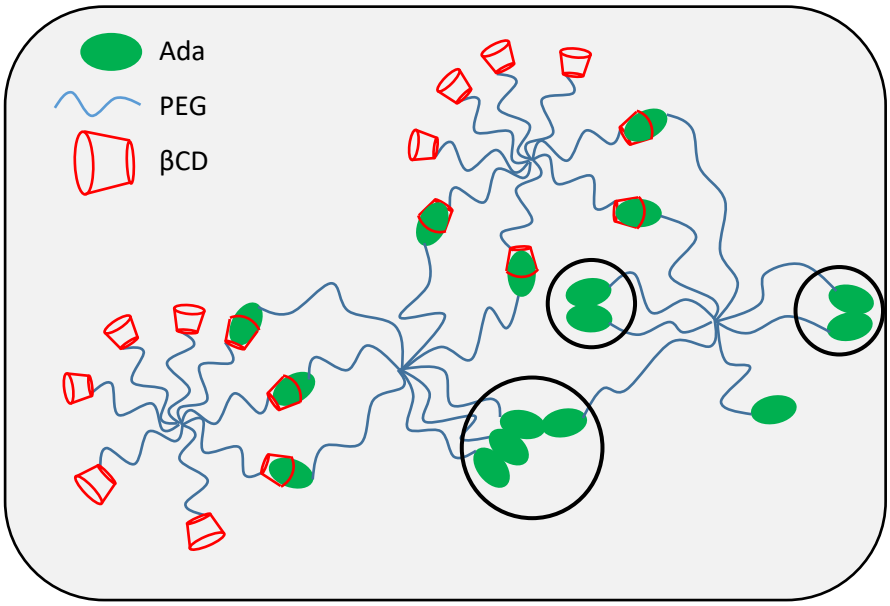

Figure 25. Schematic dynamic supramolecular network between 8arm-PEG-βCD and 8arm-PEG-Ada and hydrophobic associations (circled).

Mixing Dex_{250}-βCD DS 6% #1 with Dex_{250}-TA DS 4% resulted in a hydrogel, though after 45 minutes the gel converted into a viscous liquid. The mixture was opaque in both the gel and liquid phase (Figure 13). Gel formation validates successful HG complexation between βCD and tyramine, however this proved not optimal as the gel reorganized itself towards a viscous liquid. The opaque colour implies that besides HG complexation also hydrophobic associations between tyramines are formed. Steric hindrance and diffusion forces are also variables that influences HG complexation. The observed phase transitions suggests that the binding strength of βCD to tyramine is too weak to overcome these driving forces. However, it is remarkable that the transition of the gel-phase towards the liquid-phase depended on the DS of Dex_{250}-TA. Dex_{250}-βCD DS 6% #1 mixed with Dex_{250}-TA DS 8% resulted in a 15 minutes stable gel, whereas the Dex_{250}-βCD DS 6% #1/Dex_{250}-TA DS 4% mixture remained in the gel-phase for 45 minutes. The transition to viscous liquid was not reversible as the gel-phase of the mixture could not be reintroduced, not by vortexing nor by adjusting the temperature or pH.

It is notable that upon mixing Dex_{250}-βCD DS 6% #2 with Dex_{250}-TA DS 4% no hydrogel was formed, whereas the mixture Dex_{250}-βCD DS 6% #1/Dex_{250}-TA DS 4% resulted in a temporary gel. The Dex_{250}-βCD polymers were prepared with different βCD-NH_2 batches. However, ^{1}H NMR spectra confirmed that these βCD-NH_2 batches were both pure substances and that Dex_{250}-βCD DS 6% #1 and Dex_{250}-βCD DS 6% #2 were nearly identical (Figure 26). As aforementioned, in the case of natural polymers their purest forms are mixtures of molecules of different molecular weight and branching degrees.[93]

PEG-βCD mixed with PEG-TA did not result in a hydrogel, and neither of them could form stable gels upon mixing with the complementary dextran polymers. 8-arm-PEGs are structurally well defined and its 3D structure should promote collision between the host and guest moieties. Our gel mixing results confirmed that PEG-Ada was capable of hydrogel formation through supramolecular complexation upon 1:1 H:G molar ratio mixing with our synthesized βCD polymers (10wt%). However, these gels tended to be weak and could remain in the vial tip only for about 30 seconds. This could be a consequence of the presence of unbound adamantane in the freeze dried product. Unbound adamantanes occupying βCDs lower the degree of physical crosslinks between polymers, decreasing hydrogel stability. The viscosity reached a maximum with a 1:1 H:G molar ratio and decreased when the host or the guest concentration exceeded the other. These observations were visually obtained, and rheology measurements should be performed to confirm that these mixtures are viscoelastic hydrogels instead of viscous liquids.

Considering all these observations it is evident that mixtures of βCD conjugated and TA conjugated polymers could not be physically crosslinked by HG interactions, whereas the complexations between βCD and adamantane were capable of physical crosslinking.

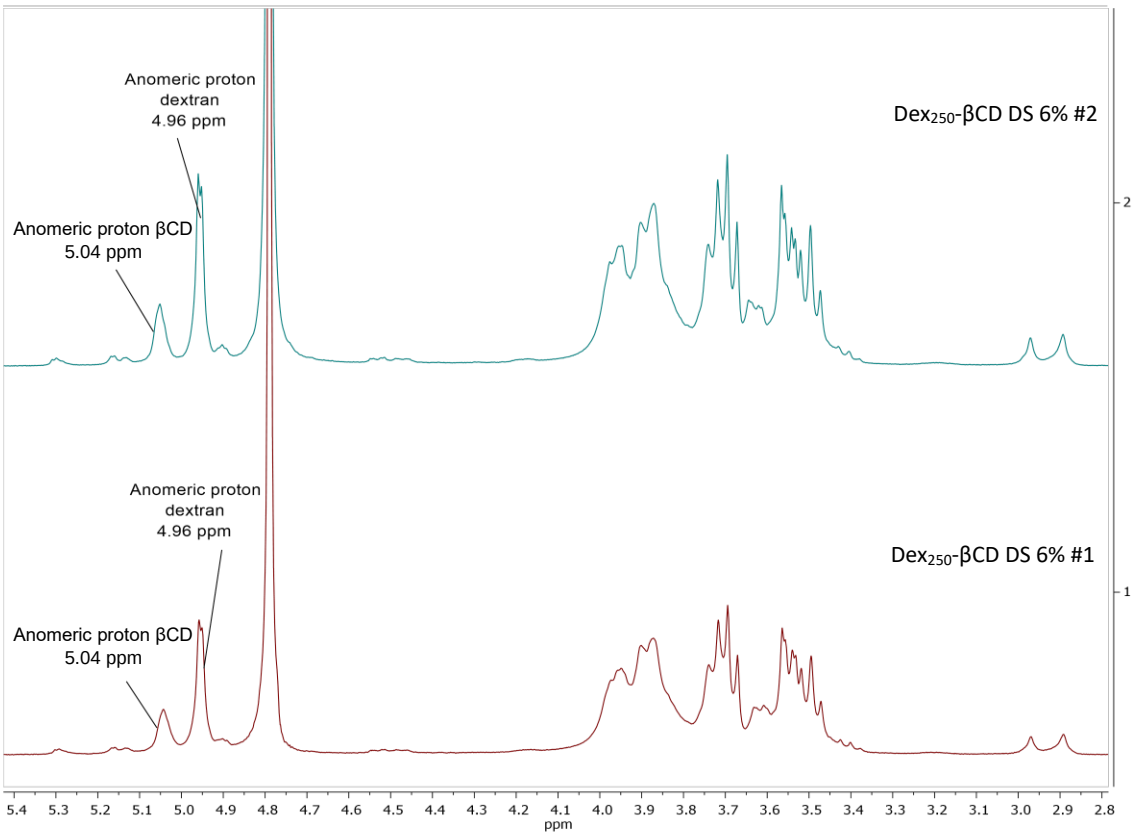

Figure 26. ^{1}H NMR spectra of Dex_{250}-βCD DS 6% #2 (blue) and Dex_{250}-βCD DS 6% #1 (red) (400 MHz, D_2O) δ: 4.96 (s, 1H, anomeric proton dextran), 5.04 (s, 7H, anomeric proton βCD)

Another interesting part of the Dex-βCD/Dex-TA mixtures are the observed fibers. These fibers were investigated by microscopic pictures and ^{1}H NMR measurements. Microscopic pictures (Figure 13) of the HG polymer solution showed the fibers, with a length of ~450 µm and a width of ~25 µm. ^{1}H NMR measurement were performed with isolated fibers. Figure 15 shows the stacked spectra of Dex_{250}-TA DS 8%, βCD and fibers. Comparing these spectra's it can be seen that βCD, tyramine and dextran are all present in the fibers. The protons signals of βCD and tyramine are low as compared to the dextran signals, and the H:G ratio of 1.0:1.7 implies a 1:2 assembling ratio.

The fibers' sensitivity to pH change was tested as well. By pH adjustment from 7 to 12 the phenol ring of tyramine deprotonates, increasing the dipolar moment and therefore increasing its hydrophilicity. However, adjusting the pH did not affect the fibers' structures. The fibers proved non-responsive to temperature change as well. Upon DMSO addition the fibers disintegrated and the solution became more liquid. Hydrophobic guest molecules are better soluble in DMSO as compared to aqueous solutions, hence disintegrated the complexes between βCD and tyramine.[109]

According to literature these macromolecular fibers are assembled in a higher tertiary structure and are hard to obtain.[85] Yan et al.[110] designed a new methodology to design molecular assemblies that could sense biomolecules and drive shape transformation. The observed macromolecular fibers structures in our mixed polymer solutions have an automatic hydrophilic–hydrophobic imbalance. It is interesting to investigate whether our system can qualify as a new methodology that can sense biomolecules and drive shape transformations by the addition of hydrophobic moieties as done by Yan et al.

Attempts to prepare hydrogels by secondary chemical crosslinking did not succeed. Concentrations of HRP (4 U/mL) and H_2O_2 (0.03%) were based on standard Dex_{40}-TA DS 10% procedures used within the DBE research group. Mixing Dex_{250}-βCD DS 6% #2 with Dex_{250}-TA DS 4% in a 1:1 H:G molar ratio (10 wt%) results in a tyramine concentration of 13.3 mM. The concentration of HRP can be rewritten in a HRP/TA ratio of 1.14 mg HRP/mmol TA. A H_2O_2 concentration of 0.03% equals 9.8 mM and is therefore present in a H_2O_2/TA ratio of 0.74 (mol/mol). Both ratios are considerably higher than the 0.25 mg HRP/mmol TA and 0.20 H_2O_2/TA ratios used in other studies. Within these studies ratios were selected based on their gelation time (within 1 minute), which offers processability of the material before crosslinking.[48,111] The higher HRP/TA and H_2O_2/TA ratios used in our tests could therefore have caused the fast enzymatic crosslinking of Dex_{250}-TA DS 4%. It is advisable to adjust the HRP and H_2O_2 concentrations according to the HRP/mmol TA and H_2O_2/TA (mol/mol) ratios used in literature and repeat these crosslinking experiments. Successful crosslinked hydrogels can then be characterized by rheology measurements.

The proposed supramolecular hydrogel system is appealing due to the physical crosslinking by HG interactions and covalent crosslinking of tyramine by HRP/H_2O_2 addition. Results have shown that βCD/TA HG complexation is not sufficient for physical crosslinking, though βCD/Ada complexation is. Novel polymers modified with two different moieties, such as Dex-βCD-TA and Dex-TA-Ada, could offer adequate physical crosslinking while the mixture can be enzymatic crosslinked as well.

5.3. Stoichiometry determination of HG complexation of βCD/TA and βCD/Ada

It was demonstrated that βCD·H_2O/TA·HCl had a 1:1 binding complexation (R=0.5) and via UV-vis spectroscopy an association constant of 1242 M^{-1} was calculated (Roy et al.[80] Supplementary Table S11). Our stoichiometry determination by UV-vis measurements was based on Job's method of continuous variation and Benesi-Hildebrand plots. The Job plots showed R=0.5 for all the HG complexes, indicating a 1:1 binding complexation (SI 4). Table 8 shows the calculated K_a values for the polymers. The calculated K_a value for βCD.H_2O/TA·HCl was 1299 M^{-1}, which does not deviate too much from the literature value (1242 M^{-1}). Dex_{250}-βCD DS 6% #2 (1457 M^{-1}) had the highest calculated K_a

value of the βCD polymers and Dex_{250}-TA DS 4% (1193 M^{-1}) of the tyramine polymers. Evidently these K_a values edge the lower limit of the needed binding strength, as these polymers could not form a hydrogel upon mixing, whereas the Dex_{250}-βCD DS 6% #1/Dex_{250}-TA DS 4% mixture did result in a temporary gel. Unfortunately the K_a value of Dex_{250}-βCD DS 6% #1 could not be determined via UV-vis measurements as there was not enough material left. Both PEG-βCD and PEG-TA had low K_a values, accounting the low viscous liquids that resulted from mixing them with eachother and the other polymers. Adamantane is optically inert and its stoichiometry cannot be determined with UV-vis measurements.

According to Pall Thordarson[95] the Benesi-Hildebrand linear regression method is out-dated, as they introduce a number of problems such as equating the total concentration of the guest $[G]_0$ with the free (unbound) concentration of the guest [G] or that the measured quantity (e.g., absorbance change ΔA) equals the change in the concentration of the complex [HG]. These problems can be avoided with modern computer-based non-linear regression methods.

Therefore the assembly ratio and K_a of the βCD.H_2O/Ada·HCl binding complex were determined via a ^{1}H NMR titration experiments and a computer-based non-linear regression method provided by Pall Thordarson. Also ^{1}H NMR titration experiments were performed with βCD.H_2O/TA·HCl and these values were compared and verified to the UV-vis obtained values. The K_a for βCD/TA·HCl calculated by the ^{1}H NMR titration experiments (46.6 M^{-1}) is significantly lower than the constant calculated by UV-vis (1299 M^{-1}) and does not match the results from Roy et al.[80] This large deviation is hard to explain, though it could be a consequence of the low concentrations ([βCD]=4.41 µM, [G]=0-44.1 µM) used in the titration experiments as compared to the 100 µM used during UV-vis measurements. However, the calculated K_a value for βCD/Ada·HCl complexation (1.19×10^4 M^{-1}) does match the values found in literature (10^4-10^5 M^{-1}) and similar concentrations were used as for the βCD/TA·HCl titration experiments.[72-74,85] The constructed binding isotherms (Figure 19) do also clearly indicate that the stronger complex is formed by βCD/Ada·HCl and the weaker complex by βCD/TA·HCl, confirming the calculated K_a values.

The observed chemical shifts ($\Delta\delta$) of the βCD's H-3' and H-5' signals are assigned to magnetic shielding of the βCD protons due to the guest inclusion and thus confirms the inclusion complex between βCD and the guest molecules.[112] Both βCD/Ada·HCl and βCD/TA·HCl ^{1}H NMR spectra show shifts of the H-3' and H-5' protons affirming the inclusion of both Ada·HCl and TA·HCl. The other protons (H-1', H-2', H-4' and H-6') were less affected. In the βCD/Ada·HCl complex was the $\Delta\delta$ of the H-3' signal higher than $\Delta\delta$ of the H-5' signal, whereas in the βCD/TA·HCl complex the $\Delta\delta$ of the H-5' signal was more pronounced than the H-3' signal (SI 5 Table S3 and Table S4Table S1). As the H-5' proton lies deeper in the βCD cavity, it would suggest that the TA·HCl penetrates the cavity deeper than the Ada·HCl and could have therefore a stronger binding. However, the association constant increases with the degree of space filled of the βCD cavity.[83] With a diameter of 4.3 Å it is likely that TA·HCl penetrates the βCD cavity deeper, but as less space is filled fewer hydrophobic and non-polar van der Waals interactions occur as compared to the near perfect fit of Ada·HCl (6.4 Å). Also, the H-2' proton in the βCD/Ada·HCl experiments showed a downfield $\Delta\delta$ of +0.06 ppm towards the H-5' signal until they overlapped. The H-2' signal of the βCD/TA·HCl had a lower downfield $\Delta\delta$ of +0.02 ppm. This implies a larger conformational change of the H-2' proton in the βCD/Ada·HCl complex and could be caused by the increased hydrophobic and non-polar van der Waals interactions. In order to investigate the structures of the complexes formed a ^{1}H ROESY (Rotating frame Overhause Effect SpectroscopY) should be conducted. ^{1}H ROESY can determine which signals arise from protons that are close to each other in space even if they are not bonded and can detect chemical and conformational change.[113]

Important to consider is the fact that free adamantane (or water soluble Ada·HCl) has a much higher reported K_a value of 10^4-10^5 M^{-1} as compared to bound adamantane guest units, which has a reported K_a value of 1500 M^{-1}.[72-74,85] Likely this observation applies as well to free and bound tyramine. Our calculated K_a values by ^{1}H NMR titration were based on the HG complexation of free molecules and therefore only an indication for the HG complexation between conjugated hosts and guests moieties. The K_a values of the conjugated hosts and guests is possibly lower due to the steric hindrance by the polymer backbone. However, multiple host and guest moieties are conjugated to one polymer. The formation of one HG complex decreases the distance of the polymer backbones to which they are bound, increasing the probability of HG complexation of the surrounding moieties. This can cause a cascade affect that overcomes the steric hindrance and increases the K_a value. ^{1}H NMR titration experiments with conjugated host and guest moieties should be performed in order to calculate the appropriate corresponding K_a values.

5.4. Printability

HG polymer combinations were selected that formed a gel or a solution with high viscosity to serve as ink or support bath. In the first test PEG-βCD/PEG-Ada (1:1 H:G molar ratio, 10 wt%) containing 0.03% H_2O_2 ink was printed in 3% Xanthan stacked on pre-crosslinked Dex_{250}-TA DS 8% (5 wt%). First 5 mg of Dex_{250}-TA DS 8% was dissolved in 70 µL, and 10 µL HRP (40 U/mL stock solution) and 20 µL H_2O_2 (0.03% stock solution) were added and vortexed. This resulted in a homogeneously crosslinked gel with a desirable viscosity for printing. However, when 1.0 mL pre-crosslinked Dex_{250}-TA DS 8% was prepared with the same ratios a gel was obtained with uneven distributed crosslinking. Therefore 100 µL H_2O_2 (0.03% stock solution) was added, which resulted in a more homogeneously crosslinked gel that could be used as printing bath. The green ink was printed in this bath in a straight line, but was discontinued at some places. This could be the result of the uneven distributed crosslinking of the support bath. The green ink did not form a periphery crosslinked "shell" and after two hours the ink printed in the pre-crosslinked Dex_{250}-TA bath was no longer visible. This indicates that the H_2O_2 concentration in the ink was too low for sufficient crosslinking of the bath. As a consequence no outer shell was formed and the green dye could diffuse freely through the medium. It is desirable to obtain a homogeneously crosslinked Dex_{250}-TA DS 8% by optimizing the HRP/mmol TA and H_2O_2/TA (mol/mol) ratios. Also various H_2O_2 concentrations (0.03-0.3%) in the ink should be tested in order to determine the optimal concentration for crosslinking the support bath and shell formation.

In the second test Dex_{250}-βCD DS 6% #2/Dex_{250}-TA DS 4% (1:1 H:G molar ratio, 15 wt%) was investigated if the solution could function as support bath. Green gelatin (0.03% H_2O_2) ink was printed in the Dex_{250}-βCD DS 6% #2/Dex_{250}-TA DS 4% bath and in a Xanthan (3%) bath as comparison. In both baths the ink was printed in continuous straight lines, though the green dye of the ink printed in Dex_{250}-βCD/Dex_{250}-TA could diffuse through the medium. After 2 hours the ink printed in Xanthan remained in place, while the ink printed in Dex_{250}-βCD DS 6% #2/Dex_{250}-TA DS 4% was distributed through the medium and no periphery crosslinked "shell" was formed. Evidently no sufficient crosslinking took place. This printing experiment shows some promise and more printing tests should be performed in order to optimizing the HRP/mmol TA and H_2O_2/TA (mol/mol) ratios.

5.5. Cytotoxicity

Unfortunately the performed live/dead assay with Jurkat cells proved unsuccessful. Jurkat cells were cultured in the gels Dex_{250}-βCD DS 6% #2/Dex_{250}-TA DS 4% (1:1 H:G molar ratio, 10 wt%) and PEG-βCD/PEG-Ada/ (1:1 H:G molar ratio, 10 wt%). Medium culture was used as control. The executed protocol was provided by our research group. Since this protocol was not yet optimal, some adjustments were made. However it was known that this protocol was not optimal. Previously

performed live/dead assays on Jurkat cells resulted in cells that were stained both green and red. This could be a result of non optimal concentrations of ethidium homodimer and calcein AM. Therefore, the concentrations were altered to the values provided in the protocol drafted by Jaqueline van der Plas. The cells were washed twice with PBS after incubation. To ensure minimal cell loss not all PBS was aspirated during these washing step, nonetheless this precaution has failed as nearly no cells were observed by EVOS microscopy (Figure 24). The observed cell debris were mainly coloured red, and some deformed cells were stained both green and red. No conclusive observations could be obtained about the cytotoxicity of the tested gels. From these results it can be concluded that the live/dead assay be repeated following a different assay suitable for Jurkat cells, such as WST-1 viability test.[114] Another option is to use alternative cells that are known to be compatible with the live/dead calcein-AM/ethidium homodimer assay should be used, such as HUVECs.

5.6. Possible applications for the proposed supramolecular hydrogel

It would be interesting to further investigate the temporary gel derived from Dex_{250}-βCD DS 6% #1/Dex_{250}-TA DS 4% mixing. To our knowledge, a hydrogel system that does not require chemical agents nor environmental adjustments in order to transition from a gel-phase into a liquid-phase has not been reported. Key factors in this "self-sacrificing" system are controllability over the duration of the gel-phase, mechanical properties of the gel-phase and reproducibility. The mechanical properties should be investigated by rheological measurements in order to determine the exact behaviour of the mixture from gel- to liquid-phase. The time that the mixture is in the gel phase can be measured, alongside with the storage modulus and whether it has self-healing abilities. Shear-thinning properties will be harder to characterize as the main feature of the gel is similar to shear-thinning behaviour. The option of secondary crosslinking of the tyramines by HRP/H_2O_2 addition should also be investigated. When these variables are characterized and controllable, the self-sacrificing hydrogel can be applied in multiple research areas.

The temporary Dex_{250}-βCD DS 6% #1/Dex_{250}-TA DS 4% gel mixture could be used for designing microfluidic networks. When this mixture is incorporated with H_2O_2 and printed in a support bath containing tyramine and HRP, crosslinking of the tyramines at the contact area occurs. As H_2O_2 can diffuse into the bath medium a mechanical stable "shell" around the printed filament will be formed by the crosslinked tyramines. When the Dex_{250}-βCD DS 6% #1/Dex_{250}-TA DS 4% mixture reaches its liquid-phase the created tunnel-like structures can be flushed without the need of additives and can then function as perfusion networks.

The self-sacrificing gel could also be applied as biomaterial for endovascular embolization during surgery. As of yet, many embolic materials are correlated with various complications, such as breakthrough bleeding, coil migration, coil compaction, recanalization, adhesion of the catheter to the embolic agent or toxicity.[115,116,117] Materials applied for endovascular embolization require to be sterile, injectability through long catheters and should offer fast gelation on site to create an occlusive seal that prevents breakthrough bleeding. The capacity to repair shear-stress induced damage is desirable as well.[115] Important is to determine whether the mechanical stability of our self-sacrificial gel is sufficient to create a proper occlusive seal. Also controllability of the duration of the gel-phase is vital to ensure that the surgeons can finish the procedure before the seal flushes away.

A recent study by Rogan et al.[118] showed that single cell encapsulation of mesenchymal stem cells (MSCs) in hydrogels led to enhanced MSC-based cartilage formation as compared to encapsulated MSC aggregates. Upon injection of the MSC encapsulated hydrogel into the cartilage defect the hydrogel should withstand the compressive load of native cartilage which is over 1 MPa.[119] However, Roy et al showed that MSCs encapsulated in soft hydrogels (0.5-10 kPa) excreted more cartilage matrix as compared to MSCs encapsulated in stiff hydrogels (20-100 kPa). When single cells are encapsulated in a layer of soft hydrogel before they are mixed into the stiffer hydrogel, specialized niches will be

created that provide a more optimal cell-matrix interactions while mechanical properties of the entire hydrogel is maintained. Interesting is to investigate if our temporary gel could be used as a single cell encapsulation system. The general idea would be to form a gel layer around single MSCs with our HRP containing temporary gel. Upon mixing these encapsulated MSCs into a stiffer hydrogel, containing H_2O_2, crosslinking of the tyramines at the hydrogels contact site can occurs. As H_2O_2 can diffuse through the gel a mechanical stable “shell” will be formed by the crosslinked tyramines. When the temporary gel remodels itself towards the liquid-phase the formed shell will prevent its diffusion into the surrounding medium. This system will result in encapsulated MSCs in the desired soft environment while being in mixed in stiffer hydrogels.

6. Conclusions

A novel supramolecular hydrogel system for embedded bioprinting was designed based on HG interactions between βCD and tyramine groups conjugated to either dextran or 8arm-PEG. Mechanical strength was obtained by enzymatic crosslinking of tyramine using HRP as a catalyst and H_2O_2 as an oxidant. Adamantane was as well conjugated to 8arm-PEG in order to compare our system with βCD/Ada HG systems. Dex-βCD and Dex-TA conjugates with desired degrees of substitution were synthesized with 250 kDa and 500 kDa dextrans. The degree of substitution of PNC to 150 kDa dextran proved too low and was excluded from successive experiments. The synthesis of Dex_{250}-TA-Ada resulted in contradicting outcomes and should be further investigated in order to determine its hydrophobic behaviour while no adamantane conjugation to the dextran was be detected by ^{1}H NMR measurements.

Our gel mixing results confirmed that PEG-Ada was capable of hydrogel formation through supramolecular complexation and reached a maximum with a 1:1 H:G molar ratio and decreased when the host or the guest concentration exceeded the other. These gels tended to be weak and could remain in the vial tip only for about 30 seconds. Temporary gels were rapidly formed by mixing Dex_{250}-βCD DS 6% #1 with Dex_{250}-TA DS 8% and Dex_{250}-TA DS 4% for respectively 15 minutes and 45 minutes. The other mixtures resulted in opaque coloured viscous liquids which were not able to remain in the vial tip upon tilting. Fibers were present in the dextran polymer mixtures and absent in PEG mixtures. Stoichiometry and association constant determination by UV-vis and ^{1}H NMR titration experiments confirmed a 1:1 HG binding ratio, strong binding between βCD/Ada and weak binding between βCD/TA conjugates. These results validated that supramolecular HG interactions between βCD and tyramine groups on dextran or 8arm-PEG backbone are not strong enough to physically crosslink and form a stable hydrogel. Also the desired potential shear-thinning and self-healing properties of the supramolecular hydrogels could not be validated by rheological measurements as no stable gels were formed. New polymers, conjugated with both host and guest moieties could offer the desired physically crosslinked hydrogel while preserving the option of enzymatic crosslinking of the tyramines.

Inadequate mechanical strength was obtained by enzymatic crosslinking of tyramine using HRP as a catalyst and H_2O_2 as an oxidant due to the use of incorrect HRP/TA and H_2O_2/TA ratios. It is advisable to adjust the HRP and H_2O_2 concentration according to the HRP/mmol TA and H_2O_2/TA ratios used in literature and repeat these crosslinking experiments.

Although our βCD/TA hydrogel system was unable to form stable physically crosslinked hydrogels, Dex_{250}-βCD DS 6% #2/Dex_{250}-TA DS 4% (1:1 H:G molar ratio, 15 wt%) was selected to function as support bath and in another tests PEG-βCD/PEG-Ada (1:1 H:G molar ratio, 10 wt%) functioned as bioink. The chosen support bath and bioink materials proved to be compatible with embedded bioprinting, however the HRP/TA and H_2O_2/TA ratios needed to be adjusted as well in order to sufficiently crosslink the tyramines.

Finally, the performed live/dead assay with Jurkat cells to determine cytotoxicity of our selected mixtures proved unsuccessful. Alternative protocols should be followed suitable for Jurkat cells or a different cell type should be used.

7. References

1. Mandrycky C, Wang ZJ, Kim K, Kim DH. 3D bioprinting for engineering complex tissues. *Biotechnology Advances.* 2016; 34(4): 422-434.
2. Chia HN, Wu BM. Recent advances in 3D printing of biomaterials. *Journal of Biological Engineering.* 2015; 9(1): 4.
3. Badylak SF, Taylor D, Uygun K. Whole-organ tissue engineering: decellularization and recellularization of three-dimensional matrix scaffolds. *Annual review of biomedical engineering.* 2011; 13: 27-53.
4. Bajaj P, Schweller RM, Khademhosseini A, West JL, Bashir R. 3D biofabrication strategies for tissue engineering and regenerative medicine. *Annual review of biomedical engineering.* 2014; 16: 247-276.
5. Annabi N, Nichol JW, Zhong X, et al. Controlling the porosity and microarchitecture of hydrogels for tissue engineering. *Tissue Engineering Part B: Reviews.* 2010; 16(4): 371-383.
6. Ford MC, Bertram JP, Hynes SR, et al. A macroporous hydrogel for the coculture of neural progenitor and endothelial cells to form functional vascular networks invivo. *Proceedings of the National Academy of Sciences.* 2006; 103(8): 2512-2517.
7. Madihally SV, Matthew HW. Porous chitosan scaffolds for tissue engineering. *Biomaterials.* 1999; 20(12): 1133-1142.
8. Mehrabanian M, Nasr-Esfahani M. HA/nylon 6, 6 porous scaffolds fabricated by salt-leaching/solvent casting technique: effect of nano-sized filler content on scaffold properties. *International journal of nanomedicine.* 2011; 6: 1651.
9. Hsu YY, Gresser JD, Trantolo DJ, Lyons CM, Gangadharam PR, Wise DL. Effect of polymer foam morphology and density on kinetics of in vitro controlled release of isoniazid from compressed foam matrices. *Journal of Biomedical Materials Research: An Official Journal of The Society for Biomaterials and The Japanese Society for Biomaterials.* 1997; 35(1): 107-116.
10. Shapiro L, Cohen S. Novel alginate sponges for cell culture and transplantation. *Biomaterials.* 1997; 18(8): 583-590.
11. Miyata T, Sohde T, Rubin AL, Stenzel KH. Effects of ultraviolet irradiation on native and telopeptide-poor collagen. *Biochimica et Biophysica Acta (BBA)-Protein Structure.* 1971; 229(3): 672-680.
12. Quirk RA, France RM, Shakesheff KM, Howdle SM. Supercritical fluid technologies and tissue engineering scaffolds. *Current Opinion in Solid State and Materials Science.* 2004; 8(3-4): 313-321.
13. Zellander A, Gemeinhart R, Djalilian A, Makhsous M, Sun S, Cho M. Designing a gas foamed scaffold for keratoprosthesis. *Materials Science and Engineering: C.* 2013; 33(6): 3396-3403.
14. Sachlos E, Czernuszka J. Making tissue engineering scaffolds work. Review: the application of solid freeform fabrication technology to the production of tissue engineering scaffolds. *Eur Cell Mater.* 2003; 5(29): 39-40.
15. Kim HJ, Park IK, Kim JH, Cho CS, Kim MS. Gas foaming fabrication of porous biphasic calcium phosphate for bone regeneration. *Tissue Engineering and Regenerative Medicine.* 2012; 9(2): 63-68.
16. Mironov V, Visconti RP, Kasyanov V, Forgacs G, Drake CJ, Markwald RR. Organ printing: tissue spheroids as building blocks. *Biomaterials.* 2009;30(12):2164-2174.
17. Moroni L, Burdick JA, Highley C, et al. Biofabrication strategies for 3D in vitro models and regenerative medicine. *Nature Reviews Materials.* May 2018;3(5).
18. Arslan-Yildiz A, El Assal R, Chen P, Guven S, Inci F, Demirci U. Towards artificial tissue models: Past, present, and future of 3D bioprinting. *Biofabrication.* 2016;8(1).
19. Groll J, Boland T, Blunk T, et al. Biofabrication: reappraising the definition of an evolving field. *Biofabrication.* 2016;8(1):013001.
20. Lind JU, Busbee TA, Valentine AD, et al. Instrumented cardiac microphysiological devices via multimaterial three-dimensional printing. *Nature materials.* 2017;16(3):303.

21. Dai X, Liu L, Ouyang J, et al. Coaxial 3D bioprinting of self-assembled multicellular heterogeneous tumor fibers. *Scientific reports.* 2017; 7(1): 1457.
22. Moroni L, Boland T, Burdick JA, et al. Biofabrication: A Guide to Technology and Terminology. *Trends in Biotechnology.* 2018;36(4):384-402.
23. Hinton TJ, Hudson A, Pusch K, Lee A, Feinberg AW. 3D Printing PDMS Elastomer in a Hydrophilic Support Bath via Freeform Reversible Embedding. *Acs Biomaterials Science & Engineering.* Oct 2016;2(10):1781-1786.
24. Cui X, Dean D, Ruggeri ZM, Boland T. Cell damage evaluation of thermal inkjet printed Chinese hamster ovary cells. *Biotechnology and bioengineering.* 2010;106(6):963-969.
25. Duan B, Hockaday LA, Kang KH, Butcher JT. 3D bioprinting of heterogeneous aortic valve conduits with alginate/gelatin hydrogels. *Journal of biomedical materials research Part A.* 2013;101(5):1255-1264.
26. Koch L, Kuhn S, Sorg H, et al. Laser printing of skin cells and human stem cells. *Tissue Engineering Part C: Methods.* 2009;16(5):847-854.
27. Rocca M, Fragasso A, Liu WJ, Heinrich MA, Zhang YS. Embedded Multimaterial Extrusion Bioprinting. *Slas Technology.* Apr 2018;23(2):154-163.
28. De Maria C, Vozzi G, Moroni L. Multimaterial, heterogeneous, and multicellular three-dimensional bioprinting. *Mrs Bulletin.* 2017; 42(8): 578-584.
29. Melchels FPW, Domingos MAN, Klein TJ, Malda J, Bartolo PJ, Hutmacher DW. Additive manufacturing of tissues and organs. *Progress in Polymer Science.* Aug 2012;37(8):1079-1104.
30. Murphy SV, Atala A. 3D bioprinting of tissues and organs. *Nature biotechnology.* 2014;32(8):773.
31. Ribeiro A, Blokzijl MM, Levato R, et al. Assessing bioink shape fidelity to aid material development in 3D bioprinting. *Biofabrication.* Jan 2018;10(1).
32. Gleadall A, Visscher D, Yang J, Thomas D, Segal J. Review of additive manufactured tissue engineering scaffolds: relationship between geometry and performance. *Burns & Trauma.* Jul 2018;6.
33. Ji S, Guvendiren M. Recent advances in bioink design for 3D bioprinting of tissues and organs. *Frontiers in bioengineering and biotechnology.* 2017;5:23.
34. Hinton TJ, Jallerat Q, Palchesko RN, et al. Three-dimensional printing of complex biological structures by freeform reversible embedding of suspended hydrogels. *Science Advances.* Oct 2015;1(9).
35. Zhang YS, Arneri A, Bersini S, et al. Bioprinting 3D microfibrous scaffolds for engineering endothelialized myocardium and heart-on-a-chip. *Biomaterials.* Dec 2016;110:45-59.
36. Zhang YS, Yue K, Aleman J, et al. 3D bioprinting for tissue and organ fabrication. *Annals of biomedical engineering.* 2017;45(1):148-163.
37. Malda J, Visser J, Melchels FP, et al. 25th Anniversary Article: Engineering Hydrogels for Biofabrication. *Advanced Materials.* Sep 2013;25(36):5011-5028.
38. Loo Y, Lakshmanan A, Ni M, Toh LL, Wang S, Hauser CA. Peptide bioink: self-assembling nanofibrous scaffolds for three-dimensional organotypic cultures. *Nano letters.* 2015;15(10):6919-6925.
39. Melchels FP, Dhert WJ, Hutmacher DW, Malda J. Development and characterisation of a new bioink for additive tissue manufacturing. *Journal of Materials Chemistry B.* 2014;2(16):2282-2289.
40. Ouyang L, Yao R, Zhao Y, Sun W. Effect of bioink properties on printability and cell viability for 3D bioplotting of embryonic stem cells. *Biofabrication.* 2016;8(3):035020.
41. Daly AC, Critchley SE, Rencsok EM, Kelly DJ. A comparison of different bioinks for 3D bioprinting of fibrocartilage and hyaline cartilage. *Biofabrication.* 2016;8(4):045002.
42. Kyle S, Jessop ZM, Al-Sabah A, Whitaker IS. 'Printability' of Candidate Biomaterials for Extrusion Based 3D Printing: State-of-the-Art. *Adv. Healthc. Mater.* Aug 2017;6(16).

43. Hong S, Sycks D, Chan HF, et al. 3D Printing: 3D Printing of Highly Stretchable and Tough Hydrogels into Complex, Cellularized Structures (Adv. Mater. 27/2015). *Advanced Materials.* 2015;27(27):4034-4034.
44. Lee J-S, Kim BS, Seo D, Park JH, Cho D-W. Three-dimensional cell printing of large-volume tissues: Application to ear regeneration. *Tissue Engineering Part C: Methods.* 2017;23(3):136-145.
45. Schacht K, Jüngst T, Schweinlin M, Ewald A, Groll J, Scheibel T. Biofabrication of cell-loaded 3D spider silk constructs. *Angewandte Chemie International Edition.* 2015;54(9):2816-2820.
46. Okay O. General properties of hydrogels. *Hydrogel sensors and actuators*: Springer; 2009:1-14.
47. Zhang H, Qadeer A, Mynarcik D, Chen W. Delivery of rosiglitazone from an injectable triple interpenetrating network hydrogel composed of naturally derived materials. *Biomaterials.* 2011;32(3):890-898.
48. Jin R, Hiemstra C, Zhong Z, Feijen J. Enzyme-mediated fast in situ formation of hydrogels from dextran–tyramine conjugates. *Biomaterials.* 2007;28(18):2791-2800.
49. Guvendiren M, Lu HD, Burdick JA. Shear-thinning hydrogels for biomedical applications. *Soft matter.* 2012;8(2):260-272.
50. Mann JL, Anthony CY, Agmon G, Appel EA. Supramolecular polymeric biomaterials. *Biomaterials science.* 2018;6(1):10-37.
51. Ghosh SK. *Self-healing materials: fundamentals, design strategies, and applications*: Wiley Online Library; 2009.
52. Peppas N, Huang Y, Torres-Lugo M, Ward J, Zhang J. Physicochemical foundations and structural design of hydrogels in medicine and biology. *Annual review of biomedical engineering.* 2000;2(1):9-29.
53. Diba M, Spaans S, Ning K, et al. Self-Healing Biomaterials: From Molecular Concepts to Clinical Applications. *Advanced Materials Interfaces.* 2018; 5(17).
54. Wang YN, Adokoh CK, Narain R. Recent development and biomedical applications of self-healing hydrogels. *Expert Opinion on Drug Delivery.* 2018;15(1):77-91.
55. Sun TL, Kurokawa T, Kuroda S, et al. Physical hydrogels composed of polyampholytes demonstrate high toughness and viscoelasticity. *Nature materials.* 2013;12(10):932.
56. Tuncaboylu DC, Argun A, Sahin M, Sari M, Okay O. Structure optimization of self-healing hydrogels formed via hydrophobic interactions. *Polymer.* 2012;53(24):5513-5522.
57. Wang H, Wang S, Su H, et al. A Supramolecular Approach for Preparation of Size-Controlled Nanoparticles. *Angewandte Chemie.* 2009;121(24):4408-4412.
58. Jin R, Moreira Teixeira LS, Dijkstra PJ, et al. Enzymatically crosslinked dextran-tyramine hydrogels as injectable scaffolds for cartilage tissue engineering. *Tissue Engineering Part A.* 2010;16(8):2429-2440.
59. Wennink JW, Niederer K, Bochyńska AI, et al. Injectable Hydrogels by Enzymatic Co-Crosslinking of Dextran and Hyaluronic Acid Tyramine Conjugates. Paper presented at: Macromolecular symposia2011.
60. Chimene D, Lennox KK, Kaunas RR, Gaharwar AK. Advanced bioinks for 3D printing: a materials science perspective. *Annals of biomedical engineering.* 2016; 44(6): 2090-2102.
61. Kolesky DB, Homan KA, Skylar-Scott MA, Lewis JA. Three-dimensional bioprinting of thick vascularized tissues. *Proceedings of the National Academy of Sciences of the United States of America.* Mar 2016;113(12):3179-3184.
62. Liu W, Heinrich MA, Zhou Y, et al. Extrusion Bioprinting of Shear-Thinning Gelatin Methacryloyl Bioinks. *Advanced Healthcare Materials.* 2017;6(12).
63. Loebel C, Rodell CB, Chen MH, Burdick JA. Shear-thinning and self-healing hydrogels as injectable therapeutics and for 3D-printing. *Nature Protocols.* Aug 2017;12(8):1521-1541.
64. Rodell CB, MacArthur Jr JW, Dorsey SM, et al. Shear-thinning supramolecular hydrogels with secondary autonomous covalent crosslinking to modulate viscoelastic properties in vivo. *Advanced functional materials.* 2015;25(4):636-644.

65. Jeong D, Joo SW, Shinde VV, Jung S. Triple-crosslinked beta-cyclodextrin oligomer self-healing hydrogel showing high mechanical strength, enhanced stability and pH responsiveness. *Carbohydrate Polymers.* Oct 2018;198:563-574.
66. Ouyang LL, Highley CB, Rodell CB, Sun W, Burdick JA. 3D Printing of Shear-Thinning Hyaluronic Acid Hydrogels with Secondary Cross-Linking. *Acs Biomaterials Science & Engineering.* Oct 2016;2(10):1743-1751.
67. Zhang YS, Pi QM, van Genderen AM. Microfluidic Bioprinting for Engineering Vascularized Tissues and Organoids. *Jove-Journal of Visualized Experiments.* Aug 2017(126).
68. Stumberger G, Vihar B. Freeform Perfusable Microfluidics Embedded in Hydrogel Matrices. *Materials.* Dec 2018;11(12).
69. Highley CB, Rodell CB, Burdick JA. Direct 3D printing of shear-thinning hydrogels into self-healing hydrogels. *Advanced Materials.* 2015;27(34):5075-5079.
70. Shi L, Carstensen H, Hölzl K, et al. Dynamic coordination chemistry enables free directional printing of biopolymer hydrogel. *Chemistry of Materials.* 2017;29(14):5816-5823.
71. Henke S, Leijten J, Kemna E, et al. Enzymatic Crosslinking of Polymer Conjugates is Superior over Ionic or UV Crosslinking for the On-Chip Production of Cell-Laden Microgels. *Macromolecular Bioscience.* Oct 2016;16(10):1524-1532.
72. Harada A, Takashima Y, Nakahata M. Supramolecular polymeric materials via cyclodextrin–guest interactions. *Accounts of chemical research.* 2014;47(7):2128-2140.
73. Appel EA, del Barrio J, Loh XJ, Scherman OA. Supramolecular polymeric hydrogels. *Chemical Society Reviews.* 2012; 41(18): 6195-6214.
74. Granadero D, Bordello J, Pérez-Alvite MJ, Novo M, Al-Soufi W. Host-guest complexation studied by fluorescence correlation spectroscopy: adamantane–cyclodextrin inclusion. *International journal of molecular sciences.* 2010;11(1):173-188.
75. Stella VJ, He Q. Cyclodextrins. *Toxicologic pathology.* 2008;36(1):30-42.
76. Del Valle EM. Cyclodextrins and their uses: a review. *Process biochemistry.* 2004; 39(9): 1033-1046.
77. Szejtli J. Introduction and general overview of cyclodextrin chemistry. *Chemical reviews.* 1998;98(5):1743-1754.
78. Crini G, Fourmentin S, Fenyvesi É, Torri G, Fourmentin M, Morin-Crini N. Cyclodextrins, from molecules to applications. *Environmental chemistry letters.* 2018; 16(4): 1361-1375.
79. Upadhyay SK, Ali SM. Molecular recognition of flunarizine dihydrochloride and β-cyclodextrin inclusion complex by NMR and computational approaches. *Chemistry Central Journal.* 2018;12(1):33.
80. Roy MN, Saha S, Kundu M, Saha BC, Barman S. Exploration of inclusion complexes of neurotransmitters with β-cyclodextrin by physicochemical techniques. *Chemical Physics Letters.* 2016;655:43-50.
81. https://pubchem.ncbi.nlm.nih.gov/compound/Tyramine#section=Structures. Accessed 17-03, 2019.
82. Chang PH, Jiang WT, Li ZH. Mechanism of tyramine adsorption on Ca-montmorillonite. *Science of the Total Environment.* 2018; 642: 198-207.
83. Fourmentin S, Ciobanu A, Landy D, Wenz G. Space filling of β-cyclodextrin and β-cyclodextrin derivatives by volatile hydrophobic guests. *Beilstein journal of organic chemistry.* 2013;9(1):1185-1191.
84. Morel-Desrosiers N, Morel J-P. Standard molar enthalpies, volumes, and heat capacities of adamantane in cyclohexane, n-hexane, and carbon tetrachloride. Interpretation using the scaled-particle theory. *Journal of Solution Chemistry.* 1979;8(8):579-592.
85. Schmidt BV, Barner-Kowollik C. Dynamic Macromolecular Material Design—The Versatility of Cyclodextrin-Based Host–Guest Chemistry. *Angewandte Chemie International Edition.* 2017;56(29):8350-8369.

86. Kobayashi S, Uyama H, Kimura S. Enzymatic polymerization. *Chemical Reviews.* 2001;101(12):3793-3818.
87. Kurisawa M, Chung JE, Yang YY, Gao SJ, Uyama H. Injectable biodegradable hydrogels composed of hyaluronic acid–tyramine conjugates for drug delivery and tissue engineering. *Chemical communications.* 2005(34):4312-4314.
88. Sofia SJ, Singh A, Kaplan DL. Peroxidase-catalyzed crosslinking of functionalized polyaspartic acid polymers. *Journal of Macromolecular Science, Part A.* 2002;39(10):1151-1181.
89. Fukuoka T, Uyama H, Kobayashi S. Polymerization of polyfunctional macromolecules: synthesis of a new class of high molecular weight poly (amino acid) s by oxidative coupling of phenol-containing precursor polymers. *Biomacromolecules.* 2004;5(3):977-983.
90. Hiemstra C, van der Aa LJ, Zhong Z, Dijkstra PJ, Feijen J. Rapidly in situ-forming degradable hydrogels from dextran thiols through Michael addition. *Biomacromolecules.* 2007;8(5):1548-1556.
91. Engler AJ, Sen S, Sweeney HL, Discher DE. Matrix elasticity directs stem cell lineage specification. *Cell.* 2006;126(4):677-689.
92. Buxboim A, Ivanovska IL, Discher DE. Matrix elasticity, cytoskeletal forces and physics of the nucleus: how deeply do cells 'feel'outside and in? *J Cell Sci.* 2010; 123(3): 297-308.
93. Su W-F. Polymer size and polymer solutions. *Principles of Polymer Design and Synthesis*: Springer; 2013:9-26.
94. Zaslavsky BY. *Aqueous two-phase partitioning: physical chemistry and bioanalytical applications*: CRC Press; 1994.
95. Thordarson P. Determining association constants from titration experiments in supramolecular chemistry. *Chemical Society Reviews.* 2011;40(3):1305-1323.
96. Fulmer GR, Miller AJ, Sherden NH, et al. NMR chemical shifts of trace impurities: common laboratory solvents, organics, and gases in deuterated solvents relevant to the organometallic chemist. *Organometallics.* 2010;29(9):2176-2179.
97. Byun HS, Zhong N, Bittman R, Shea KM, Danheiser RL. 6A-O-p-toluenesulfonyl-β-cyclodextrin [β-cyclodextrin, 6A-(4-methylbenzenesulfonate)]. *Organic Syntheses.* Vol 772000: 225.
98. Jicsinszky L, Iványi R. Catalytic transfer hydrogenation of sugar derivatives. *Carbohydrate polymers.* 2001;45(2):139-145.
99. Trotta F, Martina K, Robaldo B, Barge A, Cravotto G. Recent advances in the synthesis of cyclodextrin derivatives under microwaves and power ultrasound. *Journal of Inclusion Phenomena and Macrocyclic Chemistry.* April 01 2007;57(1):3-7.
100. Lovrinovic M, Niemeyer CM. Microtiter plate-based screening for the optimization of DNA–protein conjugate synthesis by means of expressed protein ligation. *ChemBioChem.* 2007;8(1):61-67.
101. Hamasaki K, Ikeda H, Nakamura A, et al. Fluorescent sensors of molecular recognition. Modified cyclodextrins capable of exhibiting guest-responsive twisted intramolecular charge transfer fluorescence. *Journal of the American Chemical Society.* 1993;115(12):5035-5040.
102. Nielsen TT, Wintgens V, Larsen KL, Amiel C. Synthesis and characterization of poly (ethylene glycol) based β-cyclodextrin polymers. *Journal of Inclusion Phenomena and Macrocyclic Chemistry.* 2009;65(3-4):341.
103. Goswami S, Sen D, Das NK, Fun H-K, Quah CK. A new rhodamine based colorimetric 'off–on'fluorescence sensor selective for Pd 2+ along with the first bound X-ray crystal structure. *Chemical Communications.* 2011;47(32):9101-9103.
104. Dotsikas Y, Kontopanou E, Allagiannis C, Loukas YL. Interaction of 6-p-toluidinylnaphthalene-2-sulphonate with β-cyclodextrin. *Journal of pharmaceutical and biomedical analysis.* 2000;23(6):997-1003.
105. Elmorsi TM, Aysha TS, Machalický O, Mohamed MBI, Bedair AH. A dual functional colorimetric and fluorescence chemosensor based on benzo [f] fluorescein dye derivatives for copper ions

and pH; kinetics and thermodynamic study. *Sensors and Actuators B: Chemical.* 2017;253:437-450.

106. http://www.chemistry.unsw.edu.au/research/research-groups/thordarson-group/software. Accessed 15-06, 2019.
107. https://www.rheosense.com/applications/viscosity/newtonian-non-newtonian. Accessed 24-06, 2019.
108. Wang J, Qiu Z, Wang Y, et al. Supramolecular polymer assembly in aqueous solution arising from cyclodextrin host–guest complexation. *Beilstein journal of organic chemistry.* 2016;12(1):50-72.
109. Senac C, Desgranges Sp, Contino-Pépin C, Urbach W, Fuchs PF, Taulier N. Effect of Dimethyl Sulfoxide on the Binding of 1-Adamantane Carboxylic Acid to β-and γ-Cyclodextrins. *Acs Omega.* 2018;3(1):1014-1021.
110. Yan Q, Zhao Y. ATP-triggered biomimetic deformations of bioinspired receptor-containing polymer assemblies. *Chemical science.* 2015;6(7):4343-4349.
111. Teixeira LM, Leijten J, Sobral J, et al. High throughput generated micro-aggregates of chondrocytes stimulate cartilage formation in vitro and in vivo. *Eur. Cell Mater.* 2012;23:387-399.
112. Upadhyay SK, Kumar G. NMR and molecular modelling studies on the interaction of fluconazole with β-cyclodextrin. *Chemistry Central Journal.* 2009;3(1):9.
113. Atkins PW, De Paula J. *Physical chemistry*: John Wiley & Sons; 2010.
114. Panayitou M, Pohner C, Vandevyver C, Wandrey C, Hilbrig F, Freitag R. Synthesis and characterisation of thermo-responsive poly(N,N '-diethylacrylamide) microgels. *Reactive & Functional Polymers.* Sep 2007;67(9):807-819.
115. Avery RK, Albadawi H, Akbari M, et al. An injectable shear-thinning biomaterial for endovascular embolization. *Science Translational Medicine.* 2016; 8(365).
116. Shin JH. Refractory gastrointestinal bleeding: role of angiographic intervention. *Clinical endoscopy.* 2013;46(5):486.
117. Karanicolas PJ, Colquhoun PH, Dahlke E, Guyatt GH. Mesenteric angiography for the localization and treatment of acute lower gastrointestinal bleeding. *Canadian Journal of Surgery.* 2008;51(6):437.
118. Rogan H, Ilagan F, Yang F. Comparing Single Cell Versus Pellet Encapsulation of Mesenchymal Stem Cells in Three-Dimensional Hydrogels for Cartilage Regeneration. *Tissue Engineering Part A.*
119. Saltzman WM. *Tissue engineering: engineering principles for the design of replacement organs and tissues*: Oxford university press; 2004.

Supplementary info

SI 1. Jurkat cell culturing and subculturing

The following procedures were performed by master student Dennis van der Zwaan.

Culturing Jurkat cells

Jurkat cells were thawed at 37 ^{o}C until a small clump of ice was still present. Cells were transferred to a 50 mL Greiner tube and the Cryovial was rinsed once by dropwise adding and swirling 5 mL medium which was afterwards added to the cell containing Greiner tube. Another 10 mL of medium was added to the cell suspension and afterwards centrifuged to form a pellet. Medium was removed and cells were resuspended in 10 mL medium, counted and checked for viability by adding 20 µL of cell suspension to 20 µL of trypan blue and counted. Afterwards a 90 mL cell suspension was prepared containing 300 000 cells which was divided over 30 wells (~10 000 cells/well), and incubated for 1 day. Next, 2 mL of pre-warmed medium was added to the cells and incubated for 4 days.

Subculturing Jurkat cells

Cell suspension of each well was collected in a 50 mL Greiner tube, centrifuged and the supernatant was removed. The cells were wash twice by PBS and afterwards resuspended and counted. Subculturing was performed by seeding 200 000 cells in a suspension (non-treated) flasks in 15 mL medium and subsequently incubation. After 2 days medium was refreshed and the cells were further incubated for 3 days.

SI 2. ^{1}H NMR spectra

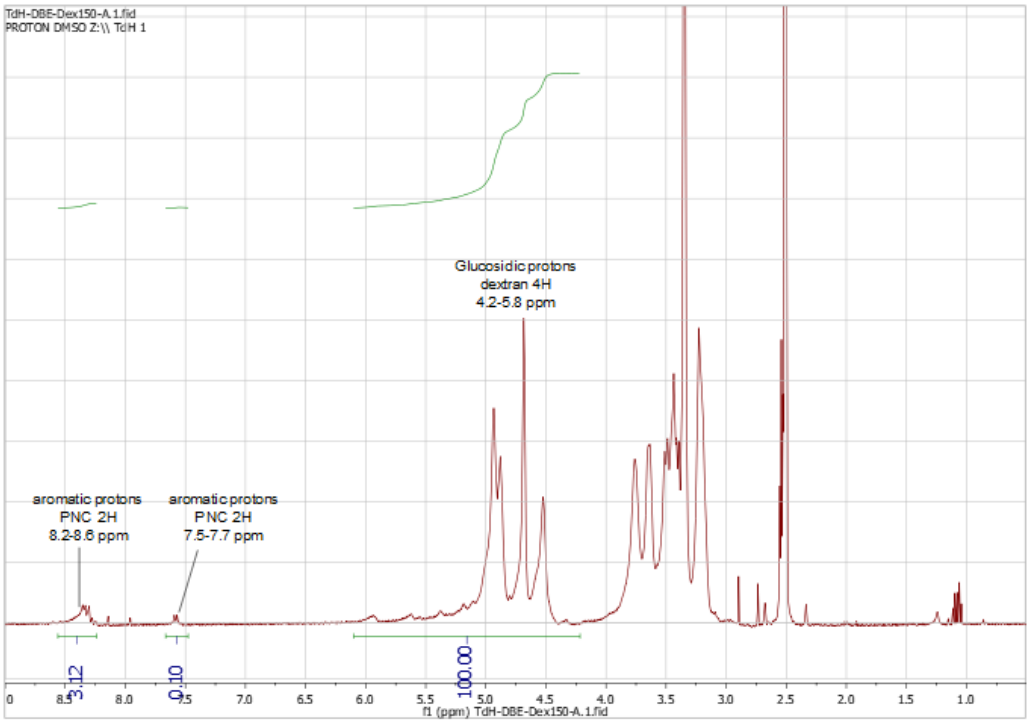

Figure S1. Dex$_{150}$-PNC DS 3%. ^{1}H NMR (400 MHz, DMSO-d$_6$) δ: 2.5-4.0 (m, –CH$_2$–CH$_2$–), 4.2-5.8 (m, 4H, glucosidic protons dextran), 7.5-7.7 (m, aromatic protons PNC), 8.2-8.6 (m, 2H, aromatic protons).

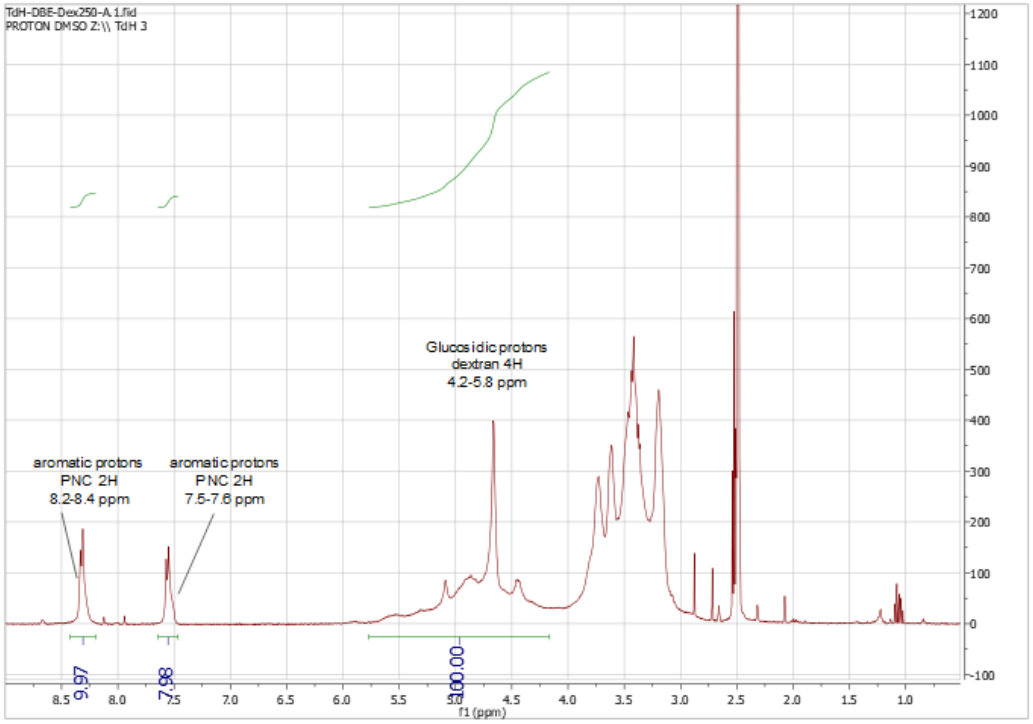

Figure S2. Dex$_{250}$-PNC DS 18%. ^{1}H NMR (400 MHz, DSMO-d$_6$) δ: 2.5-4.0 (m, –CH$_2$–CH$_2$–), 4.2-5.8 (m, 4H, glucosidic protons dextran), 7.5-7.6 (m, 2H, aromatic protons PNC), 8.2-8.4 (m, 2H, aromatic protons PNC).

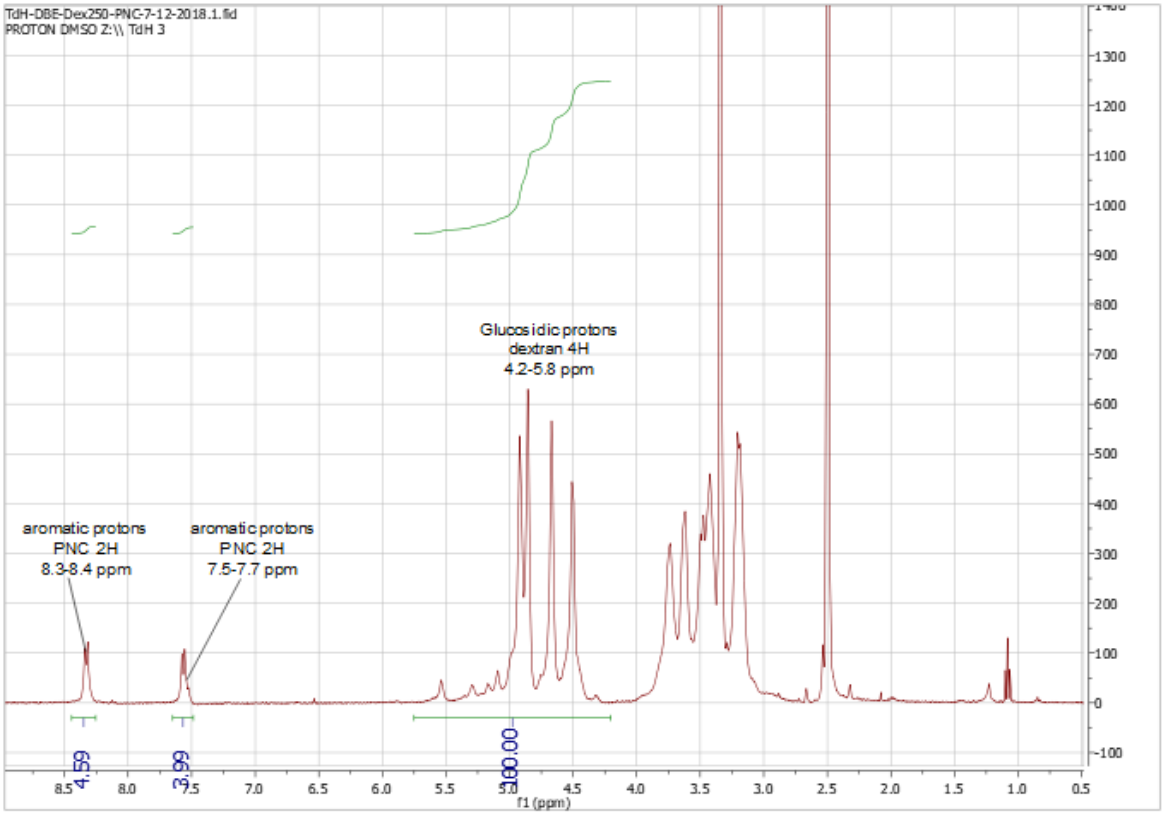

Figure S3. Dex_{250}-PNC DS 9%. ^1H NMR (400 MHz, DSMO-d_6) δ: 2.5-4.0 (m, –CH_2–CH_2–), 4.2-5.8 (m, 4H, glucosidic protons dextran), 7.5-7.7 (m, 2H, aromatic protons PNC), 8.3-8.4 (m, 2H, aromatic protons PNC).

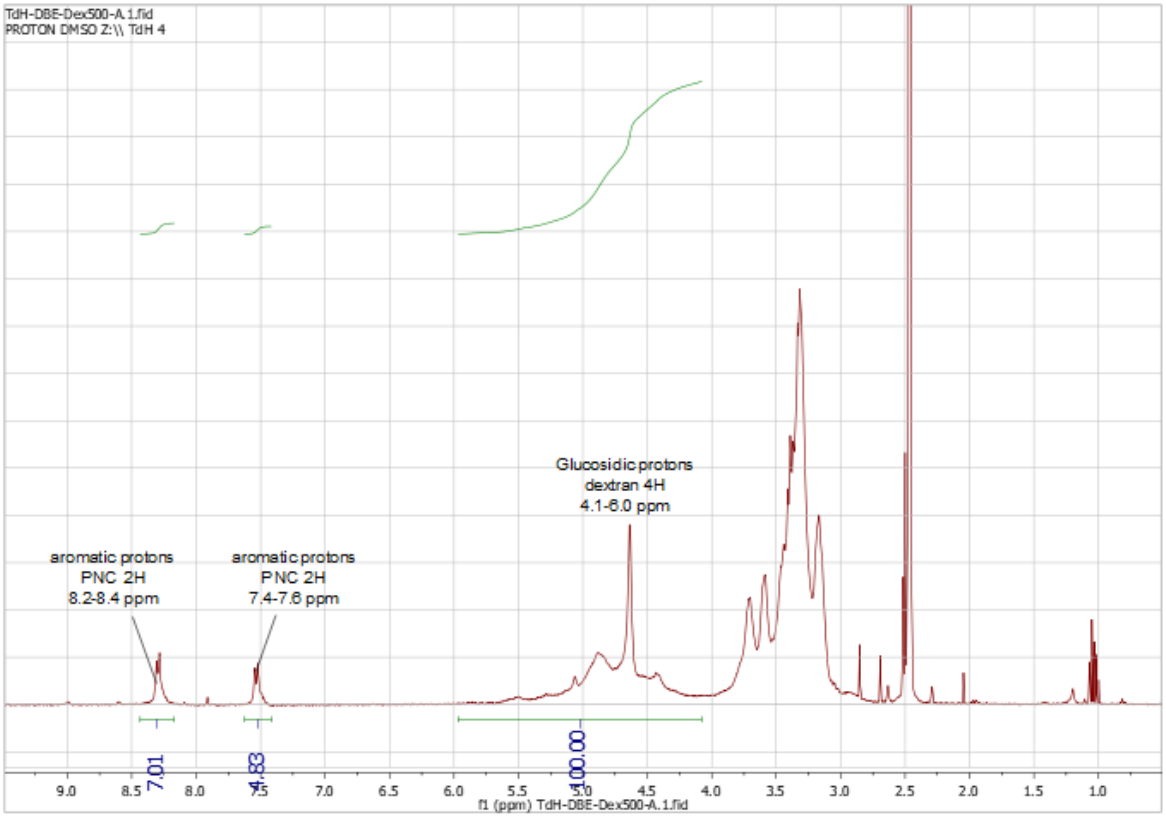

Figure S4. Dex_{500}-PNC DS 12%. % ^1H NMR (400 MHz, DSMO-d_6) δ: 2.5-4.0 (m, –CH_2–CH_2–), 4.1-6.0 (m, 4H, glucosidic protons dextran), 7.4-7.6 (m, 2H, aromatic protons PNC), 8.2-8.4 (m, 2H, aromatic protons PNC).

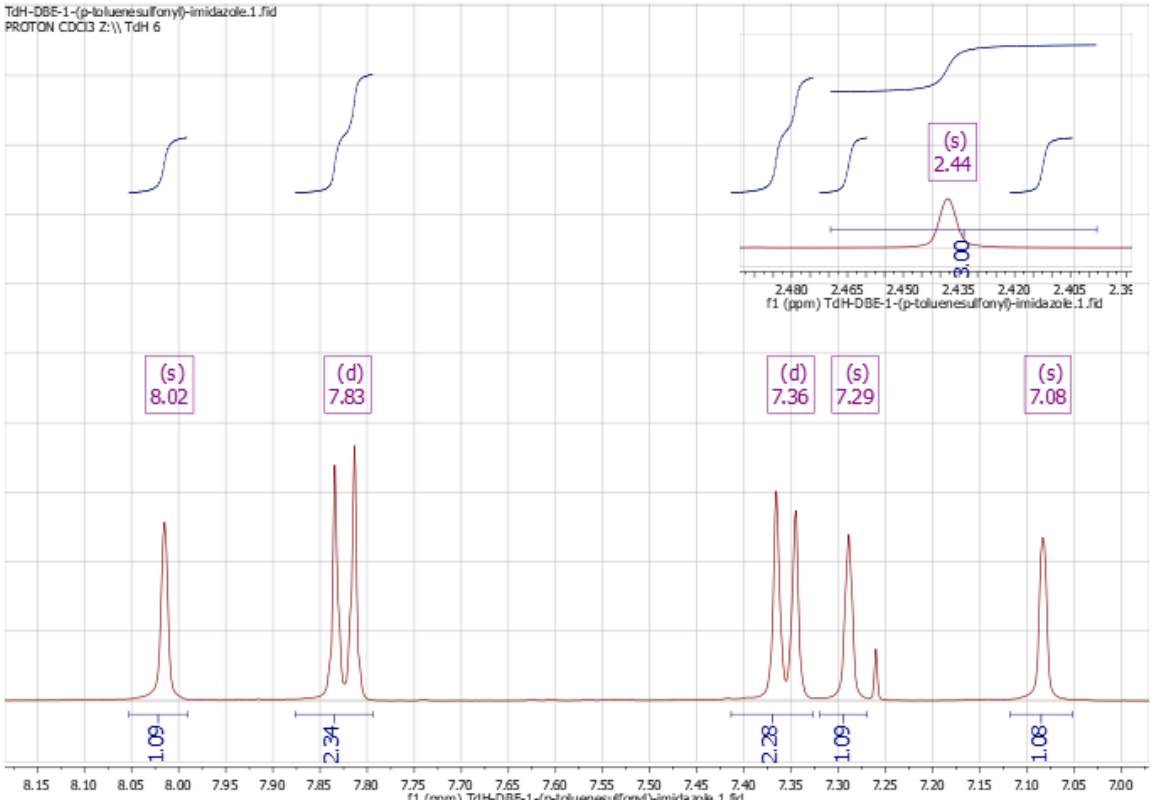

Figure S5. Tosyl-imidazole. ^{1}H NMR (400 MHz, $CDCl_3$) δ: 2.44 (s, 3H), 7.08 (s, 1H), 7.29 (s, 1H), 7.36 (d, 2H), 7.83 (d, 2H), 8.02 (s, 1H).

Figure S6. Tosyl-βCD. ^{1}H NMR (400 MHz, DMSO-d_6) δ: 2.49 (overlap with DMSO-d_6, s, 3H) 3.11- 3.83 (m. overlap with HDO), 4.11-4.23 (m, 1H), 4.27-4.41 (m, 2H), 4.41-4.48 (m, 2H), 4.52 (br s, 3H), 4.76 (br s, 2H), 4.83 (br s, 5H), 5.58-5.92 (m, 14H), 7.43 (d, 2H), 7.75 (d, 2H).

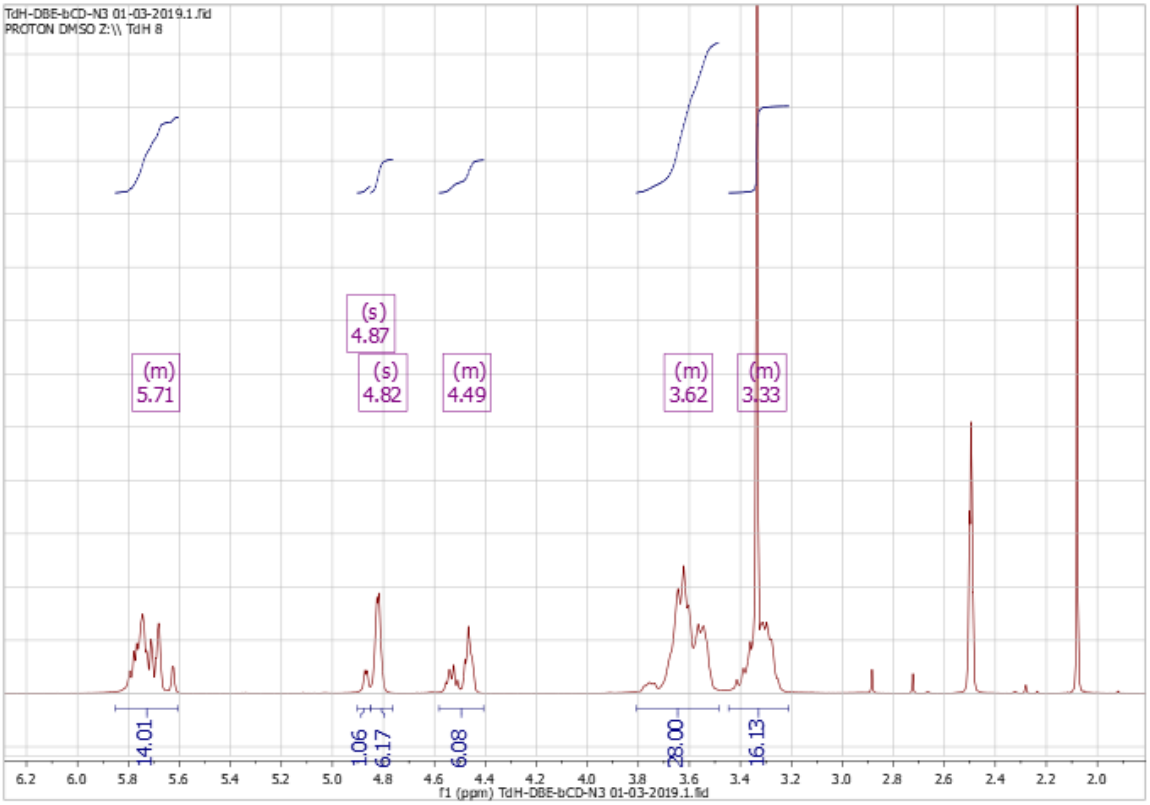

Figure S7. βCD-N_3. ^{1}H NMR (400 MHz, DMSO-d_6) δ: 3.21-3.45 (m, overlap with HDO), 3.48-3.81 (m, 28H), 4.41-4.58 (m, 6H), 4.82 (br s, 6H), 4.87 (shoulder, 1H), 5.61-5.85 (m, 14H).

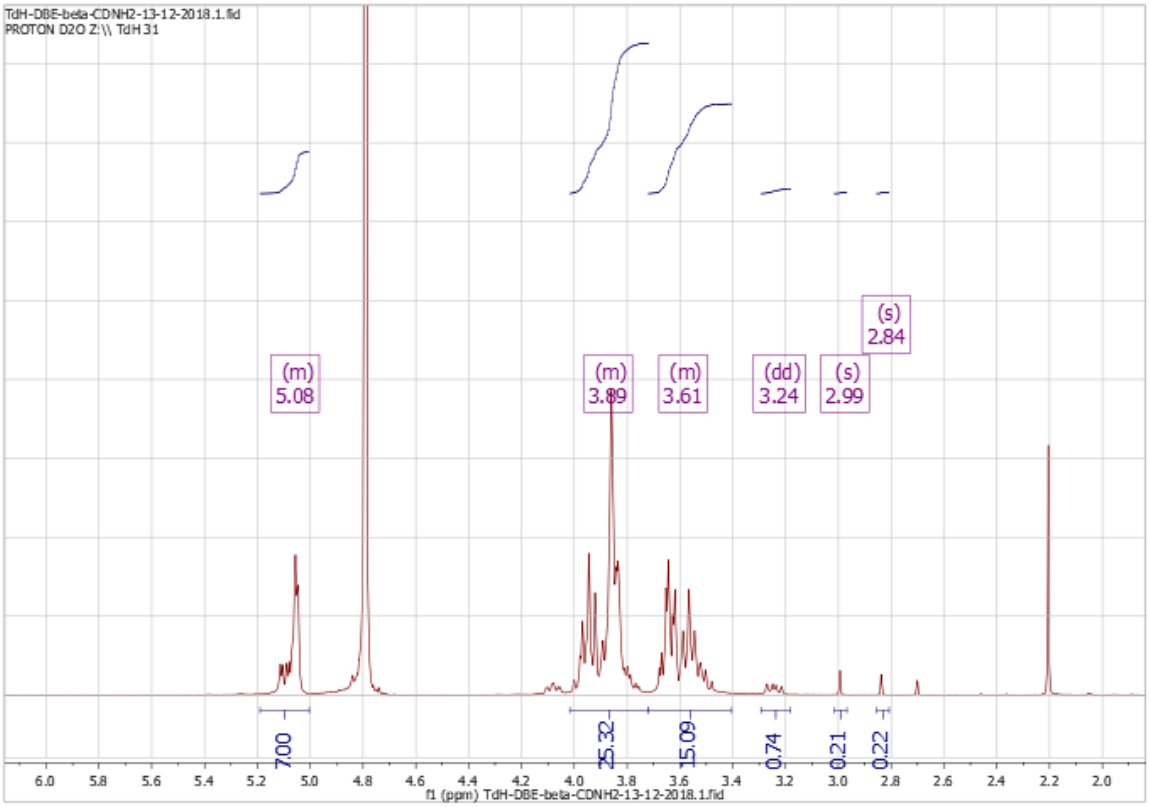

Figure S8. βCD-NH_2 Pd/C. ^{1}H NMR (D_2O, 400 MHz) δ: 2.84 (s, 0H), 2.99 (s, 0H), 3.24 (dd, 1H), 3.40-3.72 (m), 3.72-4.02 (m), 5.00-25.19 (m, 7H).

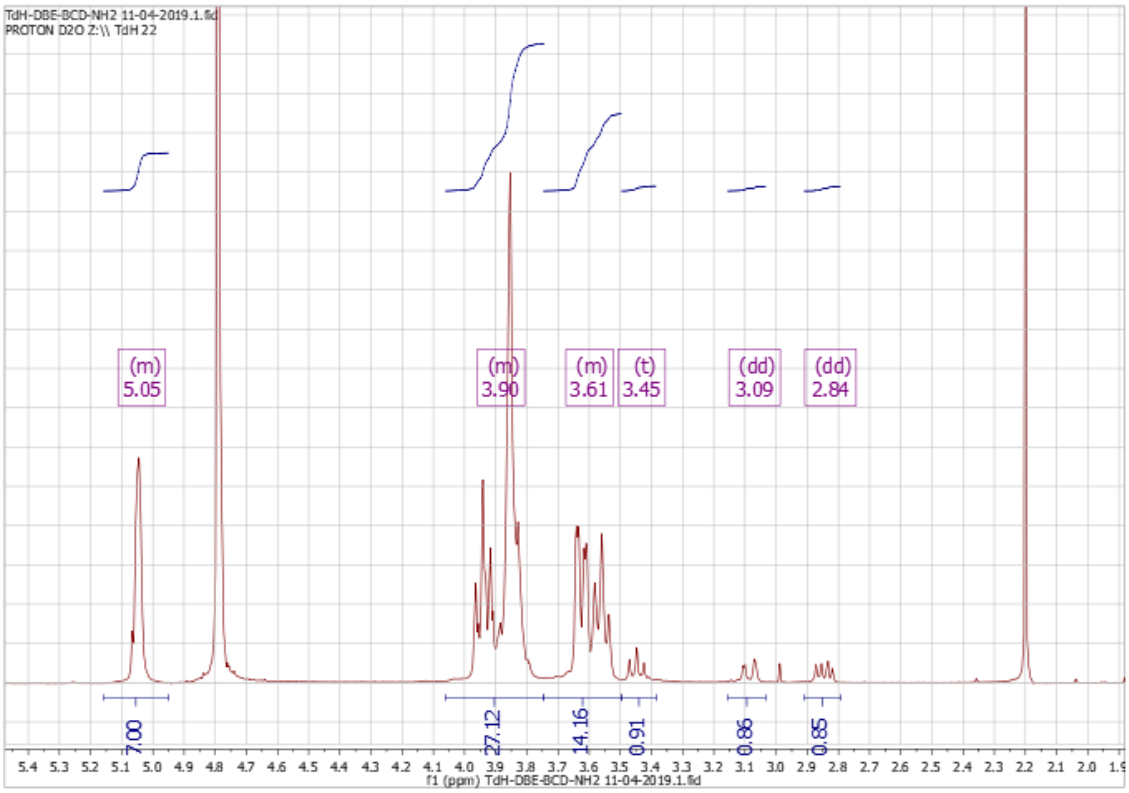

Figure S9. βCD-NH_2 PPh_3. ^1H NMR (400 MHz, D_2O) δ: 2.85 (dd, 1H, H-6'), 3.09 (dd, 1H, H-6'), 3.45 (t, 1H, H-4'), 3.49-3.74 (m), 3.75-4.11 (m), 4.99-5.16 (m, 7H, H-1').

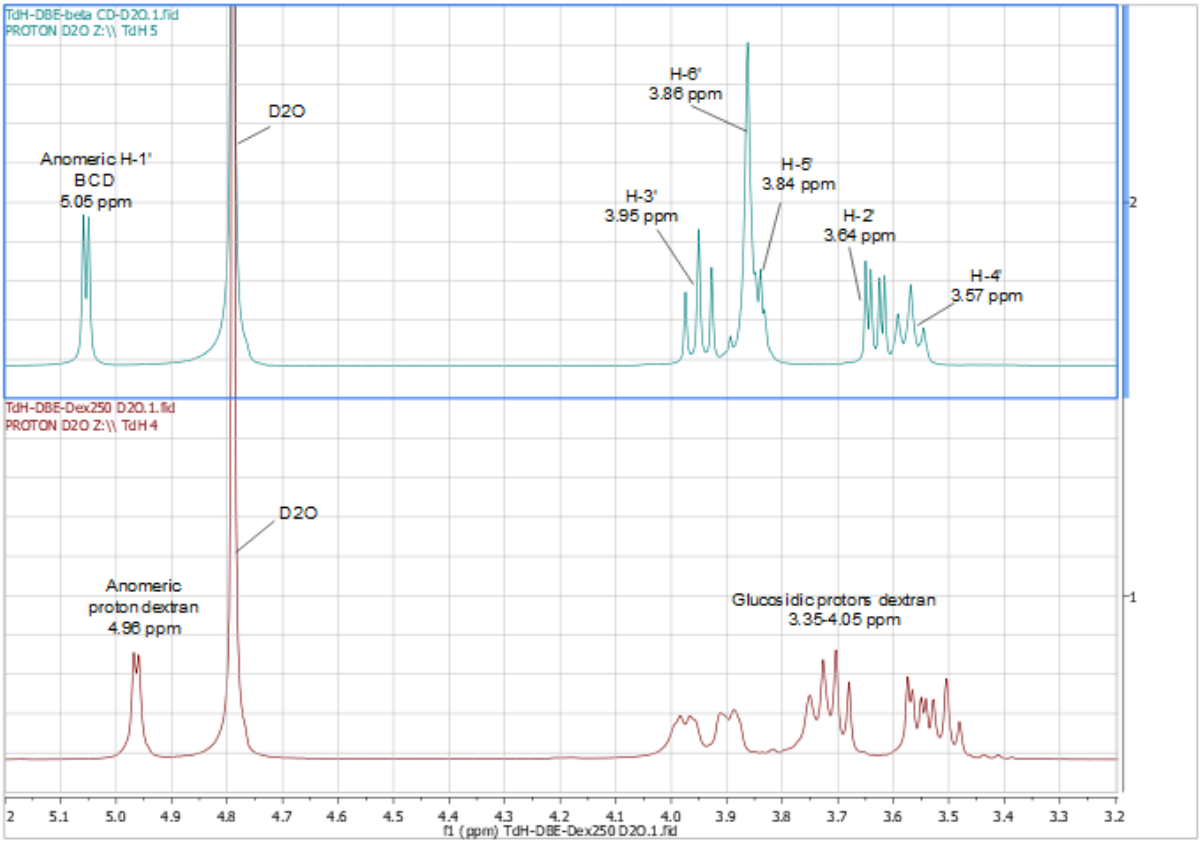

Figure S10. βCD and dextran in D_2O.

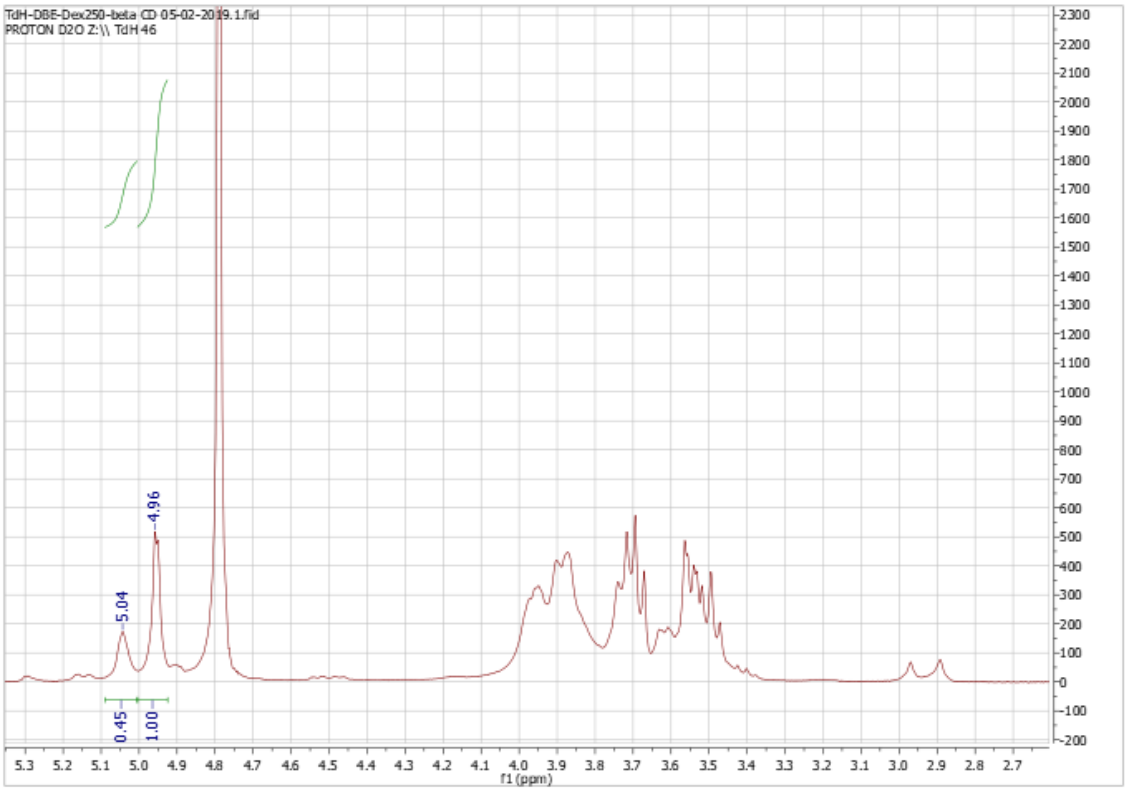

Figure S11. Dex_{250}-βCD DS 6% #1. ^1H NMR (400 MHz, D_2O) δ: 4.96 (s, 1H, anomeric proton dextran), 5.04 (s, 7H, anomeric proton βCD).

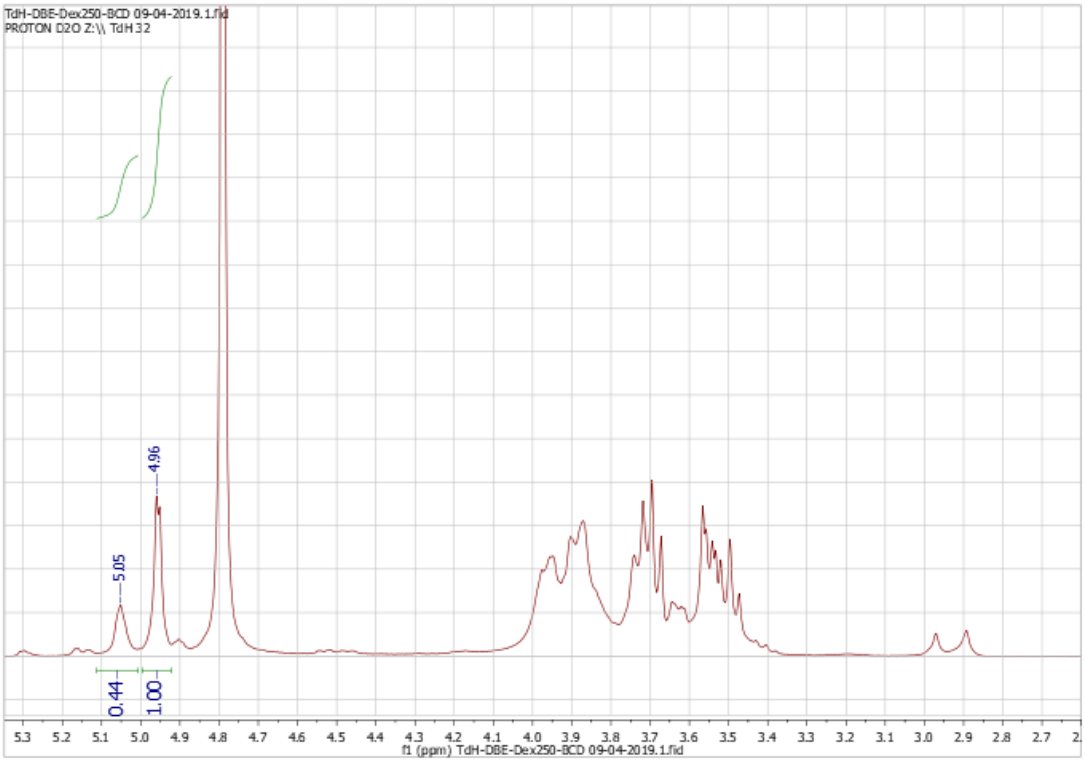

Figure S12. Dex_{250}-βCD DS 6% #2. ^1H NMR (400 MHz, D_2O) δ: 4.96 (s, 1H, anomeric proton dextran), 5.05 (s, 7H, anomeric proton βCD).

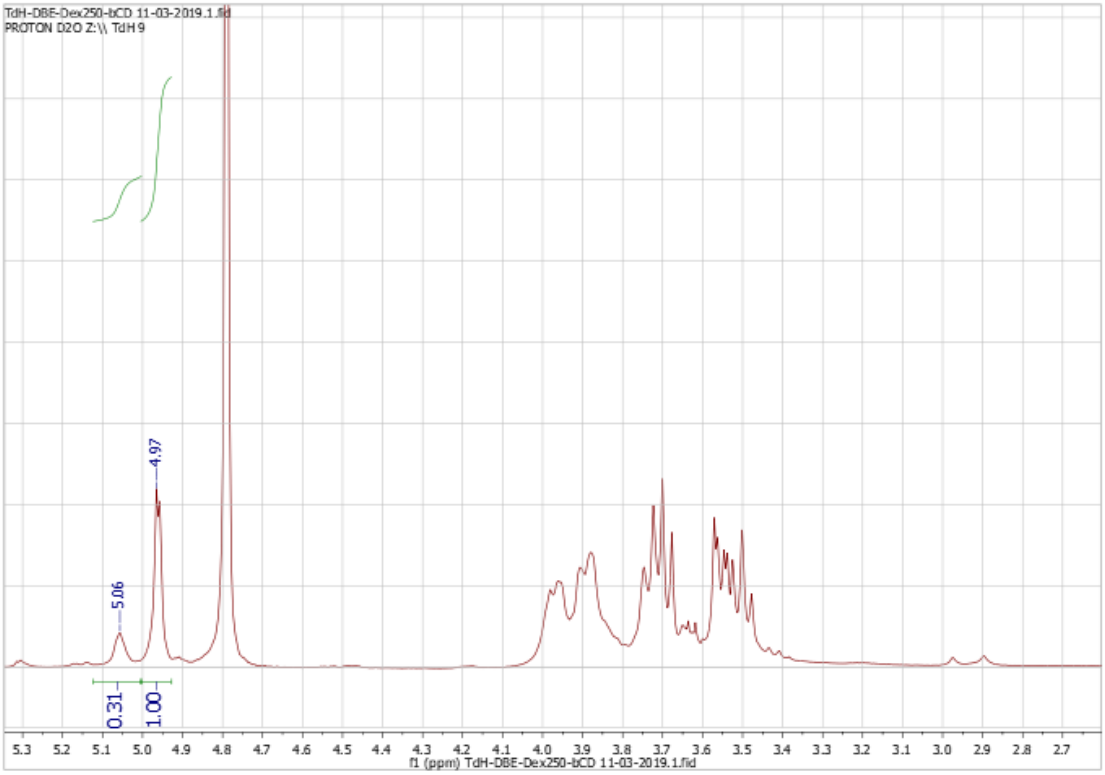

Figure S13. Dex_{250}-βCD DS 5%. ^1H NMR (400 MHz, D_2O) δ: 4.97 (s, 1H, anomeric proton dextran), 5.06 (s, 7H, anomeric proton βCD).

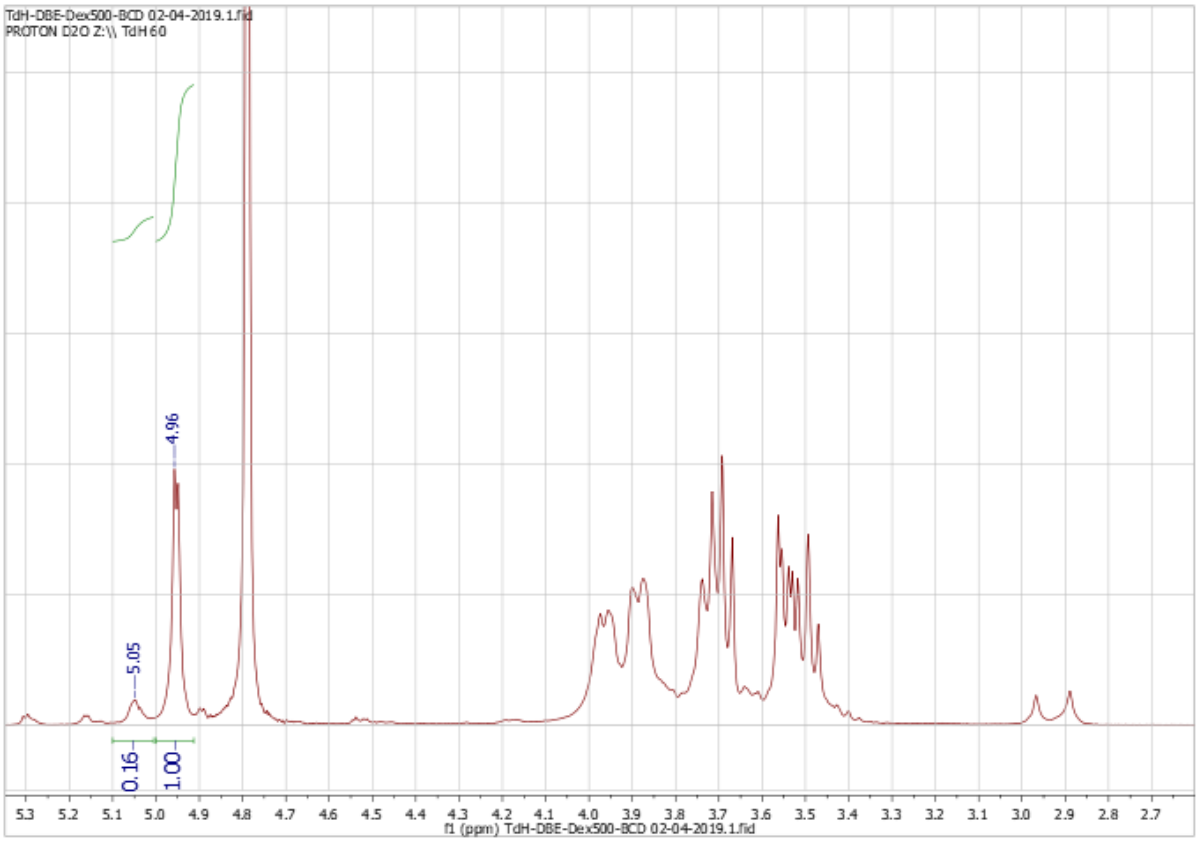

Figure S14. Dex_{500}-βCD DS 2%. ^1H NMR (400 MHz, D_2O) δ: 4.96 (s, 1H, anomeric proton dextran), 5.05 (s, 7H, anomeric proton βCD).

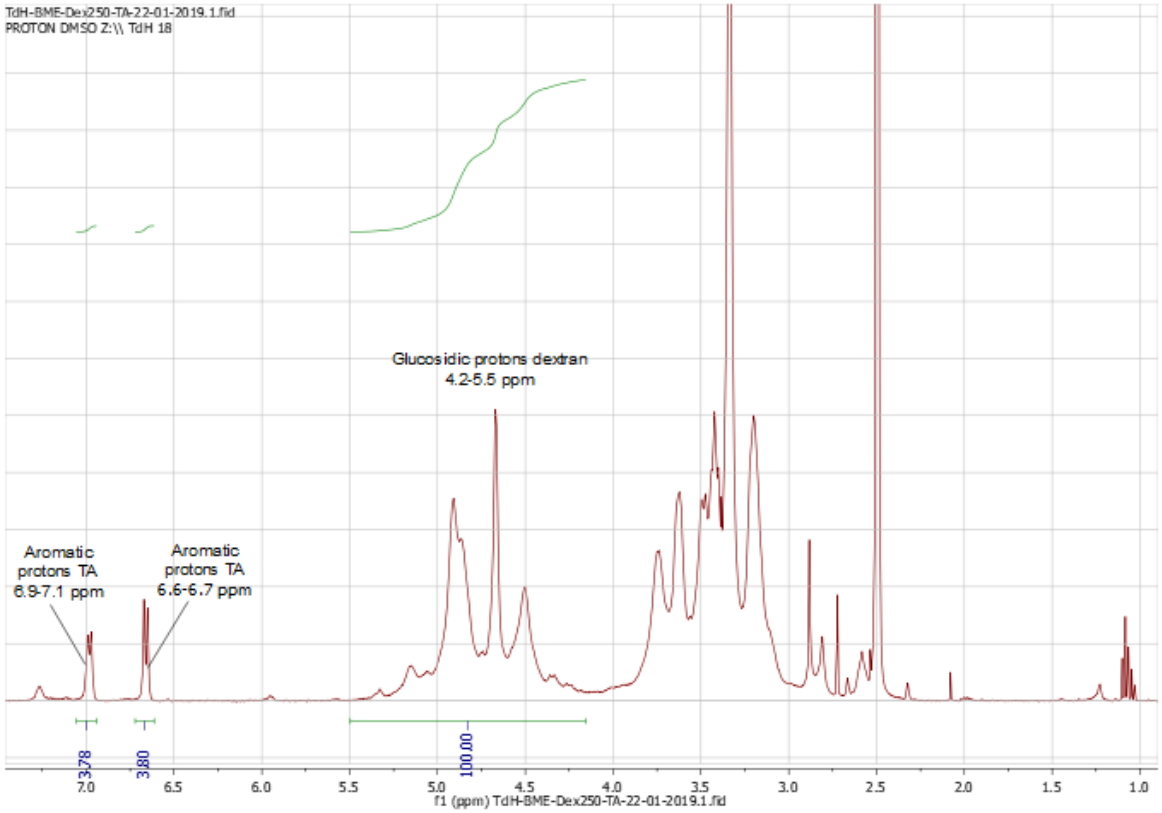

Figure S15. Dex_{250}-TA DS 8%. ^1H NMR (400 MHz, DSMO-d_6) δ: 2.5-4.0 (m, –CH_2–CH_2–), 4.2-5.5 (m, 4H, glucosidic protons dextran), 6.6-6.7 (m, 2H, aromatic protons TA), 6.9-7.1 (m, 2H, aromatic protons TA).

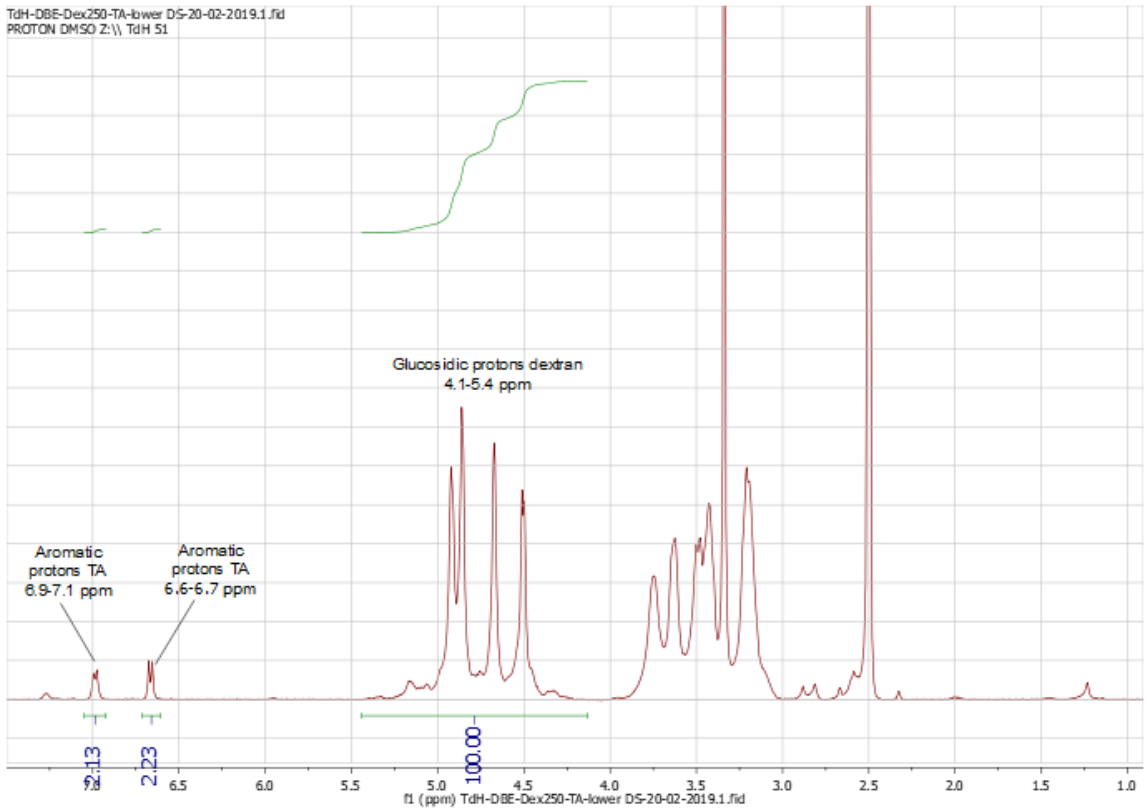

Figure S16. Dex_{250}-TA DS 4%. ^1H NMR (400 MHz, DSMO-d_6) δ: 2.5-4.0 (m, –CH_2–CH_2–), 4.1-5.4 (m, 4H, glucosidic protons dextran), 6.6-6.7 (m, 2H, aromatic protons TA), 6.9-7.1 (m, 2H, aromatic protons TA).

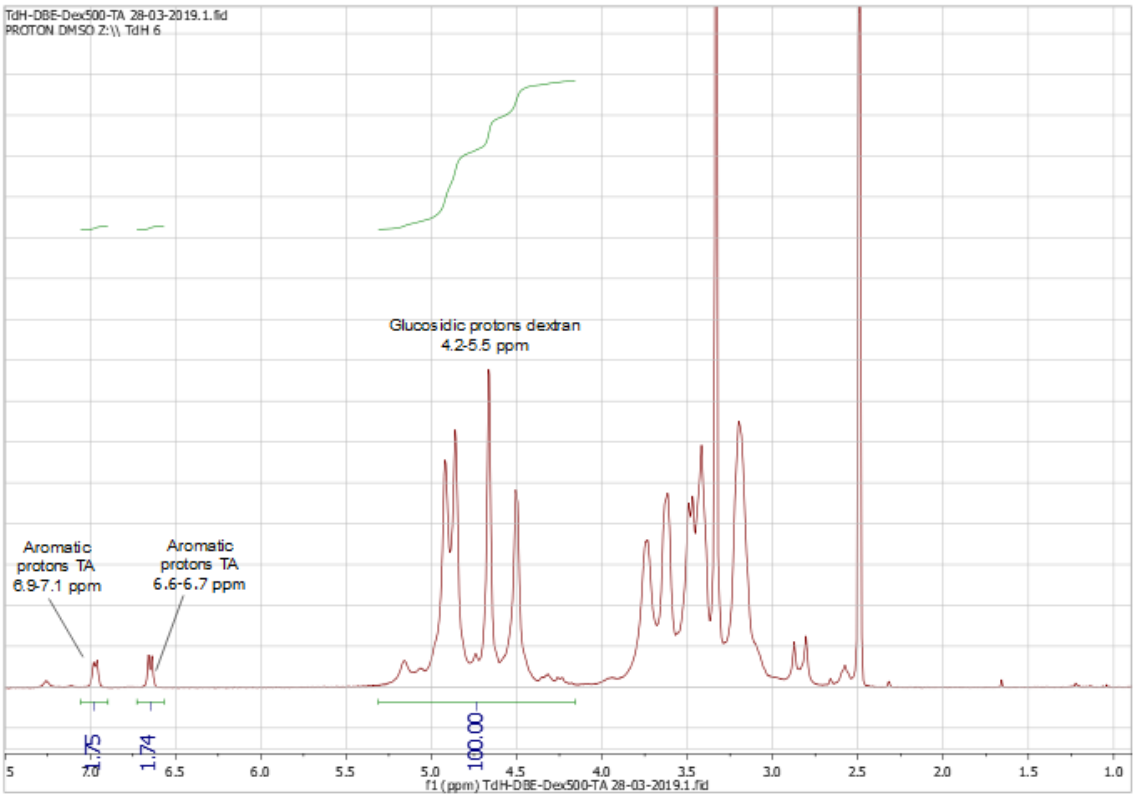

Figure S17. Dex_{500}-TA DS 4%. ^1H NMR (400 MHz, DSMO-d_6) δ: 2.5-4.0 (m, –CH_2–CH_2–), 4.2-5.3 (m, 4H, glucosidic protons dextran), 6.6-6.7 (m, 2H, aromatic protons TA), 6.9-7.1 (m, 2H, aromatic protons TA).

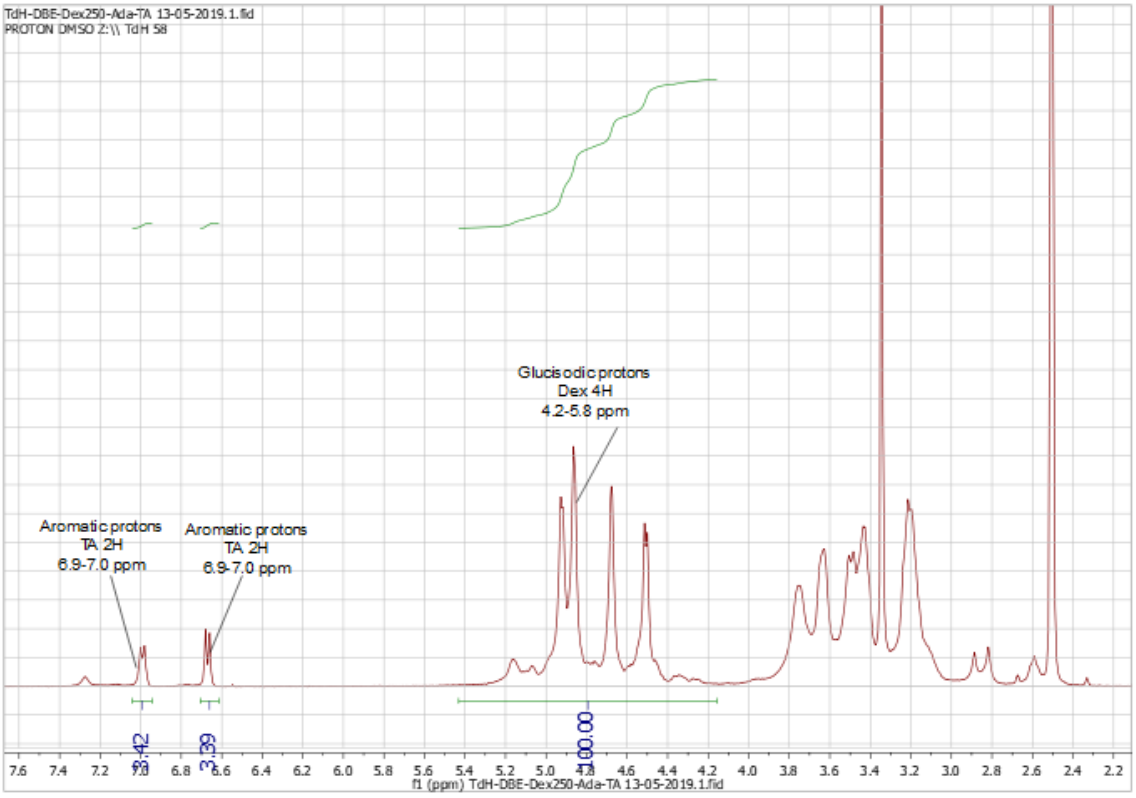

Figure S18. Dex_{250}-TA-Ada DS TA 6.8%, DS Ada 0%. ^1H NMR (400 MHz, DSMO-d_6) δ: 2.5-4.0 (m, –CH_2–CH_2–), 4.2-5.4 (m, 4H, glucosidic protons dextran), 6.6-6.7 (m, 2H, aromatic protons TA), 6.9-7.0 (m, 2H, aromatic protons TA).

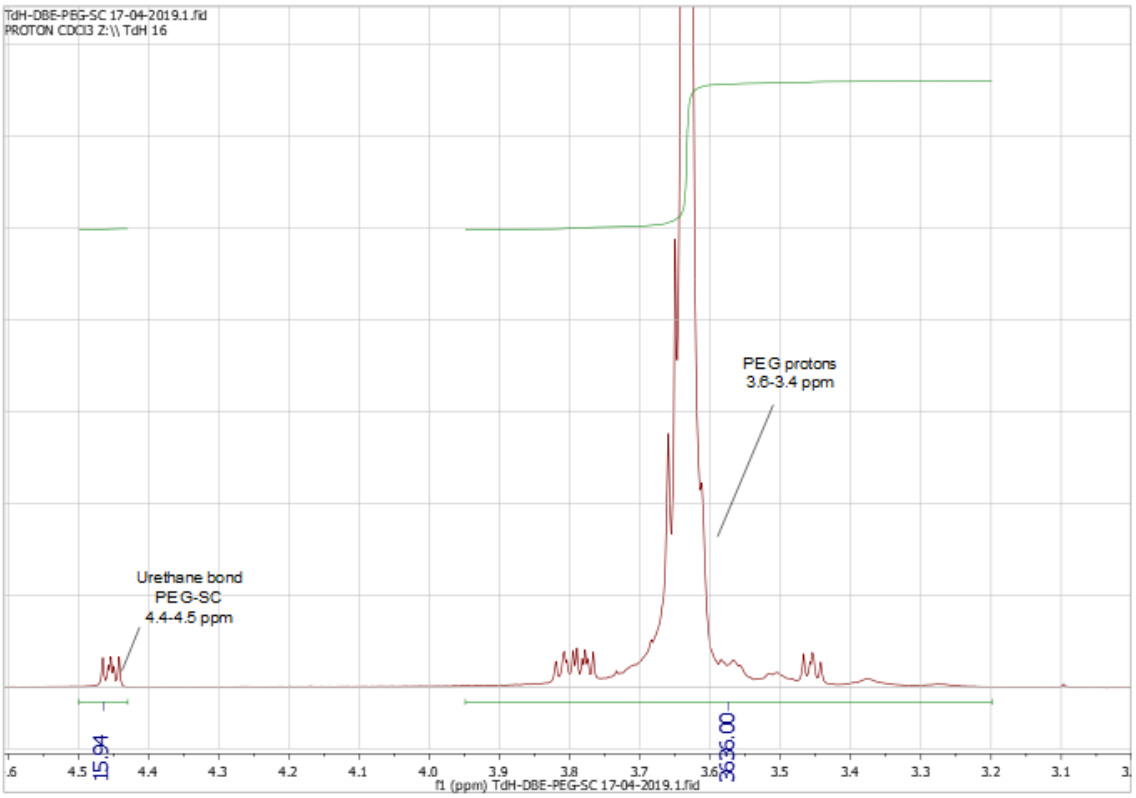

Figure S19.PEG-SC DS 100%. ^{1}H NMR (400 MHz, $CDCl_3$) δ: 3.20-3.95 (m, 3636H, protons PEG), 4.43-4.50 (t, 2H, urethane bond).

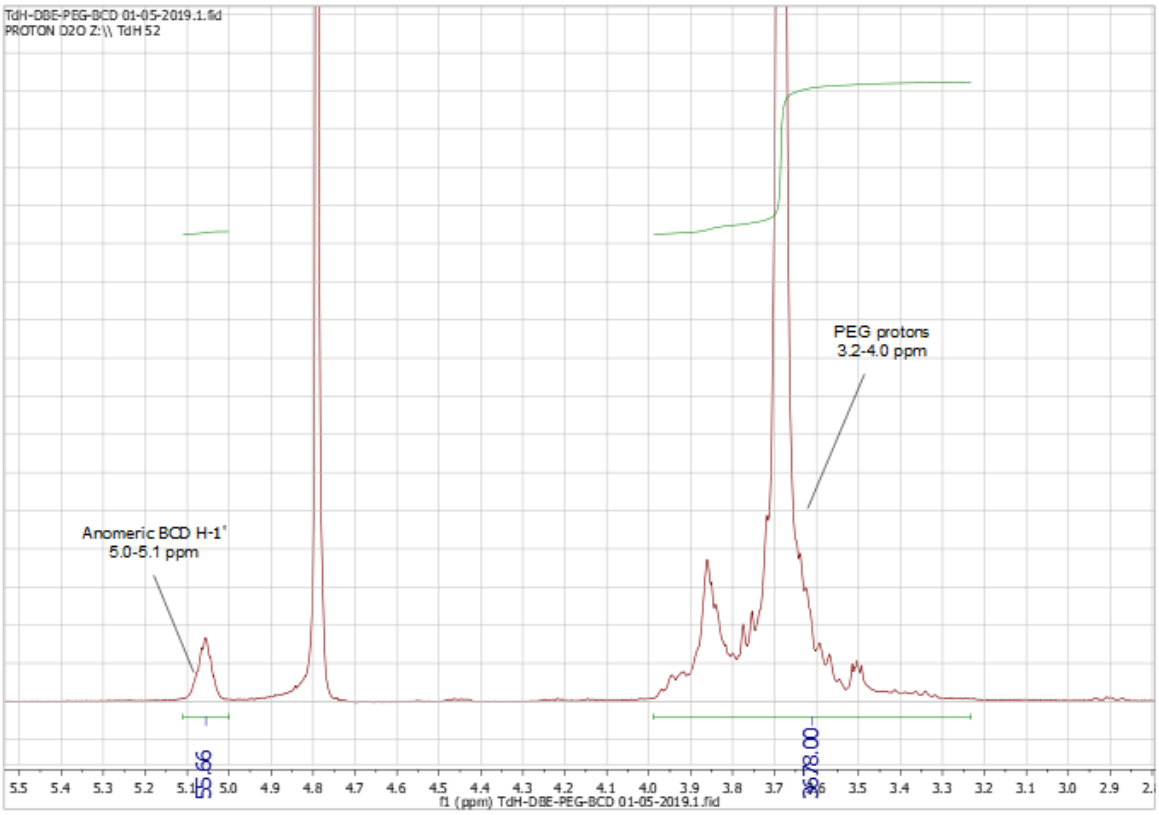

Figure S20. PEG-βCD 99%. ^{1}H NMR (400 MHz, $CDCl_3$) δ: 3.23-4.00 (m, 3636H, protons PEG), 5.00-5.11 (s, 7H, anomeric βCD H-1').

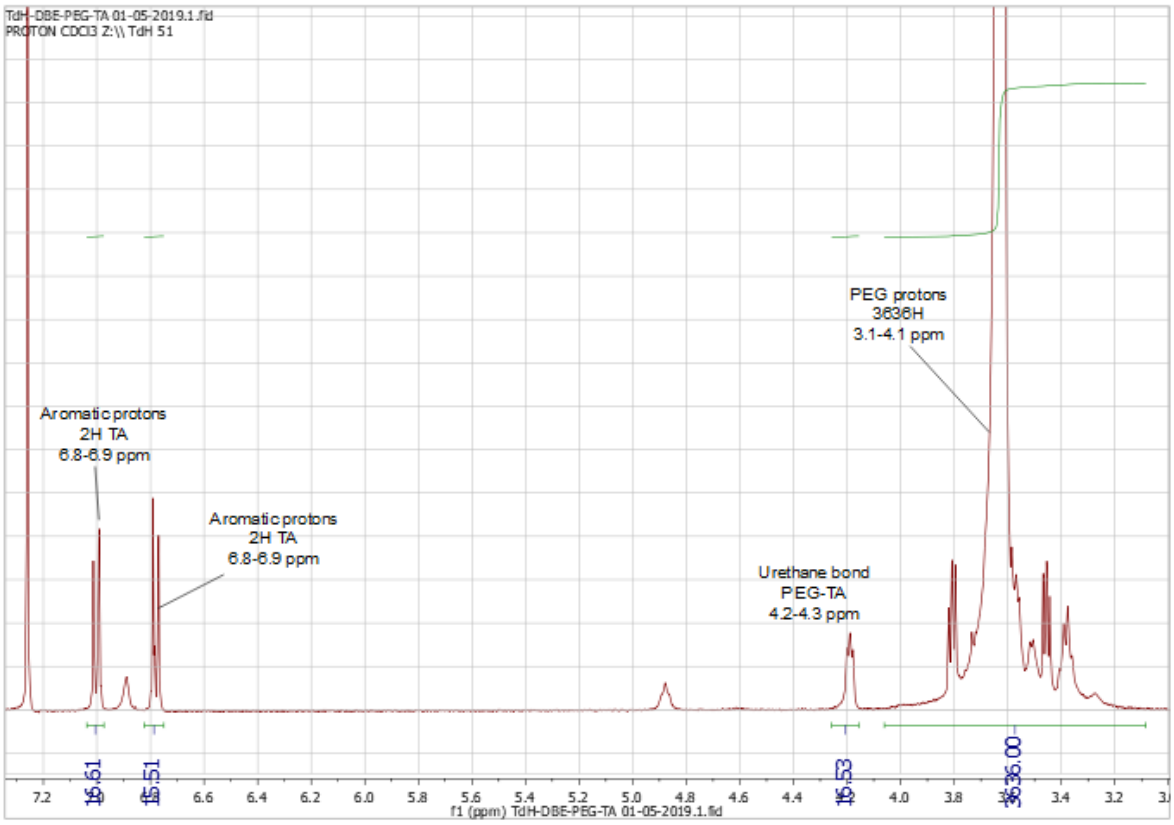

Figure S21. PEG-TA 103%. ^{1}H NMR (400 MHz, $CDCl_3$) δ: 3.08-4.06 (m, 3636H, protons PEG), 4.16-4.26 (t, 2H, urethane bond PEG-TA), 6.75-6.82 (m, 2H, aromatic protons TA), 6.97-7.04 (m, 2H, aromatic protons TA).

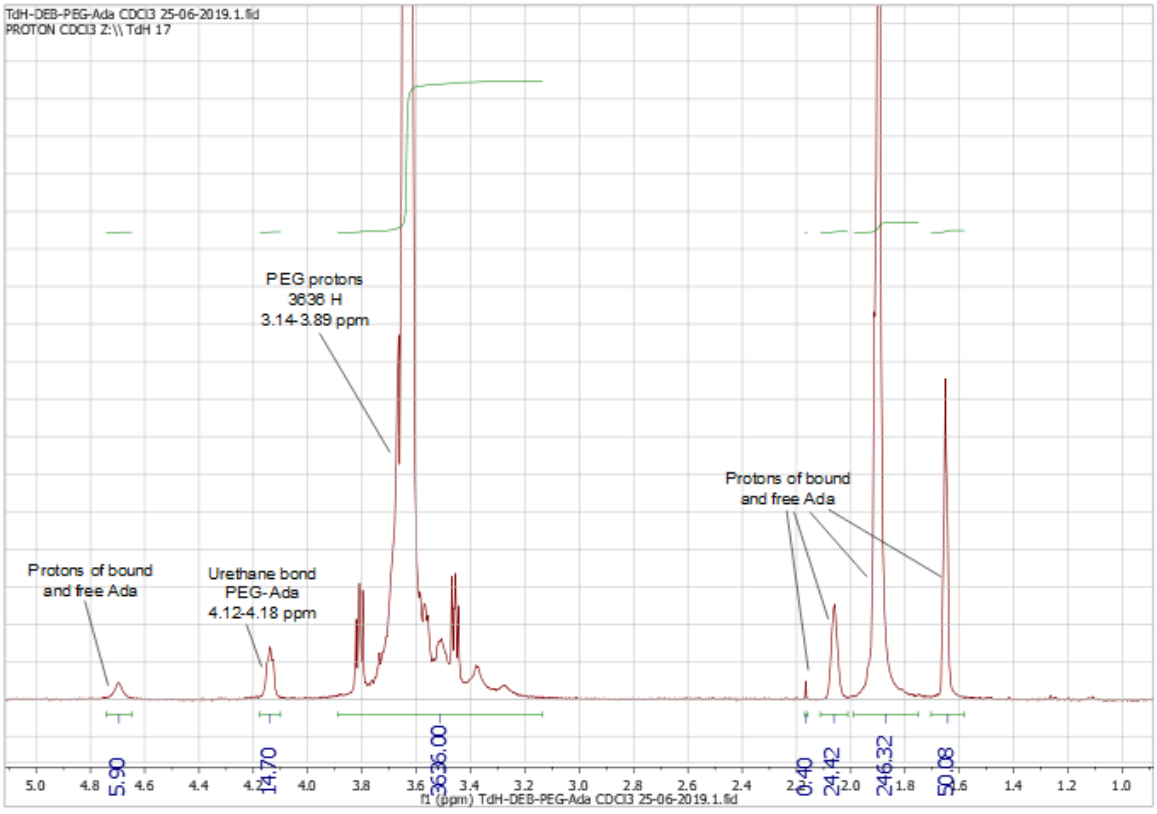

Figure S22. PEG-Ada DS 92%. ^{1}H NMR (400 MHz, $CDCl_3$) δ: 3.14-3.89 (m, 3636H, protons PEG), 4.12-4.18 (t, 2H, urethane bond PEG-TA). Remaining signals indicate that free adamantane is still present.

SI 3. ATR FTIR spectra

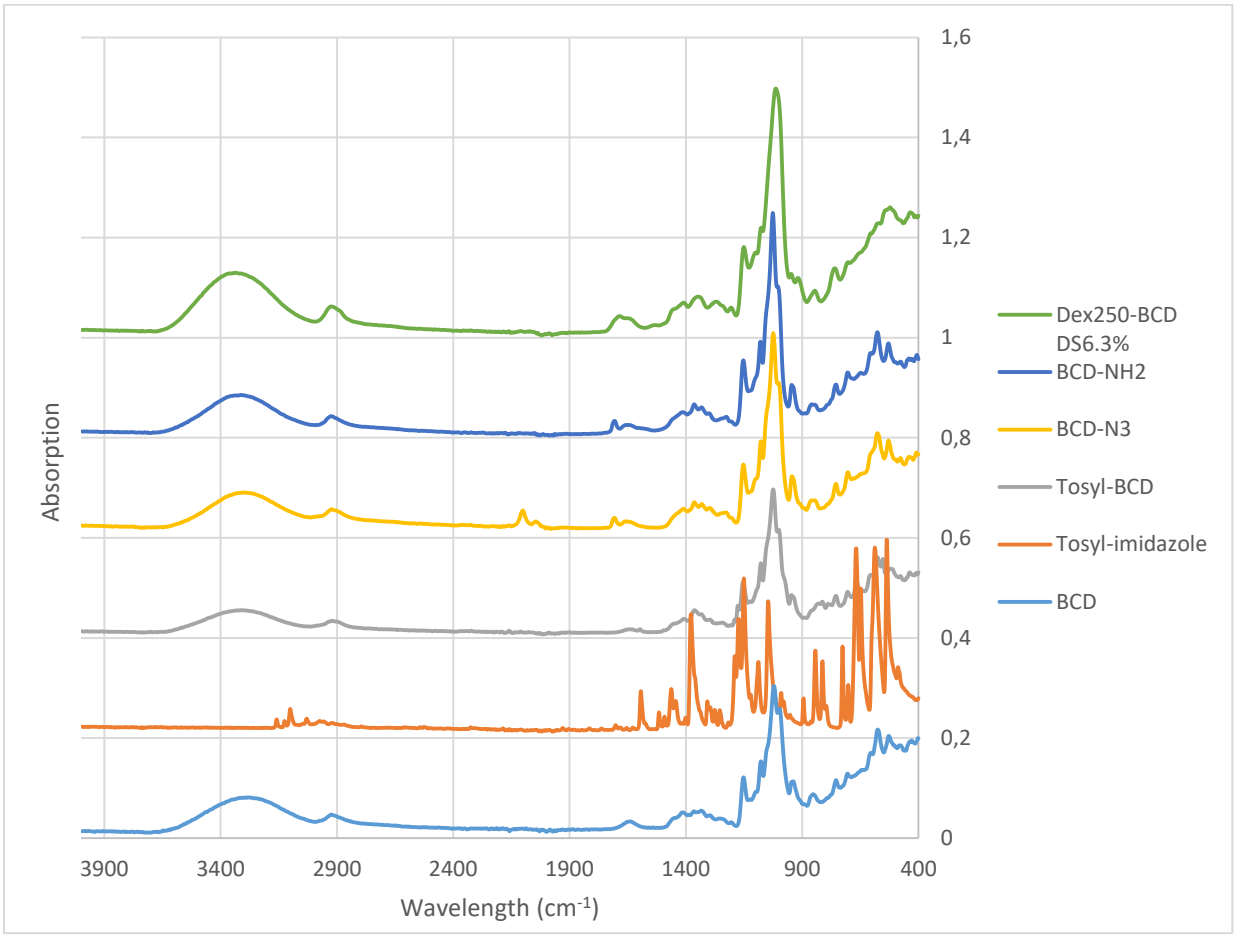

Figure S23. ATR FTIR spectra of βCD, tosyl, imidazole, tosyl- βCD, βCD-N_3, βCD-NH_2 and Dex_{250}- βCD DS6% #2.

βCD: 3282 (O-H, stretch), 2925 (C-H, stretch), 1638 (H-O-H), 1152 (C-C, stretch) and 1020 (O-H, bend) cm^{-1}.

Tosyl-imidazole: 3160-3125 (N-H, stretch), 3101-2974 (C-H, stretch), 1593 (N-H, bend), 1463 (C=C, stretch), 1377 (S=O, sulfonyl, stretch) and 1047 (S=O, sulfoxide, stretch) cm^{-1}.

Tosyl-βCD: 3310 (O-H, stretch), 2923 (C-H_2, stretch), 1362 (S=O, sulfonyl, stretch), 1153 (C-C, stretch) and 1047 (S=O, sulfoxide, stretch), 1024 (O-H, bend) cm^{-1}.

βCD-N_3: 3304 (O-H), 2923 (C-H_2), 2101 (N≡N, stretch), 1228 (C-N), 1146 (C-C) and 1024 (O-H, bend) cm^{-1}.

βCD-NH_2: 3350 (N-H, stretch), 3333 (O-H, stretch), 2925 (C-H_2, stretch), 1654 (N-H, bend), 1226 (C-N), 1152 (C-C, stretch) and 1026 (O-H, bend) cm^{-1}.

Dex_{250}-βCD DS 6%: 3335 (O-H, stretch), 2923 (C-H, stretch), 1685 (C=O urethane, stretch), 1215 (C-N, stretch), 1150 (C-C, stretch) and 1013 (O-H, bend) cm^{-1}.

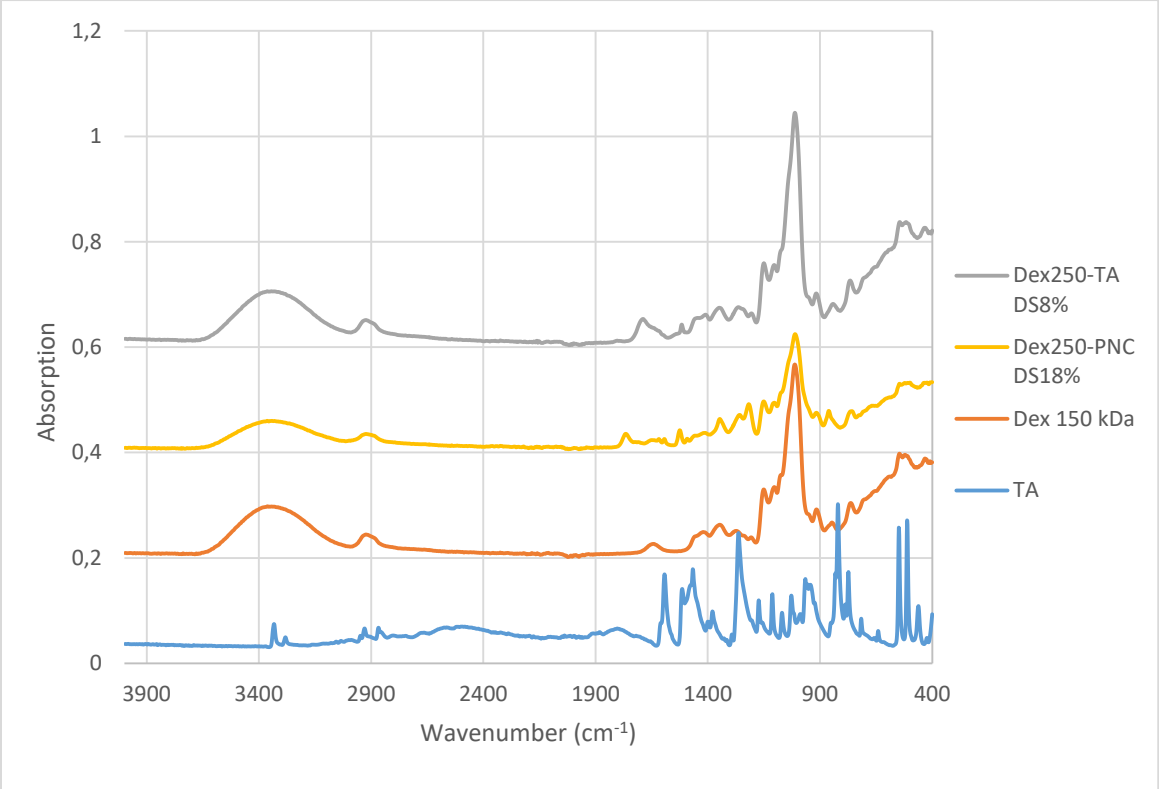

Figure S24. ATR FTIR spectra of TA, 150 kDa dextran, Dex_{250}-PNC DS 18% and Dex_{250}-TA DS 8%.

TA: 3333 (N-H), 3282 (N-H), 2929 (C-H), 2866 (C-H), 1593 (N-H), 1487-1381 (C-H), 1262 (C-O), 964 (C-C) and 820-463 (C-H) cm^{-1}.

Dextran 150 kDa: 3362 (O-H), 2923 (C-H), 1640 (H-O-H), 1151 (C-C, stretch) and 1011 (O-H, bend) cm^{-1}.

Dex_{250}-PNC DS 18%: 3341 (O-H, stretch), 2923 (C-H, stretch), 1765 (C=O carbonate, stretch), 1650 (C=C, stretch), 1346 (C-H, bend), 1524 (N-O, stretch) 1217 (C-O, stretch) and 1010 (O-H, bend) cm^{-1}.

Dex_{250}-TA DS 8%: 3361 (O-H), 2923 (C-H), 1689 (C=O urethane, stretch), 1650 (C=C, stretch), 1205 (C-N, stretch), 1151 (C-C, stretch) and 1012 (O-H, bend) cm^{-1}.

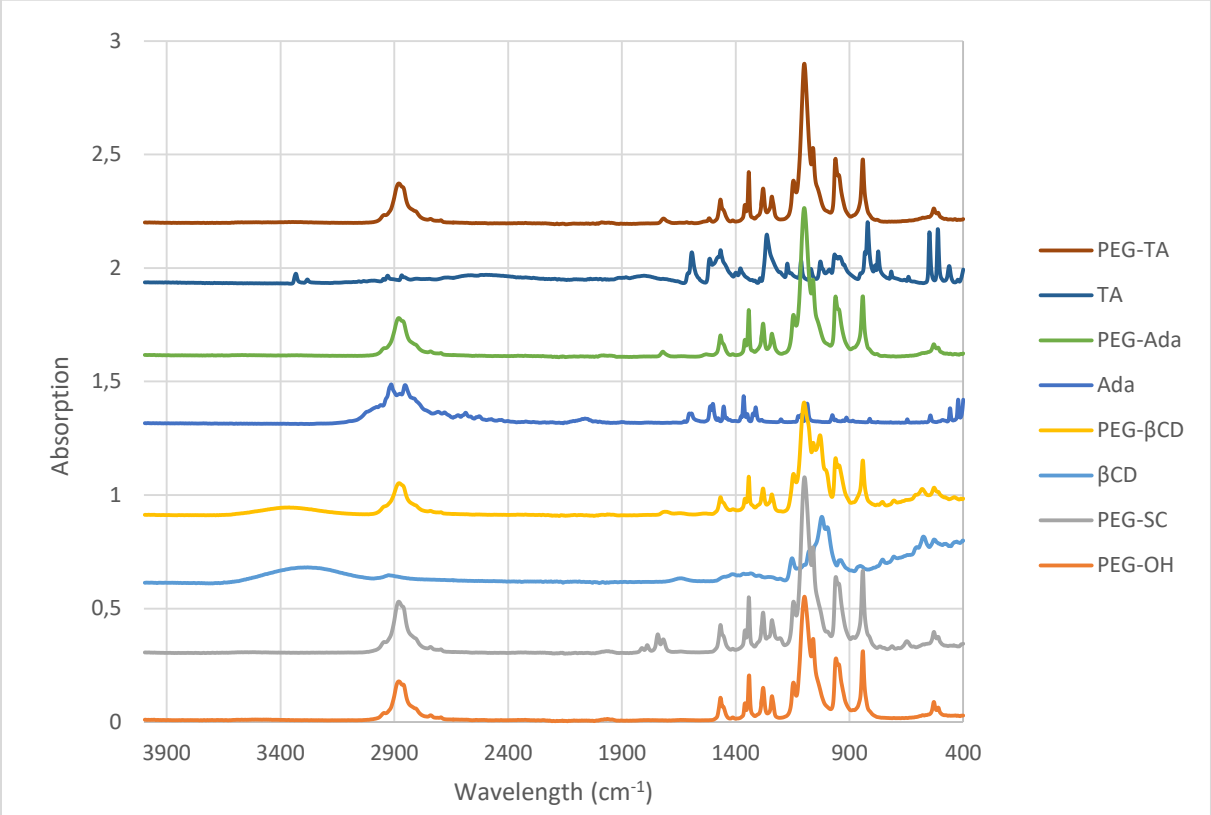

Figure S25. ATR FTIR spectra of PEG-OH, PEG-SC, βCD, PEG- βCD, Ada, PEG-Ada, TA and PEG-TA.

PEG-OH: 3501 (O-H, stretch), 2880 (C-H, stretch), 1466 (C-H, bend), 1340 (C-H, bend), 1280 (O-H, stretch), 1240 (O-H, stretch), 1097 (C-O-H, bend), 958 (C-H, bend) and 840 (C-H, bend) cm^{-1}.

PEG-SC: 2880 (C-H, stretch), 1811 (C=O, stretch), 1742 (C=O, stretch), 1466 (C-H, bend), 1340 (C-H, bend), 1279 (O-H, stretch), 1240 (O-H, stretch), 1197 (C-O, ester stretch), 1146 (C-N, stretch), 1099 (C-O-H, bend), 960 (C-H, bend) and 840 (C-H, bend) cm^{-1}.

βCD: 3282 (O-H, stretch), 2925 (C-H, stretch), 1638 (H-O-H), 1152 (C-C, stretch) and 1020 (O-H, bend) cm^{-1}.

PEG-βCD: 3380 (O-H, stretch), 2878 (C-H, stretch), 1467 (C-H, bend), 1342 (C-H, bend), 1279 (O-H, stretch), 1240 (O-H, stretch), 1146 (C-N, stretch), 1100 (C-O-H, bend), 960 (C-H, bend) and 840 (C-H, bend) cm^{-1}.

Ada: 2913 (C-H), 2851 (C-H), 1600-1457 (NH2) and 1300-1400 (C-N) cm^{-1}.

PEG-Ada: 3325 (O-H, stretch), 2880 (C-H, stretch), 1719 (C=O, urethane, stretch), 1467 (C-H, bend), 1342 (C-H, bend), 1279 (O-H, stretch), 1240 (O-H, stretch), 1146 (C-N, stretch), 1098 (C-O-H, bend), 960 (C-H, bend) and 840 (C-H, bend) cm^{-1}.

TA: 3333 (N-H), 3282 (N-H), 2929 (C-H), 2866 (C-H), 1593 (N-H), 1487-1381 (C-H), 1262 (C-O), 964 (C-C) and 820-463 (C-H) cm^{-1}.

PEG-TA: 3343 (O-H, stretch), 2880 (C-H, stretch), 1717 (C=O, urethane, stretch), 1467 (C-H, bend), 1342 (C-H, bend), 1279 (O-H, stretch), 1242 (O-H, stretch), 1146 (C-N, stretch), 1098 (C-O-H, bend), 960 (C-H, bend) and 840 (C-H, bend) cm^{-1}.

SI 4. Stoichiometry determination by using Job's plot method

Table S1. Pipetting scheme TA HCl and polymer-βCD with a final concentration of 100 µM.

TA HCl (1mM) [µL]	Dex-βCD (100 µM) [µL]	Water [µL]
0	2000	0
20	1800	180
40	1600	360
60	1400	540
80	1200	720
100	1000	900
120	800	1080
140	600	1260
160	400	1440
180	200	1620
200	0	1800

Table S2. Pipetting scheme polymer-TA and βCD.H2O with a final concentration of 100 µM.

Dex-TA (100 µM) [µL]	βCD.H_2O (1mM) [µL]	Water [µL]
0	200	1800
200	180	1620
400	160	1440
600	140	1260
800	120	1080
1000	100	900
1200	80	720
1400	60	540
1600	40	360
1800	20	180
2000	0	0

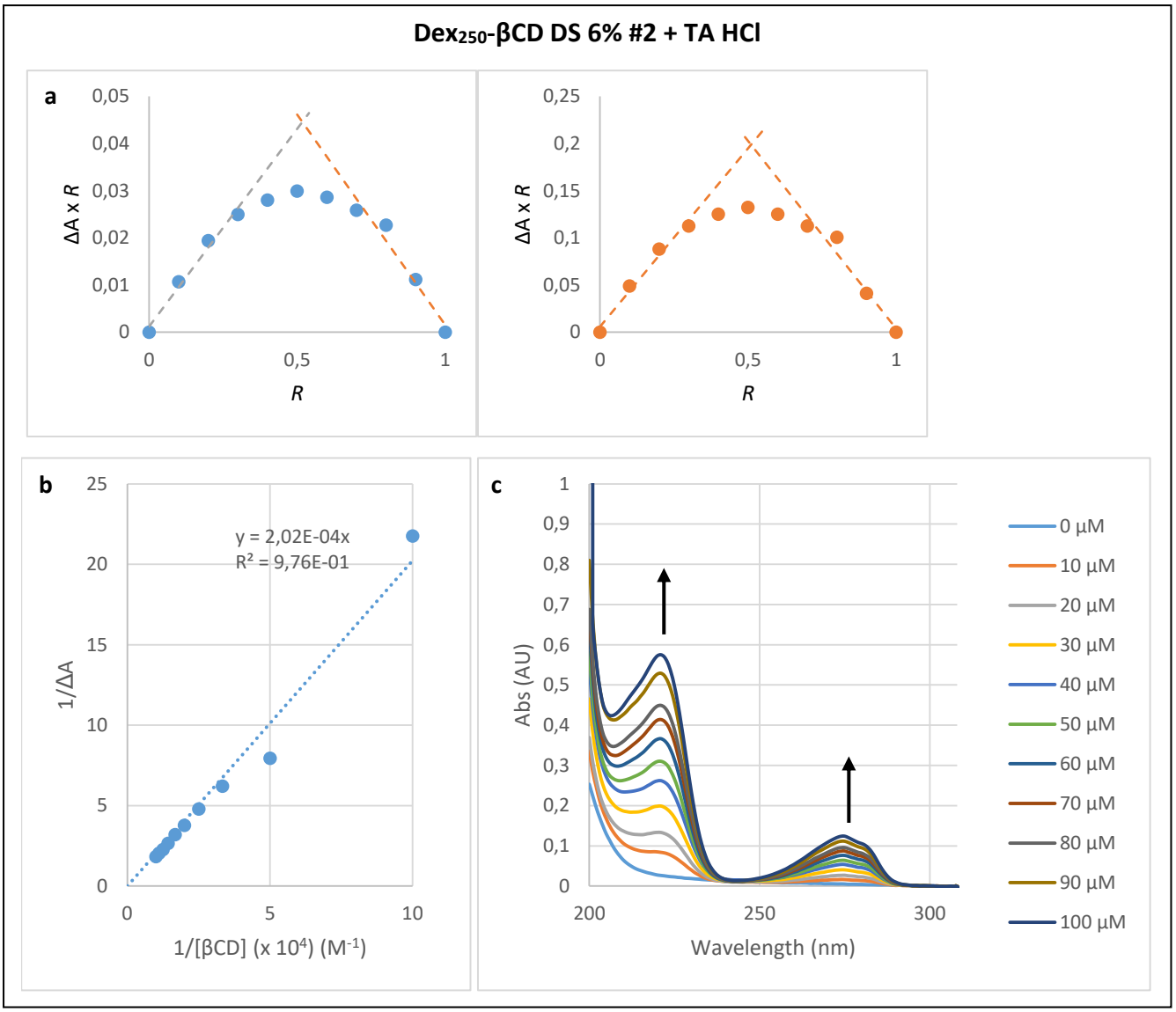

Figure S26. (a) Job plots of Dex$_{250}$-βCD DS 6% #2/TA HCl complex at 274 nm (blue) and 221 nm (orange). (b) Benesi-Hildebrand plot (221nm) for 1:1 inclusion Dex$_{250}$-βCD DS 6% #2/TA HCl complex. (c) UV-vis spectral changes of Dex$_{250}$-βCD DS 6% #2 upon addition of TA HCl (0-100 µM).

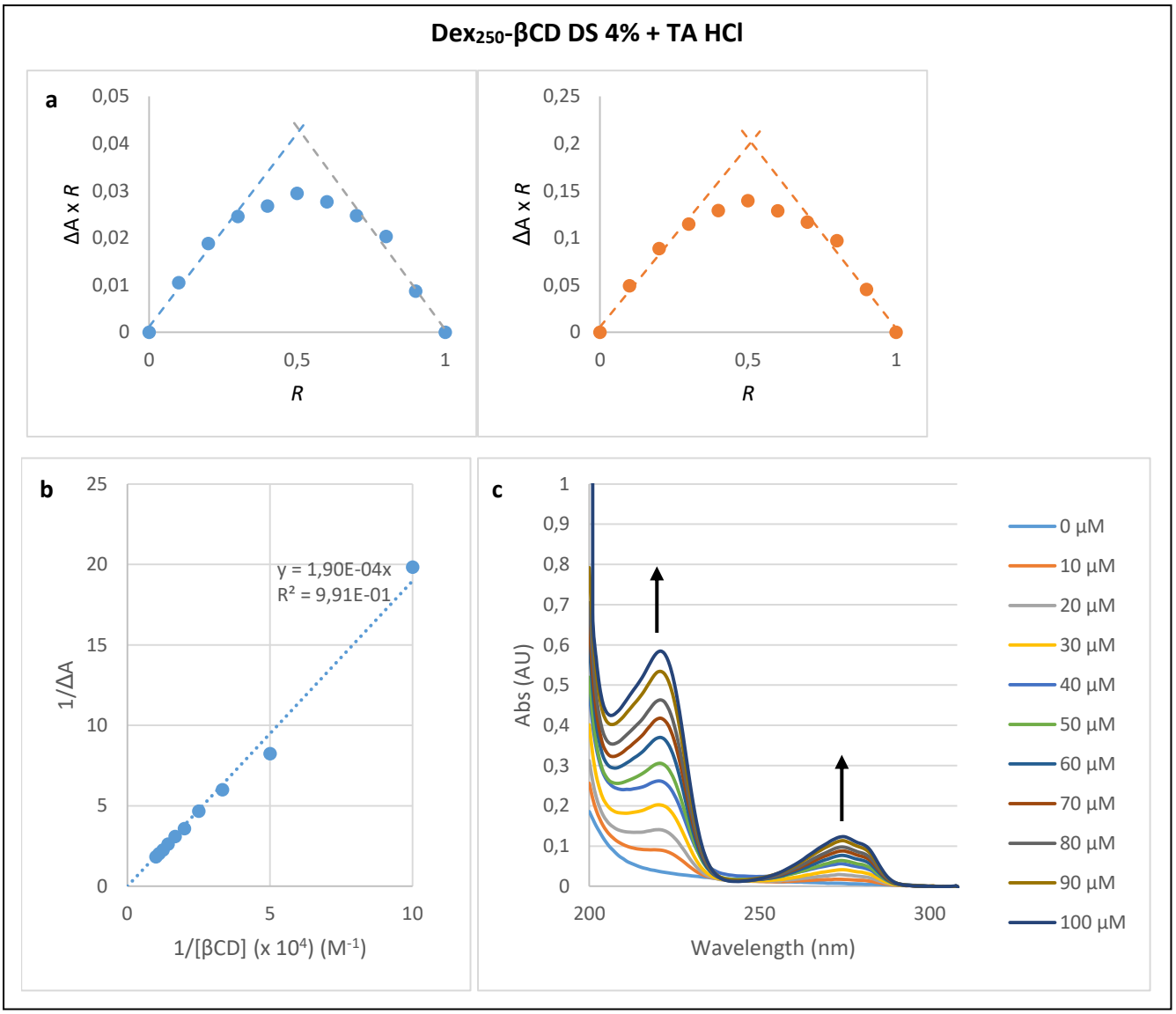

Figure S27. (a) Job plots of Dex$_{250}$-βCD DS 4%/TA HCl complex at 274 nm (blue) and 221 nm (orange). (b) Benesi-Hildebrand plot (221nm) for 1:1 inclusion Dex$_{250}$-βCD DS 4%/TA HCl complex. (c) UV-vis spectral changes of Dex$_{250}$-βCD DS 4% upon addition of TA HCl (0-100 µM).

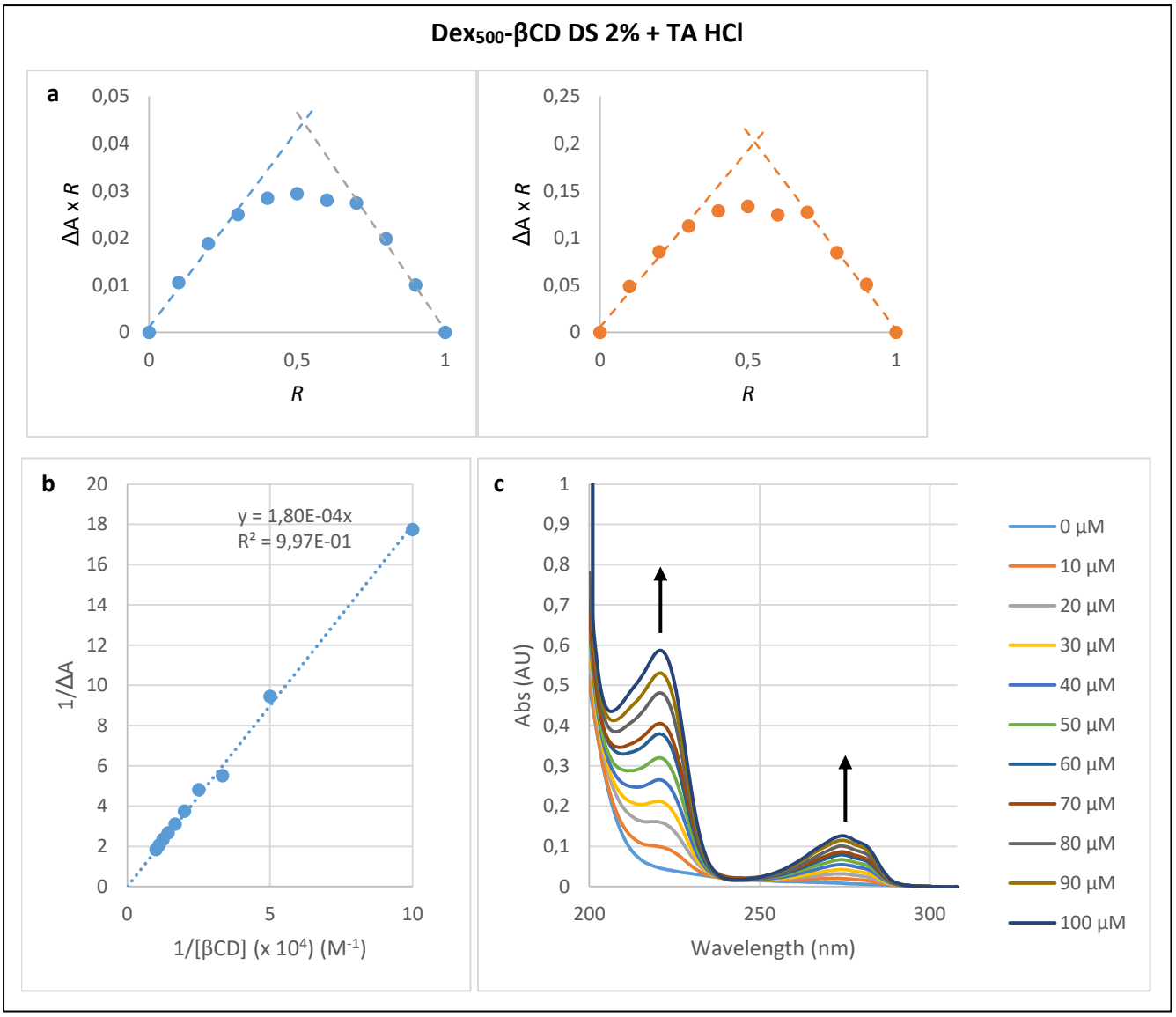

Figure S28. (a) Job plots of Dex_{500}-βCD DS 2%/TA HCl complex at 274 nm (blue) and 221 nm (orange). (b) Benesi-Hildebrand plot (221nm) for 1:1 inclusion Dex_{500}-βCD DS 2%/TA HCl complex. (c) UV-vis spectral changes of Dex_{500}-βCD DS 2% upon addition of TA HCl (0-100 µM).

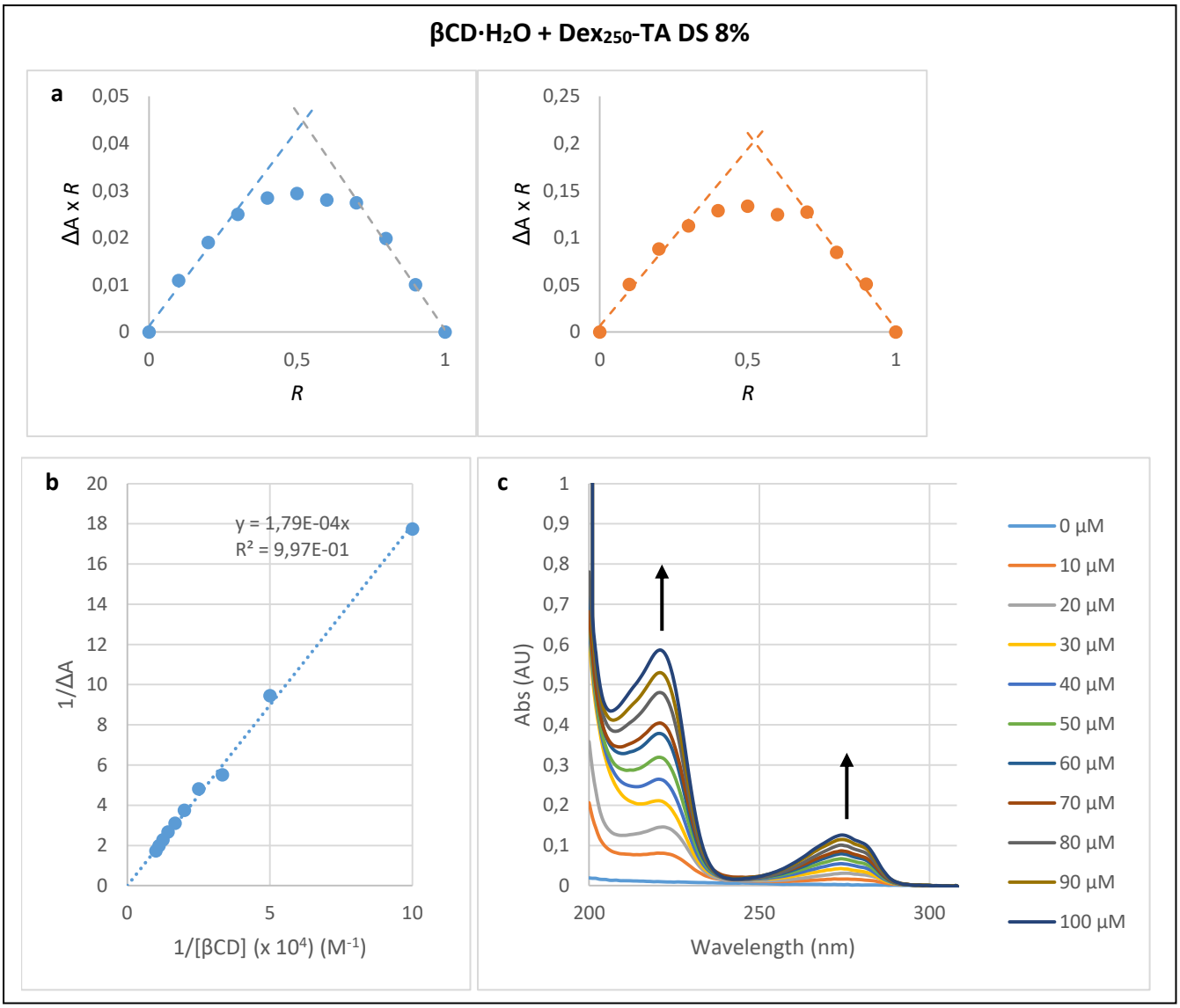

Figure S29. (a) Job plots of βCD·H2O/Dex₂₅₀-TA DS 8% complex at 274 nm (blue) and 221 nm (orange). (b) Benesi-Hildebrand plot (221nm) for 1:1 inclusion βCD·H₂O/Dex₂₅₀-TA DS 8% complex. (c) UV-vis spectral changes of βCD·H₂O upon addition of Dex₂₅₀-TA DS 8% (0-100 µM).

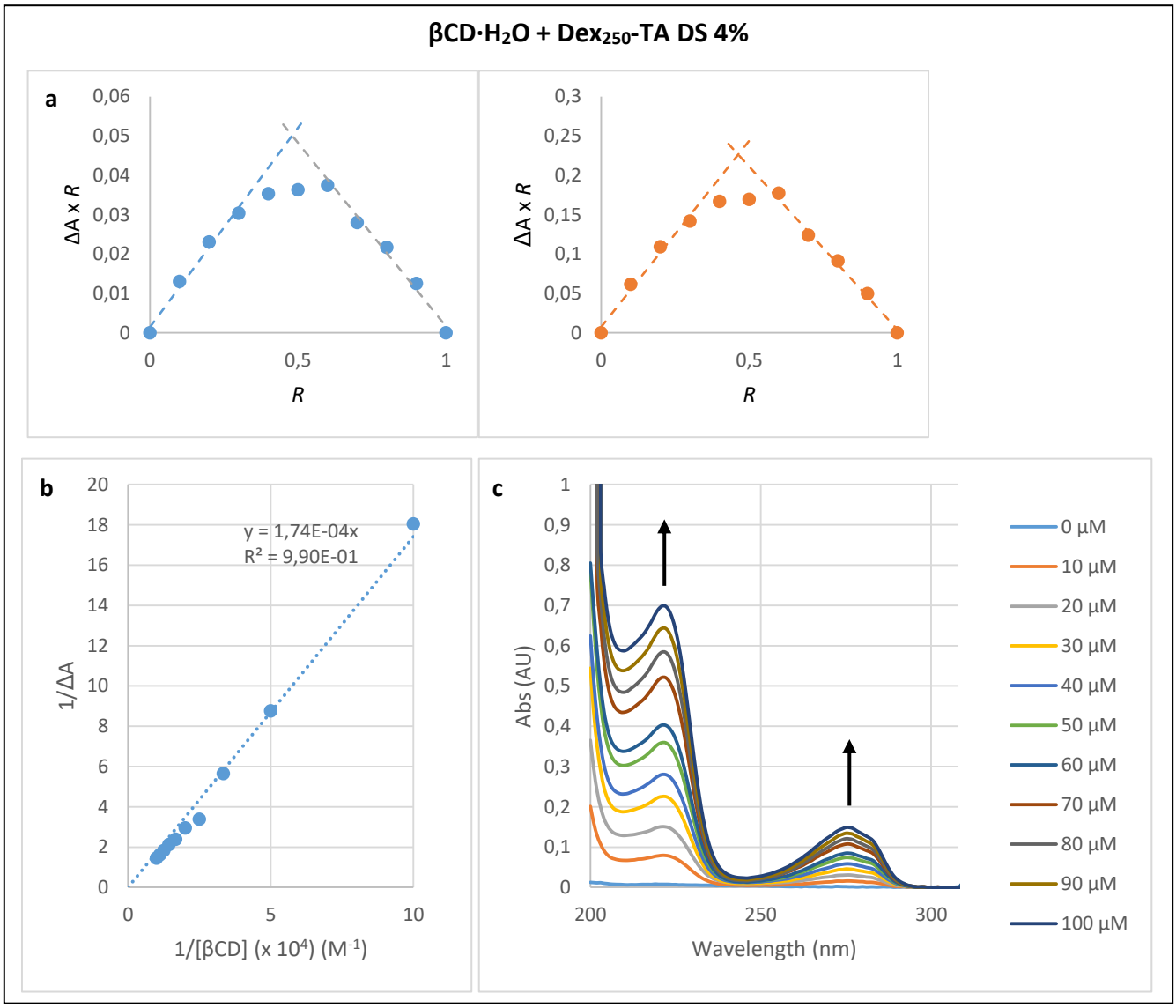

Figure S30. (a) Job plots of βCD·H2O/Dex$_{250}$-TA DS 4% complex at 274 nm (blue) and 221 nm (orange). (b) Benesi-Hildebrand plot (221nm) for 1:1 inclusion βCD·H$_2$O/Dex$_{250}$-TA DS 4% complex. (c) UV-vis spectral changes of βCD·H$_2$O upon addition of Dex$_{250}$-TA DS 4% (0-100 µM).

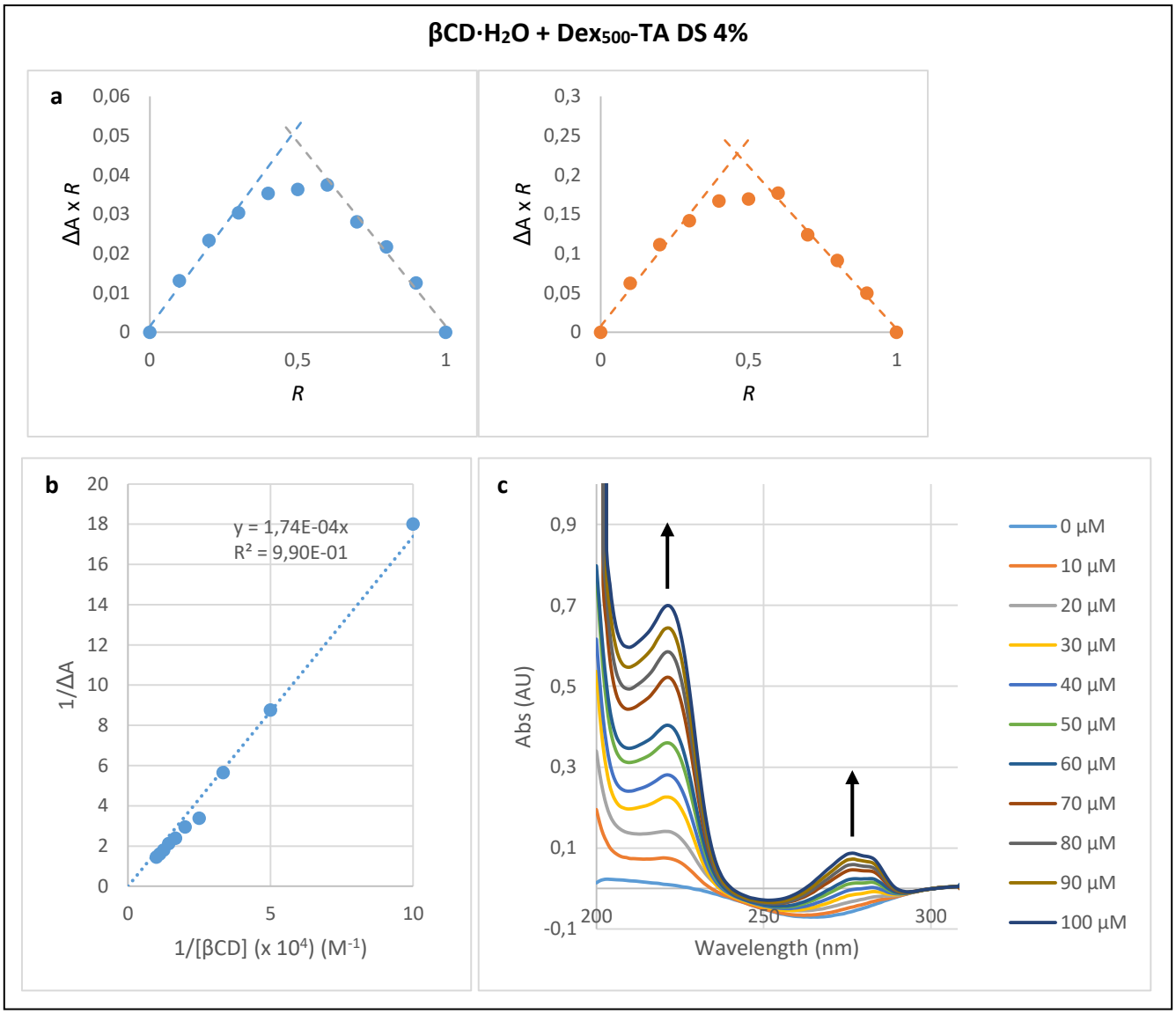

Figure S31. (a) Job plots of βCD·H2O/Dex$_{500}$-TA DS 4% complex at 274 nm (blue) and 221 nm (orange). (b) Benesi-Hildebrand plot (221nm) for 1:1 inclusion βCD·H$_2$O/Dex$_{500}$-TA DS 4% complex. (c) UV-vis spectral changes of βCD·H$_2$O upon addition of Dex$_{500}$-TA DS 4% (0-100 µM).

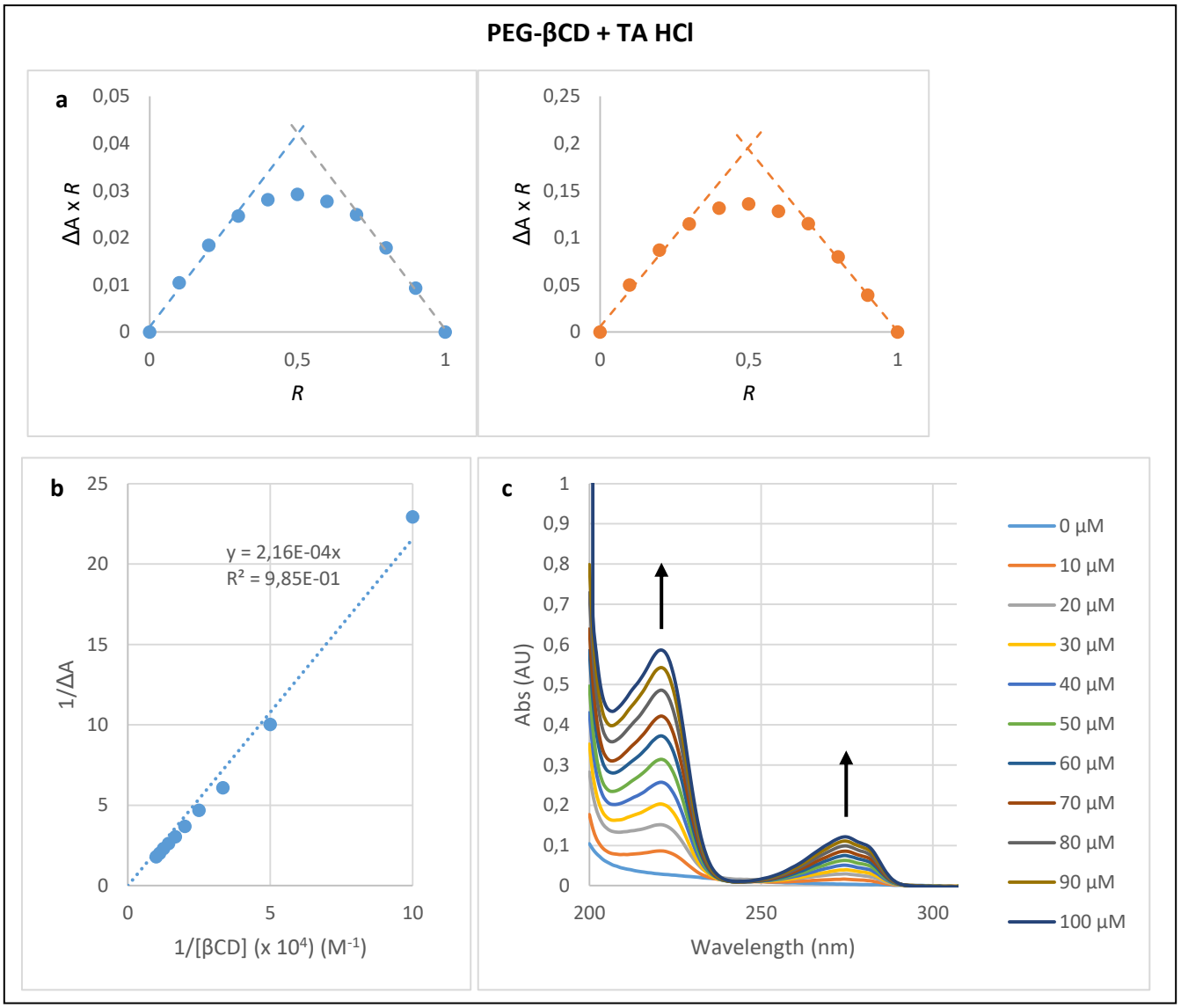

Figure S32. (a) Job plots of PEG-βCD/TA HCl complex at 274 nm (blue) and 221 nm (orange). (b) Benesi-Hildebrand plot (221nm) for 1:1 inclusion PEG-βCD/TA HCl complex. (c) UV-vis spectral changes of PEG-βCD DS 2% upon addition of TA HCl (0-100 µM).

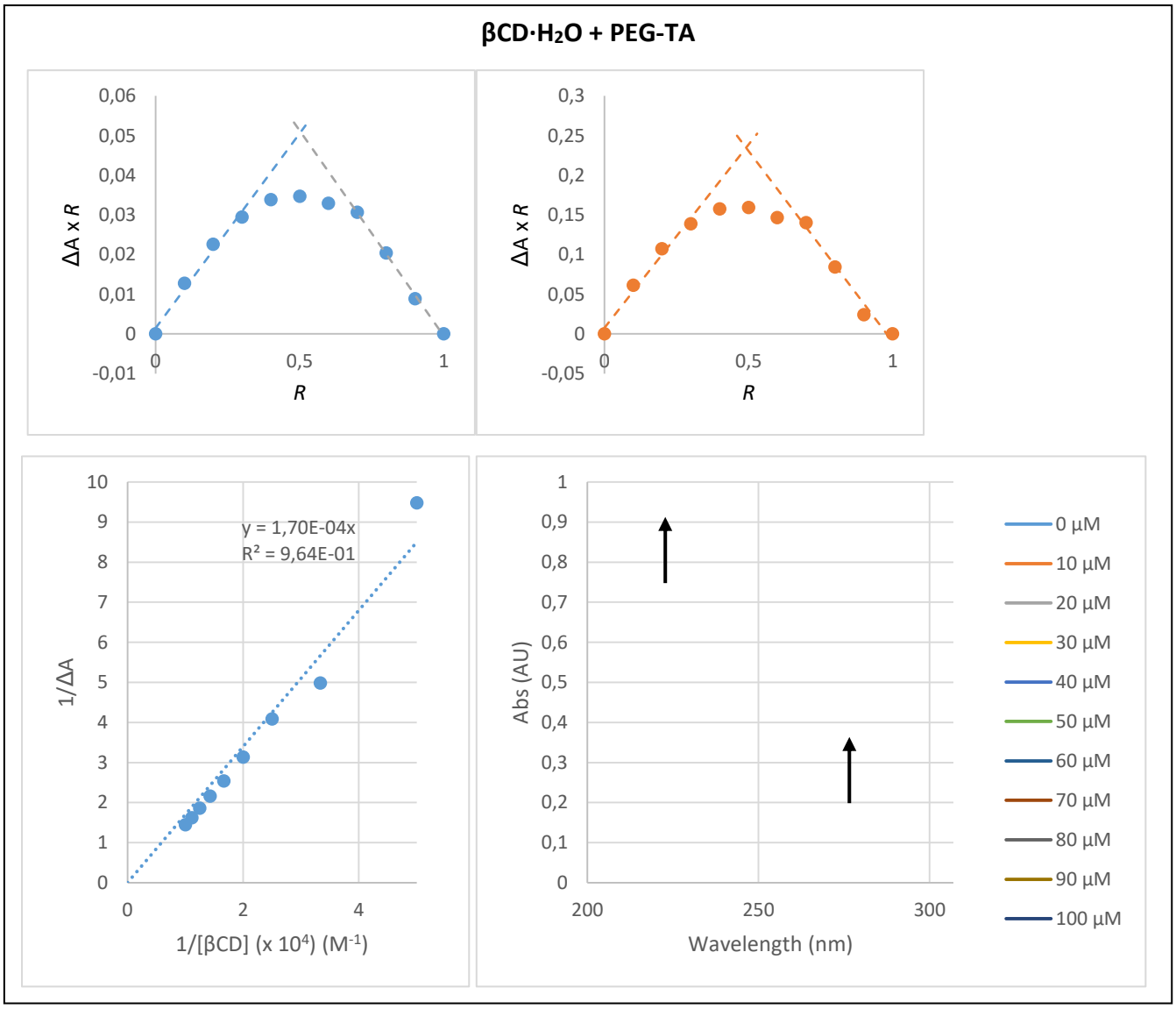

Figure S33. (a) Job plots of βCD·H2O/PEG-TA complex at 274 nm (blue) and 221 nm (orange). (b) Benesi-Hildebrand plot (221nm) for 1:1 inclusion βCD·H_2O/PEG-TA complex. (c) UV-vis spectral changes of βCD·H_2O upon addition of PEG-TA (0-100 µM).

SI 5. Stoichiometry determination by ^{1}H NMR tritration

Table S3. ^{1}H NMR chemical shift (Δδ) of the the βCD protons between the Ada/βCD complex and the pure host ($[H]_0$=4.41 mM).

[Ada]/[βCD]	H1	H2	H3	H4	H5	H6
0,00	0,00	0,00	0,00	0,00	0,00	0,00
0,10	0,01	0,01	-0,01	0,00	0,00	0,00
0,20	0,00	0,01	-0,02	0,00	-0,01	-0,01
0,30	0,00	0,02	-0,04	0,00	-0,02	0,00
0,45	0,00	0,02	-0,07	0,00	-0,03	0,00
0,60	0,00	0,03	-0,09	0,01	-0,06	0,00
0,80	0,00	0,04	-0,11	0,01	-0,08	0,00
1,00	0,00	0,04	-0,12	0,01	-0,09	0,01
1,25	0,00	0,04	-0,13	0,01	-0,10	0,01
1,50	0,00	0,05	-0,13	0,01	-0,10	0,01
2,50	0,01	0,06	-0,13	0,02	-0,11	0,02
5,00	0,01	0,06	-0,13	0,02	-0,11	0,02
7,50	0,01	0,06	-0,13	0,02	-0,12	0,02
10,0	0,01	0,06	-0,13	0,03	-0,12	0,02

Table S4. ^{1}H NMR chemical shift (Δδ) of the the βCD protons between the TA/βCD complex and the pure host ($[H]_0$=4.41 mM).

[TA]/[βCD]	H1	H2	H3	H4	H5	H6
0,00	0,00	0,00	0,00	0,00	0,00	0,00
0,10	0,01	0,00	0,00	0,00	0,00	0,00
0,20	0,00	0,00	0,00	0,00	0,00	0,00
0,30	0,00	0,00	-0,01	0,00	0,00	-0,01
0,45	0,00	0,00	-0,01	0,00	-0,01	0,00
0,60	0,01	0,01	-0,01	0,00	-0,01	0,00
0,80	0,00	0,01	-0,02	0,00	-0,03	0,00
1,00	0,00	0,00	-0,03	0,00	-0,04	-0,01
1,25	0,00	0,00	-0,04	0,00	-0,05	-0,01
1,50	0,00	0,01	-0,05	0,00	-0,06	-0,01
2,50	0,00	0,01	-0,06	0,00	-0,07	-0,01
5,00	0,00	0,01	-0,08	0,00	-0,11	-0,01
7,50	0,00	0,02	-0,10	0,00	-0,14	-0,02
10,0	0,00	0,02	-0,11	0,00	-0,16	-0,02